ABSTRACT

Title of dissertation: NON-PERTURBATIVE METHODS IN
                           QUANTUM FIELD THEORY
                           AND QUANTUM GRAVITY

                           Anton de la Fuente, Doctor of Philosophy, 2016

Dissertation directed by: Professor Raman Sundrum
                            Department of Physics

This thesis considers non-perturbative methods in quantum field theory with applications to gravity and cosmology. In particular, there are chapters on black hole holography, inflationary model building, and the conformal bootstrap.

NON-PERTURBATIVE METHODS IN
QUANTUM FIELD THEORY AND QUANTUM GRAVITY

by

Anton de la Fuente

Dissertation submitted to the Faculty of the Graduate School of the
University of Maryland, College Park in partial fulfillment
of the requirements for the degree of
Doctor of Philosophy
2016

Advisory Committee:
Professor Raman Sundrum, Chair/Advisor
Professor Thomas Cohen
Professor Jonathan Rosenberg
Professor Zackaria Chacko
Professor Rabindra Mohapatra

Table of Contents

List of Figures

Chapter 1:   Introduction

Quantum field theory has been an outstandingly successful theoretical framework for describing nature. Essentially, any relativistic and quantum mechanical system of interacting particles can be described by a quantum field theory [2]. Furthermore, on distance scales larger than the Compton wavelength of a given particle, there exists an effective description without that particle which is again a quantum field theory. Such a theory is called an effective field theory (EFT). Conversely, on short enough distance scales, a given EFT will often break down, signaling that it must be replaced by a new EFT that incorporates new physics.

Contrary to what the popular literature may suggest, the gravitational field can be quantized as an EFT just as well as any other field. The result is simply the EFT of interacting spin-2 particles. As with most EFTs, gravitational EFT breaks down and must be replaced at some small scale, which in this case is called the Planck scale. However, this is where the problem of quantizing gravity actually shows up. On distances scales smaller than the Planck scale, the entire quantum field theory framework must break down and it is not possible to replace gravitational EFT with any other EFT [3]. String theory provides a replacement theory in terms of a perturbative expansion in the string coupling. For a long time, there was only this perturbative definition string theory. In other words, there was no

non-perturbative theory whose expansion was equal to the string perturbation series.

Surprisingly (and perhaps ironically), it turned out that almost any quantum field theory secretly knows how to sum the string perturbation series and provide a non-perturbative definition of string theory in certain classes of spacetimes. This is the AdS/CFT duality [4–6]. AdS/CFT was discovered in the process of trying to understand the quantum mechanics of black holes. Basically, by decreasing the value of the string coupling, a black hole disintegrates and the system is described by the quantum mechanics of its constituents. In special cases, this back and forth was used to explicitly account for the microstates that comprised black hole entropy [7]. Various other calculations eventually led to the realization that underlying this back and forth was really an exact duality between the non-gravitational interactions of the black hole constituents and string theory in the near-horizon AdS region of an extremal black hole. The non-gravitational interactions are described by a conformal field theory (CFT) in fewer spacetime dimensions than that in which the black hole lives, giving rise to the name holography.

The reason black holes were being studied so intensively was because of the black hole information problem [8]. Basically, black hole evaporation requires one of three things, 1) non-unitary evolution, 2) superluminal propagation of information, or 3) tiny Planck-sized objects with an infinite amount of entropy. Since the dual CFT is a standard quantum mechanical system with a finite density of states, 1) and 3) are ruled out. Furthermore, the holographic nature of the duality made 2) seem like the perfect match. However, there was never any explicit description on the gravitational side of the superluminal propagation of information. Various failed attempts to construct such a description resulted in the currently infamous no-go theorem [9–11] known as the firewall paradox. Basically, [9–11]

2

convincingly argued that it is impossible to have the needed superluminal propagation of information without also having an infalling observer experiencing large violations of gravitational effective field theory or of quantum mechanics in general.

This remains the current state of affairs. Although many possible scenarios to avoid the firewall paradox have been proposed, all remain problematic. Furthermore, some scenarios involving seemingly arbitrary CFT constructions are hinting that the non-perturbative definition of string theory via AdS/CFT has its limitations. We will likely need an independent non-perturbative gravitational definition of quantum gravity in order to come to a satisfactory answer. However, instead of directly working on this highly ambitious goal, most of the current effort by those who think about the firewall paradox is actually spent on doing concrete calculations involving entanglement entropy, quantum information, or conformal field theories. These subfields are rapidly evolving, and hopefully the stage will soon be set for a large conceptual breakthrough. Perhaps the current situation is akin to the time just before AdS/CFT was discovered, when there was also a flurry of concrete calculations, which at that time involved various properties of black holes in string theory.

As with the work just mentioned, this thesis does not directly attack the problem of constructing a non-perturbative definition of quantum gravity that is independent of AdS/CFT. Instead, the main focus is in gaining a better understanding of AdS/CFT along with some possible phenomenological consequences of quantum gravity in general. What follows is the plan of the thesis, with a summary of each chapter and how it fits into the broader introduction just given.

Plan of the Thesis

In chapter 2, we investigate black holes in three spacetime dimensions. We propose a scenario in which the black hole interior is encoded in the correlation functions of certain non-local CFT operators. Due to the simplicity of three dimensions, we are able to give explicit expressions for these non-local operators. In particular, the three dimensional black hole is an orbifold of empty AdS. Motivated by the fact that local boundary correlators in empty AdS can be suitably interpreted as bulk scattering amplitudes, we define orbifolded versions of these correlators that have the interpretation of particles scattering behind the horizon. The dual construction involves the aforementioned non-local operators in the CFT. These non-local operators differ from the more standard ones used in bulk reconstruction. Perhaps most intriguingly, they are defined without reference to bulk perturbation theory.

In chapter 3, we consider the possibility that not all gravitational EFTs can be consistently completed by a non-perturbative theory of quantum gravity. The set of theories that cannot arise from a complete theory of quantum gravity has been termed the "swampland." In particular, many models of cosmic inflation involve a dynamical scalar field rolling down a potential in field space. The resulting field displacement is often larger than the Planck scale. This has raised concern because there have been arguments suggesting that any theory with transplanckian field transits must reside in the swampland. More specifically, the argument is twofold. First, the claim is that any theory which violates the " weak gravity conjecture" (WGC) must resides in the swampland. Second, the claim is that any model of transplanckian field transits must violate the WGC. In this chapter, we prove that the second claim is false by providing an explicit counterexample. Our model involves axions

and extra-dimensions, but reduces to natural inflation with small corrections during inflation. Although these small corrections do not ruin inflation, they potentially give rise to distinct observable signals in the CMB.

Chapter 4 was originally motivated by the above claim that any gravitational EFT which violates the WGC must reside in the swampland. The idea was to translate this claim into CFT language, and investigate its validity using the newly developed tools of the conformal bootstrap. We eventually realized that such an undertaking was too large and the project morphed into a non-gravitational investigation using the bootstrap. In terms of the introduction, this chapter is a concrete CFT calculation for the purpose of better understanding our tools. Now, a CFT is so constrained by symmetry that all its correlation functions are completely determined by its set of 2- and 3-point functions, which are in turn determined by a discrete set of numbers, known as the conformal data of the CFT. In order for the conformal data to consistently determine all higher-point functions, they must satisfy a highly nontrivial set of consistency conditions, known as the conformal bootstrap equations. It has recently been discovered that numerical methods can efficiently identify large regions in the space of conformal data that are inconsistent with the bootstrap equations. Using these methods, we give evidence that the 2D Ising CFT is the only CFT with a $\mathbb{Z}_2$ symmetry and two relevant operators. This shines a new light on the concept of universality in the study of critical phenomena.

Chapter 2: Holography of the BTZ Black Hole, Inside and Out

2.1 Introduction

Nearly a century after the discovery of the Schwarzschild metric,

$$ds^2 = \left(1 - \frac{r_S}{r}\right) dt^2 - \frac{dr^2}{1 - \frac{r_S}{r}} - r^2 \left(d\theta^2 + \sin^2\theta \, d\phi^2\right), \tag{2.1}$$

black holes remain a source of mystery and fascination. In theoretical physics, they provide key insights for our most ambitious attempts to unify gravity, relativity and quantum mechanics. Viewed from the outside as robust endpoints of gravitational collapse, and decaying subsequently via Hawking radiation, black holes pose the information paradox. Falling inside, the roles of "time", τ, and "space", r, apparently trade places, the horizon now encompassing a universe within, with the future singularity its "big crunch". Understanding these dramatic phenomena seems tantalizingly close to our grasp, just beyond the horizon, a region comprised of familiar, smooth patches of spacetime. And yet, the local simplicity of the horizon belies its global subtlety, which still lacks an explicit inside/outside description within a fundamental framework for quantum gravity (as exemplified by the recent "firewall" paradox [9–11][1]) regarding evaporating black holes. Nevertheless, powerful ideas and results

---

[1]See also [12] for a prediction similar to firewalls from different assumptions.

in holography [13] [14], complementarity [15], string theory and AdS/CFT duality [4] [5] [6] (reviewed in [16] [1] [17]), have combined with gravitational effective field theory (EFT) to give us a much clearer picture of the central issues (reviewed in [18] [19]).

In such a situation, it is natural to look for an "Ising model", a special case that enjoys so many technical advantages that we can hope to solve it exactly, and whose solution would test and crystalize tentative grand principles, and brings new ones to the fore. For this purpose, the $2 + 1$-dimensional BTZ black hole [20, 21] is, in many ways, an ideal candidate. The BTZ geometry solves Einstein's Equations with negative cosmological constant in $2 + 1$ dimensions, and is given in Schwarzschild coordinates by,

$$ds^2_{\text{BTZ}} = \frac{r^2 - r_S^2}{R_{\text{AdS}}^2} d\tau^2 - \frac{R_{\text{AdS}}^2}{r^2 - r_S^2} dr^2 - r^2 d\phi^2 \qquad (-\pi \leq \phi \leq \pi, \ r > 0), \qquad (2.2)$$

not that dissimilar from (2.1). The geometry asymptotes for large r to that of global anti-de Sitter spacetime, AdS$_{3\,\text{global}}$, with radius of curvature R_{AdS} and AdS boundary at $r = \infty$. The horizon is at the Schwarzschild radius, $r = r_S$. It is the simplest of the "large" AdS Schwarzschild black holes, eternal in that they do not decay via Hawking radiation, but rather are in equilibrium with it [22]. It retains many of the key interesting features of black holes in general. In what follows it will be more convenient to rescale coordinates,

$$\frac{R_{\text{AdS}}}{r_S} r \to r \qquad\qquad \frac{r_S}{R_{\text{AdS}}} \tau \to \tau \qquad\qquad \sigma \equiv r_S \phi, \qquad (2.3)$$

and to switch to $R_{\text{AdS}} \equiv 1$ units, so the metric becomes

$$ds^2_{\text{BTZ}} = (r^2 - 1)d\tau^2 - \frac{dr^2}{r^2 - 1} - r^2 d\sigma^2 \qquad (-\pi r_S \leq \sigma \leq \pi r_S, \, r > 0). \qquad (2.4)$$

The horizon is now at $r = 1$.

Although pure $2 + 1$-dimensional general relativity does not contain propagating gravitons, it does have gravitational fluctuations and backreactions, and coupled to propagating matter the EFT is non-renormalizable as in higher dimensions (in fact, it may be a compactification of higher dimensions, and contain propagating Kaluza-Klein gravitons), requiring UV completion. It also shares with higher-dimensional eternal AdS Schwarzschild black holes, the central consequence of AdS/CFT duality: as an object inside $\text{AdS}_{\text{global}}$ the black hole inherits a holographic dual in terms of a "hot" conformal field theory (CFT) (for BTZ, a $1 + 1$ CFT on a spatial circle), the CFT temperature being dual to the BTZ Hawking temperature. More precisely [23] (see also the earlier steps and insights of [24] [25] [26]), the duality is framed in terms of the Kruskal extension of BTZ,

$$ds^2 = \frac{4 du dv}{(1 + uv)^2} - \left(\frac{1 - uv}{1 + uv} \right)^2 d\sigma^2 \qquad (|uv| < 1). \qquad (2.5)$$

The horizon, "singularity" and AdS boundaries are now as follows:

$$
\begin{aligned}
\text{boundary:} \quad & uv = -1 \\
\text{horizon:} \quad & u = 0 \text{ or } v = 0 \\
\text{singularity:} \quad & uv = 1.
\end{aligned}
\qquad (2.6)
$$
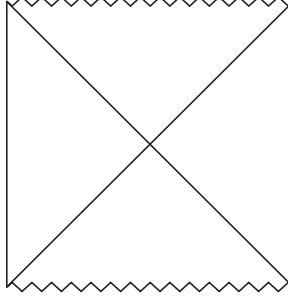
Figure 2.1: The Penrose diagram of the extended BTZ black hole spacetime. The vertical lines represent the boundaries of two asymptotically AdS regions.

The Penrose diagram of this spacetime is shown in Fig. 2.1. BTZ is seen to interpolate between two distinct asymptotically-AdS$_{\text{global}}$ boundary regions. The holographic dual is then given by two CFTs, dynamically decoupled, but in a state of "thermofield" [27–33] entanglement,

$$|\Psi\rangle_{\text{BTZ}} \equiv \sum_n e^{-\pi E_n} |\bar{n}\rangle \otimes |n\rangle. \tag{2.7}$$

The entangled state is dual to the Hartle-Hawking choice of vacuum [34] for the BTZ black hole.

There remains the puzzle of detailing just how this CFT description incorporates processes inside the BTZ horizon. We know that in asymptotic AdS spacetimes, the set of local boundary correlators gives a beautiful diffeomorphism-invariant quantum gravity description of scattering which generalizes the S-matrix construction of asymptotic Minkowski spacetimes, and, in the sense described in [35], is even richer in structure. Furthermore, these boundary correlators have a non-perturbative and UV-complete description in terms of correlators of local CFT operators "living" on the AdS boundary, ∂AdS. But in AdS-Schwarzchild spacetimes like BTZ it is not apparent what CFT questions give a diffeomorphism-invariant and non-perturbative description of scattering inside the horizon: one can send in wavepack-

ets from outside the horizon aimed to scatter within, but the products of any scattering must causally end up at the singularity rather than returning to the exterior AdS boundaries. While one can connect Witten diagrams from interaction points in the interior of the (future) horizon to the boundaries shown in Fig. 2.1, these connections cannot sharply capture the fate of such interactions since they are at best spacelike.

This does not mean that the interior of the horizon is out of bounds to the CFT description. In a sense, what is required is a set of "out states" consisting of approximately decoupled bulk particles located on a spacelike hypersurface before the (future) singularity, with which one can compute the overlap with the state resulting from the scattering process. Even in (the simpler) AdS spacetime, particles inside the bulk are described by *non-local* disturbances of the CFT, so one can anticipate that any holographic description of scattering inside the horizon will necessarily involve correlators of *non-local* CFT operators. But specifically which non-local CFT operators correspond to the simplest basis of "out states", so that their correlators (with other CFT operators) provide a sharp diagnostic of scattering inside the horizon? In this chapter, we identify such non-local CFT operators and demonstrate that they correspond to the intuitive notion of scattering inside the horizon. Our proposal is precisely and non-perturbatively framed. We test it by applying it to scattering inside the horizon but far from the singularity where, at short distances $\ll R_{\text{AdS}}$, the behavior is very much like scattering outside the horizon or in flat spacetime, and so we know what to expect. We then show how to apply our proposal to probe the more mysterious regime near the singularity, where EFT breaks down and even perturbative string theory may be blind to important non-perturbative effects (see for example, [23]). Since the interior of the horizon is a cosmological spacetime, finding the non-local CFT operators can be thought of

as giving the holographic description of a quantum cosmology with singularity, a signficant step beyond the more familiar holography of static AdS.

2.2 Overview and Organization

2.2.1 Diffeomorphism invariance in Non-perturbative Formulation

The issue of diffeomorphism invariance, and the challenge it poses for a description of the interior of the horizon, may seem unfamiliar to those who routinely use local field operators to sharply describe processes in the real world (which of course includes quantum gravity in some form). This would naively suggest that in the BTZ context we should use local bulk operators acting on the Hartle-Hawking state to create "in/out" states inside the horizon, and then translate these operators to (non-local) operators of the CFT. However, fundamentally *all* local fields (composite or elementary) violate the diffeomorphism gauge symmetry of quantum gravity (their spacetime argument at least is not generally coordinate-invariant), just as the local electron and gauge fields violate gauge invariance in QED. Of course, we are used to using gauge non-invariant local operators within a gauge-fixed formalism, but these are, in essence, non-local constructions in the gauge-invariant data. For example in electromagnetism, the gauge-invariant data (in Minkowski spacetime) are provided by specifying some field strength, $F_{\mu\nu}(x)$, subject to the Bianchi identity, $\epsilon^{\mu\nu\rho\sigma}\partial_\nu F_{\mu\nu}(x) = 0$. This uniquely determines a "local" gauge potential, $A_\mu(x) : \partial_\mu A_\nu - \partial_\nu A_\mu = F_{\mu\nu}$, once we stipulate some gauge-fixing condition (and behavior at infinity), such as

$$\partial^\mu A_\mu = c(x). \tag{2.8}$$

11

$A_\mu(x)$ is thereby a *non-local* functional of $F_{\mu\nu}(y)$. In this way, gauge-fixing is seen as a method for giving non-local gauge-invariant operators a superficially local (and useful) form. In gravity, the gauge-fixing approach is useful for perturbatively small fluctuations of the metric, but not when there are violent fluctuations of the metric (or when the notion of spacetime geometry itself breaks down). And yet it is precisely large fluctuations of the metric that we are interested in when we are concerned with non-perturbative effects (in G_{Newton}) saving us from information loss (see discussion in [23]), or in the approach to the singularity. Therefore, in the non-perturbative framing of our proposal we avoid the intermediate step of gauge-fixed local bulk fields, instead exploiting the greater simplicity of BTZ over other black holes to directly identify the (diffeomorphism-invariant) CFT observables.

Nevertheless, it is useful to see how our approach reduces to gauge-fixed EFT of bulk fields, when that is valid, and this also provides an arena for testing the proposal. To this end, we will show that correlators of local field operators inside the horizon can be re-expressed as correlators of non-local EFT observables outside the horizon (in principle accessible to an outside observer). Even though this "dictionary" is between gravitational EFT descriptions, the "translating" operation is non-perturbative in form. It resonates with the ideas of complementarity [15], where the interior of the horizon is not independent of the exterior, but rather a very different probe of it.
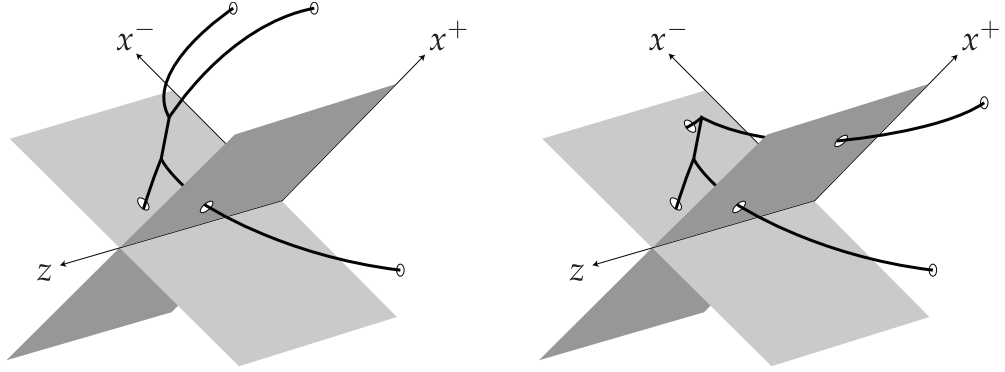
(a) The two boundary operators at the top are timelike separated from the scattering event.

(b) Boundary operators on the left and right Rindler wedges are spacelike separated from the scattering event.

Figure 2.2: Boundary operators in the future region are needed to sharply probe scattering behind the horizon.

2.2.2 Strategy for BTZ

BTZ is particularly well-suited to address the above issues for two reasons. First, the enhanced conformal symmetry of $1 + 1$-dimensional CFTs over higher dimensions provides us with a better understanding of their properties. The second reason is that BTZ can be realized as a quotient of AdS spacetime itself, by identifying points related by a discrete AdS isometry [20, 21]. At the technical level, BTZ Green functions can be easily obtained from the highly symmetric AdS Green functions using the method of images [36] [37]. Most importantly, the BTZ horizon emerges as the quotient of a "mere" Rindler horizon, as would be seen by a class of accelerating observers in AdS [38]. (See [39] for a related discussion, and [40] for a higher-dimensional discussion.) The Rindler view of AdS, the BTZ "black string", is given by (2.2) and (2.4) again, but now with non-compact $\sigma \in (-\infty, +\infty)$, $r_S \equiv \infty$. Our approach is based on a novel reanalysis of Rindler AdS/CFT [23] [40], in a manner that can then be straightforwardly quotiented to the BTZ case of interest.

The central issue from the Rindler view can be seen in Fig. 2.2a, depicting the Poincaré patch of AdS, where the intersecting planes are the Rindler horizons, light rays travel at 45 degrees to the vertical time axis, the boundary is at $z = 0$, and

$$x^{\pm} \equiv t \pm x \tag{2.9}$$

are boundary $(1 + 1$ Minkowski$)$ lightcone coordinates. Two particles are seen to enter the future horizon, scatter inside, and then the resultant particle lines "measured" by local boundary correlators ending in the boundary region inside the horizon. Such correlators can sharply diagnose the results of the scattering because the endpoints are causally connected to the scattering point (or region). In Minkowski CFT these endpoints correspond to local operators in the "Milne" wedge inside the Rindler horizon. However, the dual Rindler CFT picture corresponds to two CFTs "living" only in the left and right regions outside the horizon (entangled with each other in the thermofield state), so that correlators of *local* CFT operators correspond to boundary correlators only ending in the boundary regions outside the horizon. As seen in Fig. 2.2b, such local Rindler CFT correlators correspond to boundary correlators with endpoints at best *spacelike* separated from the scattering point, not useful for a sharp diagnosis of the scattering (as we already saw from the Penrose diagram of Fig. 2.1).

However, the desired local operators of the Minkowski CFT (as opposed to the Rindler CFTs) inside the horizon have the form,

$$\mathcal{O}(t, x) \equiv e^{iH_{\text{Mink}}t} \mathcal{O}(0, x) e^{-iH_{\text{Mink}}t}, \qquad |t| > |x|, \tag{2.10}$$

where the operator at $t = 0$ is now within the Rindler region and equivalent to a local Rindler CFT operator. The Minkowski CFT Hamiltonian H_{Mink} is also some operator on the tensor product of the Hilbert spaces of the two Rindler CFTs ($=$ Hilbert space of the Minkowski CFT, as is apparent at $t = 0$), so $\mathcal{O}(t, x)$ must also be some operator of the Rindler CFTs. But because $H_{\text{Mink}} \neq H_{\text{Rindler}}$, $\mathcal{O}(t, x)$ is not simply a *local* Heisenberg operator of the Rindler CFTs, but rather *non-local* from the Rindler perspective. We conclude that non-local correlators of the Rindler CFTs are able to sharply capture scattering inside the Rindler horizon, the same way that local correlators of the Minkowski CFT ending inside the horizon do. The problem in taking the BTZ quotient of this nice story is that the quotient of H_{Mink} does not exist: the associated t-translation isometry is broken by quotienting.

An important result of ours is to reproduce the correlators of (2.10), which sharply capture scattering inside the Rindler horizon, with a new set of non-local Rindler CFT operators,

$$\mathcal{O}_{\text{non-local}} \equiv e^{\frac{\pi}{2}(H_{\text{Rindler}} - P_{\text{Rindler}})} \mathcal{O}_{\text{local}} e^{-\frac{\pi}{2}(H_{\text{Rindler}} - P_{\text{Rindler}})}, \tag{2.11}$$

constructed from local Rindler CFT operators $\mathcal{O}_{\text{local}}$ and the Rindler Hamiltonian and momentum, $H_{\text{Rindler}}, P_{\text{Rindler}}$. Note that we are not equating these new non-local operators with those of (2.10); they will have different matrix elements within generic states. We only show that they have the same matrix elements in a fixed, special state, namely the thermofield state of the two Rindler CFTs, namely $|\Psi\rangle$ for $r_S = \infty$. This suffices to capture scattering inside the Rindler horizon. But unlike (2.10), the new operators are straightforwardly "quotiented" to the CFT dual of BTZ. Indeed, this quotient is simply the compactification of the spatial Rindler direction, so that P_{Rindler} becomes the conserved
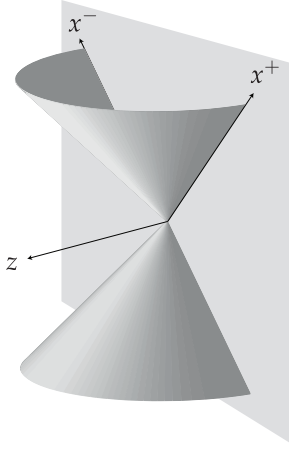
Figure 2.3: These lightcones becomes the singularity of the BTZ black hole after the quotient.

angular momentum of the thermofield CFTs on a spatial circle, and H_{Rindler} becomes their Hamiltonian. We will show that the resulting non-local operators in the thermofield CFTs have correlators which provide some sharp probes of scattering inside the BTZ horizon.

This conclusion is certainly subtle and delicate, as illustrated in Fig. 2.3. After quotienting AdS to BTZ, the lightcones in Fig. 2.3 become the future and past singularities. So it would appear that the quotient construction of correlators to "see" the scattering inside the horizon will correspond to the analog of Fig. 2.2a in BTZ, a diagram that necessarily traverses the singularity. This raises the question of whether the quotienting procedure outlined above is straightforward and trustworthy. Indeed we claim it is, but to double-check this requires studying the singularity more closely, and Feynman diagrammatics in its vicinity.

2.2.3 Through the Singularity: the "Whisker" Regions

Purely at the level of the spacetime geometry (before any dynamics is considered), the quotient construction gives BTZ a perfectly smooth passage (with finite curvature) through the "singularity", the quotient of the lightcones of Fig. 2.3 ($r = 0$ or $uv = 1$ in

Schwarzchild and Kruskal coordinates respectively). However, after the quotient the regions inside these lightcones contain closed timelike curves, dubbed "whiskers" in [41]. (In the Rindler limit, $r_S \to \infty$, these closed curves become infinitely long and the whiskers revert to just ordinary parts of AdS.) The smoothness of the quotient geometry is also deceptive, and the singularity well deserves its name once one makes any attempt to physically probe it. After quotienting the lightcones of Fig. 2.3, they are comprised of closed lightlike curves where even small (quantum) fluctuations [42] [43] can backreact divergently with divergent curvatures, and general considerations imply the breakdown of ordinary (effective) field theory [44]. See [45] for a concise review of these general considerations. Similar singularities have also been studied in the context of string theory. Attempts to scatter *through* the singularity in string theory failed to obtain well-defined amplitudes (see [46] for a concise review and original references). Ref. [47] found that stringy effects involving the twisted sector smoothed out the large backreactions, but so as to isolate the spacetime regions outside the singularity from the whisker (and other) regions beyond the singularity. In any case, much of the literatures suggests that the whisker regions are both wildly unphysical and inaccessible because of the singularity. This seems at odds with our claim that diagrams ending in the whisker regions are the dual of the non-local CFT correlators described above, and that these capture scattering inside the horizon.

However, we will show that local boundary correlators with some endpoints in the whisker regions are in fact well-defined, and a protected sub-class are dominated within EFT, parametrically insensitive to what happens very close to the singularity, even when the associated (Witten) diagrams traverse the singularity. This protected sub-class is specified

by first noting that the maximal extension of the BTZ black hole spacetime is given by [21]

$$\text{BTZ} = \text{AdS}_{\text{global}}/\Gamma, \tag{2.12}$$

where Γ is a quotient discrete isometry group of AdS. An intermediate extension of the black hole spacetime is then given by replacing $\text{AdS}_{\text{global}}$ with just the Poincaré patch, $\text{AdS}_{\text{Poincaré}}$. This still includes the entire Kruskal extension of BTZ as well as two whisker regions,

$$\text{BTZ}_{\text{Kruskal}} \subset \text{AdS}_{\text{Poincaré}}/\Gamma. \tag{2.13}$$

The protected class of boundary correlators is precisely the set confined to $\text{AdS}_{\text{Poincaré}}/\Gamma$, rather than all of $\text{AdS}_{\text{global}}/\Gamma$. For this reason, we confine ourselves in this chapter to $\text{AdS}_{\text{Poincaré}}/\Gamma$, and simply identify it in what follows as the "BTZ spacetime". We will return in future work to a treatment of the boundary correlators of the maximally extended BTZ spacetime given by $\text{AdS}_{\text{global}}/\Gamma$ [48].

Technically, in the $\text{AdS}_{\text{Poincaré}}/\Gamma$ realization of BTZ, naive divergences appear when Witten diagram interaction vertices approach the singularity, but are rendered finite by (a) using and tracking the correct "$i\epsilon$" prescription in BTZ propagators, following from AdS propagators by the method of images, and (b) including the whiskers in the integration region for interaction vertices. Roughly,

$$\int_{r_1<0}^{r_2>0} dr \frac{\ln^p r}{r^q} \to \int_{r_1<0}^{r_2>0} dr \frac{\ln^p(r+i\epsilon)}{(r+i\epsilon)^q} < \infty, \tag{2.14}$$

where r is the Schwarzchild radial coordinate for $r > 0$ and a related coordinate inside the

18

whisker region for $r < 0$. Clearly, the finiteness of such expressions as $\epsilon \to 0$ requires integrating into the whisker region, $r < 0$. (Similar cancellations were noted in [49]).

More strongly, we will show that many of the BTZ local boundary correlators are well-approximated by the analogous diagrams in (unquotiented) $\text{AdS}_{\text{Poincaré}}$ itself, where the interpretation in terms of scattering behind the (Rindler) horizon is unambiguous. This is the basis of our claim that we have found a class of correlators sensitive to scattering behind the BTZ horizon.

2.2.4 Space $\leftrightarrow$ Time inside the Horizon

Despite these good features, correlators in regions with timelike closed curves seem at odds with a physical interpretation and connection to the standard thermofield CFT dual. Relatedly, it is puzzling *why* we are lucky enough that the associated Witten diagrams should be insensitive to what is happening close to the singularity. We show that these correlators can be put into a more canonical form by performing a well-defined "space $\leftrightarrow$ time" transformation which takes local operators inside the horizon into non-local operators outside the horizon (and thereby make them accessible to external observers). This transformation is particularly plausible in the dual $1 + 1$ CFT where the causal (lightcone) structure is symmetric between space and time, and indeed we show that the transformation can be viewed as a kind of "improper" conformal transformation. It is this transformation that ultimately leads to the non-local operators arising from local ones, seen in (2.11). Such a symmetry seems much less manifest from the AdS perspective where there is no such isometry, but we prove that it indeed exists as an unexpected symmetry of boundary

19

correlators, by a careful Witten-diagrammatic analysis.

In more detail, the transformation is also accompanied by complex phases that are necessary for ensuring relativistic causality constraints in correlators, naively threatened because "spacelike ↔ timelike".) We thereby interpret our results as having found (i) non-local CFT operators that simply describe scattering inside the BTZ horizon (but outside the singularity), and (ii) an auxiliary but bizarre spacetime extension of the BTZ black hole, "whiskers", in which these non-local CFT operators are rendered as *local* operators, and in which some of their properties become more transparent. Whether or not one thereby considers the whiskers to be "physical" regions is left to the reader.

2.2.5   Comparing Whiskers and Euclidean space as auxiliary spacetimes

The notion of an auxiliary spacetime grafted onto the physical spacetime, where one uses path integrals and operators in the former to implant certain types of wavefunctionals in the latter, is already familiar when the auxiliary spacetime is Euclidean. For example, such constructions are used to create the Hartle-Hawking wavefunctional [34] or its perturbations in the physical spacetime, and can have a non-perturbative CFT dual [23]. Indeed, they too can be used to create quite general bulk states in the interior of BTZ, *in principle* including the kind of "out states" for scattering that we seek. However, the simple Euclidean constructions yield physical states at the point of time symmetry, $u + v = 0$ (or $\tau = 0$). We would need to evolve these states to late time and take superpositions in order to find "out states" that consist of several approximately free bulk particles. The problem then is that identifying such superpositions is equivalent to solving the scattering dynamics itself!

By contrast, the virtue of our Lorentzian auxiliary spacetime "whisker" is that it allows us to create simple out states with simply defined operators. In this way, we can pose explicit (non-local) CFT correlators which capture the fate of scattering inside the horizon. A well-programmed "CFT computer" would then output the answers to such questions without first requiring equally difficult computations as input.

2.2.6 Whisker correlators as generalizing "in-in" correlators

It is not simply fortuitous that Witten diagrams are insensitive to the singularity, even with some endpoints on the boundary of the whisker regions. Rather, we will show that the approach to the singularity in the bulk EFT is given by

$$\cdots U^\dagger e^{-\frac{\pi}{2}(H_\tau - P_\sigma)} U \cdots \,, \tag{2.15}$$

where U is a time evolution approaching the (future, say) singularity, and H_τ, P_σ are the isometry generators corresponding to τ and σ translations in Schwarzschild coordinates. (Of course, τ represents a spacelike direction near the singularity, and therefore H_τ is really a "momentum" here, despite the notation.) The $U^\dagger$ factor arises from the whisker region. The exponential weight is a non-trivial consequence of our "space $\leftrightarrow$ time" transformation, where the timelike circles become standard spacelike circles. One can think of the whisker-related factor, $\cdots U^\dagger e^{-\frac{\pi}{2}(H_\tau - P_\sigma)}$, as setting up a useful "out" state inside the horizon of the physical region.

If there are no sources (endpoints of correlators) in the vicinity of the singularity, the time evolution U commutes with the isometry generators, H_τ, P_σ and hence cancels against

$U^\dagger$. This cancellation, which also can be seen non-perturbatively in the CFT description, is the deep reason behind the insensitivity of boundary correlators to the details of UV physics. It matches the cancellations in Witten diagrams (before massaging by space $\leftrightarrow$ time) in the manner of (2.14). Such $U^\dagger U$ cancellation in the far future is reminiscent of what happens for correlators in the "in-in" formalism [50,51] (see [52] for a modern discussion and review). Indeed, we will show using the space $\leftrightarrow$ time transformation that local boundary correlators traversing the singularity are equivalent to a generalization of in-in correlators involving non-local operators, where all time evolution takes place after the past singularity and before the future singularity.

2.2.7 Studying the Singularity

Our ability to discover and check our proposal for describing scattering inside the BTZ horizon rests on the existence of the protected set of local boundary correlators, which we can prove in a simple way are insensitive to the singularity. However, the ultimate goal is not to merely describe scattering inside the horizon far from the singularity, since such scattering is approximately the same as scattering in a static spacetime. This regime is only useful to vet our proposal, precisely because we know the answers already, dominated by EFT. Rather the goal is to use our non-perturbative CFT proposal to describe scattering close to the singularity where cosmological blueshifts take us out of the EFT domain, and where even perturbative string theory may miss important features. This interesting kind of sensitivity to the singularity is not outright absent from the protected set of correlators, but it is suppressed by $\sim 1/\text{blueshift}$. However, one can study processes with kinematics chosen

such that they would not proceed but for such cosmological blueshifts (that is, they would not proceed for $r_S = \infty$), in which case the leading effects are sensitive to the singularity.

Furthermore, more general (gauge-fixed EFT) bulk correlators are order one sensitive to the singularity and UV physics, but not mathematically divergent. The same is also true for local boundary correlators in the more extended $\text{AdS}_{\text{global}}/\Gamma$ realization of BTZ, as we will discuss in [48].

2.2.8 Relation to the literature

Several earlier attacks have been made on more explicitly extending holography into the black hole interior, some specific to BTZ, while others apply also to higher-dimensional eternal black holes. The most direct approach has been to study the thermofield CFT formulation carefully, and to identify those subtle, non-local features that might encode key aspects of the black hole interior [53] [54] [23] [55] (see [56] for higher-dimensional discussion). Our work is certainly in the same spirit, but we claim our non-local CFT operators more sharply and more knowably probe the interior. Another general direction is to try and construct the CFT dual of interior field operators [57] [58] [59], in part by using the gravitational EFT equations of motion to evolve exterior field operators in "infaller" time into the interior. This is necessarily restricted to situations in which the bulk metric fluctuates modestly, whereas we propose a non-perturbative formulation. Yet another general approach is to try to enter the horizon by a variety of analytic continuations of external (Lorentzian or Euclidean) correlators [60] [49] [61] [62] [63]. Our work has this aspect to it, but it is governed and understood from a physical perspective in which analytic continuation merely

provides an efficient means of calculation, rather than a first principle. The symmetry-quotient structure of BTZ has led to attempts to construct a "symmetry-quotient" form of a dual CFT [25]. Another BTZ-specific approach is to take advantage of being able to follow the BTZ geometry beyond the "singularity", where further AdS-like boundary regions exist. One then tries to make sense of CFT on the various boundary regions and how they connect together [64] [60]. Our work furthers these directions, of making sense of the quotient structure from the CFT perspective, and using it to show how different boundary regions are entangled. A number of variants of BTZ have also been constructed and studied [65, 66].

2.2.9   Organization of chapter

We start from the symmetry quotient construction of BTZ from $\text{AdS}_{\text{Poincaré}}$, and try to make sense of the idea of a "quotient CFT" dual. In Section 2.3, we review the quotient construction of BTZ geometry from $\text{AdS}_{\text{Poincaré}}$ and how this extends the spacetime smoothly past the singularity, although gravitational EFT diagrams ending at the singularity do diverge. In Section 2.4, we identify the boundary regions of the BTZ spacetime, outside the horizon and inside the whiskers. We point out the central challenges for formulating a dual CFT on the boundary of BTZ, related to the presence of lightlike and timelike closed curves. In Section 2.5 we explore the BTZ singularity with the simplest examples, before beginning a more general attempt to formulate a CFT dual. The relevant BTZ correlators, with end points inside and outside the singularity and horizon, are obtained by the method of images applied to $\text{AdS}_{\text{Poincaré}}$. We illustrate how naive divergences encountered as interaction vertices approach the singularity in fact cancel to give mathematically well-defined correlators. In

Section 2.6, in order to massage the CFT on the BTZ boundary into a non-perturbatively well-defined form, we introduce the transformation switching time and space inside the horizon, arriving in (2.58) at our central result, a generalization of the thermofield CFT formulation allowing probes of physics inside the horizon. Eq. (2.58) is manifestly well-defined and manifestly respects the symmetry construction of BTZ. In Section 2.7, we recast (2.58) in canonical thermofield form, resulting in (2.64), with probes inside the horizon appearing as non-local probes of the thermofield-entangled CFTs. Many of our manipulations in sections 2.6 and 2.7 are formally based on the CFT path integral. But for concrete confirmation we must turn to the dual AdS diagrammatics.

In Section 2.8 we study the Rindler AdS/CFT correspondence ($r_S = \infty$) in detail, and prove the above results in this limit in bulk EFT, allowing us to probe inside the Rindler horizon by studying specific non-local correlators *outside* the horizon. We check that our proposal reproduces the AdS$_{\text{Poincaré}}$ correlators everywhere. In Section 2.9, we finally check that Eq. (2.58) does indeed act as the dual of BTZ by showing that it gives the associated local boundary correlators, including the whisker regions, and that these correlators are finite and dominated by EFT (despite traversing the singularity). This follows from the analogous Rindler proof in Section 2.8 by applying the method of images in EFT. We explain how these local boundary correlators are generally insensitive to the breakdown of EFT near the singularity, allowing us to use EFT to check our CFT proposal is sharply sensitive to scattering inside the horizon just as in the Rindler ($r_S = \infty$) limit. In Section 2.10, we demonstrate that bulk correlators are sensitive to the singularity and UV physics there, although still mathematically finite. We also show how to design special boundary correlators where the near-singularity UV physics dominates, so that our CFT proposal is needed to

describe them. In Section 2.11, we comment on our derivations and some aspects of the physical picture that emerges from our work, and outline future directions.

2.3 BTZ as Quotient of AdS$_{\text{Poincaré}}$

In higher-dimensional black holes, the Kruskal extension into the interior ends at a curvature singularity. In the BTZ case however, $uv = 1$ in (2.5) does not represent a true curvature singularity and the geometry can be smoothly extended beyond it. Such an extension is most simply given by a quotient of the Poincaré patch of AdS (AdS$_{\text{Poincaré}}$) [67] [38] [68],

$$ds^2 = \frac{dx^+ dx^- - dz^2}{z^2} \qquad (z > 0), \tag{2.16}$$

where $x^\pm \equiv t \pm x$ and we identify points related by the discrete rescaling

$$(x^\pm, z) \equiv (e^{rs} x^\pm, e^{rs} z). \tag{2.17}$$

As straightforwardly checked, the Poincaré coordinates are related to the Kruskal coordinates by

$$x^+ = \frac{2e^\sigma v}{1 - uv} \qquad x^- = \frac{2e^\sigma u}{1 - uv} \qquad z = \frac{1 + uv}{1 - uv} e^\sigma, \tag{2.18}$$

and to the Schwarzschild coordinates by

$$x^{\pm} = \begin{cases} \pm\sqrt{1 - \frac{1}{r^2}}\, e^{\pm\sigma^{\pm}}, & \text{if } r > 1; \\[2ex] \sqrt{\frac{1}{r^2} - 1}\, e^{\pm\sigma^{\pm}}, & \text{if } r < 1 \end{cases} \qquad z = \frac{e^{\sigma}}{r} \tag{2.19}$$

$$\sigma^{\pm} \equiv \tau \pm \sigma.$$

The horizon, singularity and asymptotic AdS boundaries now reside at:

$$\begin{aligned} \text{boundary:} \quad & z = 0 \\[1ex] \text{horizon:} \quad & x^{\pm} = 0 \\[1ex] \text{singularity:} \quad & z^2 - x^+ x^- = 0. \end{aligned} \tag{2.20}$$

The true nature of the apparent black hole singularity becomes clearer. While the BTZ black hole spacetime has locally AdS geometry and finite curvature everywhere, the singularity surface consists of closed lightlike curves, given by $x = t\cos\gamma$, $z = t\sin\gamma$, parametrized by γ. The region inside this surface consists of closed timelike curves, which we will call the "whisker" region similarly to [41].

The presence of such curves does not in itself constitute a geometric singularity[2], but it does pose a conceptual challenge for physical interpretation, and on general grounds implies the breakdown of quantum (effective) field theory in the vicinity of the closed lightlike curves [44]. See [45] for a concise review, and [42] [43] for computations of stress-tensor divergences at the BTZ singularity. Similar features have also been studied in string theory

---

[2]In the BTZ realization as a quotient of AdS$_{\text{global}}$ the singularity also includes a breakdown of the spacetime manifold (Hausdorff) structure itself. But the points at which this further complication takes place are pushed off to infinity in our Poincaré patch realization of BTZ. This breakdown is relevant to some of the studies in the literature but not to the correlators discussed in this chapter. We will more thoroughly clarify this point in [48].

(as reviewed in [46].) We illustrate the basic problem by looking at an EFT amplitude for a scalar field in the BTZ background. Following [49] we focus on the scalar propagator from a point on an AdS boundary, $x^{\pm}$, external to the black hole to a point inside the horizon and near the "singularity", $(y_{\pm}, z)$. Because BTZ is a quotient of AdS$_{\text{Poincaré}}$, we can easily work out this propagator by the method of images applied to the boundary-bulk propagator of AdS$_{\text{Poincaré}}$ [37] [49]:

$$K_{\text{BTZ}}(x^{\pm}, y^{\pm}, z) = \sum_{n \in \mathbb{Z}} \frac{(e^{nr_S} z)^{\Delta}}{[e^{2nr_S} z^2 - (x^+ - e^{nr_S} y^+)(x^- - e^{nr_S} y^-)]^{\Delta}} \qquad (2.21)$$

where $m^2 = \Delta(\Delta - 2)$ and we have summed over images of the bulk point. Generically, the image sum clearly converges, the summand behaving asymptotically as $\sim e^{-|n|r_S \Delta}$. The exception is the singular surface $z^2 - y^+ y^- = 0$, where the summand becomes n-independent for large n, and the series diverges. (We omit a discussion of the $i\epsilon$ prescription in the propagator as it does not avoid the divergence as $\epsilon \to 0$, although it will play an important role later in the chapter.) This feature is general for correlators with some points ending on the surface $z^2 - y^+ y^- = 0$, the perturbative incarnation of divergent backreactions that justifies this surface being called the "singularity". A subtler question is whether one can propagate or scatter *through* the singularity within gravitational EFT. If so, one can just avoid probes (correlator endpoints) very near the singularity and trust EFT calculations elsewhere. This question is particularly relevant for correlators ending on the full BTZ boundary (including inside the whiskers) since these would define local operator correlators of a possible CFT dual to BTZ. Before tackling this question, we first study the BTZ boundary itself.

2.4 The Extended BTZ Boundary and Challenges for the CFT Dual

Since BTZ is at least locally AdS-like, it seems very natural to guess that BTZ quantum gravity has a holographic dual given by a $1+1$ dimensional CFT "living" on the BTZ boundary. Within the Kruskal extension, this boundary, $uv = -1$, consists of the two disjoint solutions with $u > 0$, $v < 0$ or $u < 0$, $v > 0$, corresponding to the two asymptotically $\text{AdS}_{\text{global}}$ regions outside the horizon, as in higher-dimensional AdS black holes. This is then consistent with the now-standard thermofield picture of two CFTs living on two copies of the boundary of $\text{AdS}_{\text{global}}$, namely two separate CFTs each living on a spatial circle $\times$ infinite time, but in an entangled state. However, this Kruskal boundary corresponds in our $\text{AdS}_{\text{Poincaré}}$ coordinates to $z = 0$, $x^+ x^- < 0$, whereas in the $\text{AdS}_{\text{Poincaré}}$ realization the boundary is straightforwardly all of $z = 0$. The regions $z = 0$, $x^+ x^- > 0$ are missed in the Kruskal extension because they lie inside the singularity, while the Kruskal extension stops there. The question then arises whether these inside-singularity boundary regions play an important role in the CFT dual of BTZ (the view taken in [64] [60]), even for "projecting" the part of BTZ outside the singularity but inside the horizon. We will show that there are in fact two equivalent formulations of the CFT dual of BTZ, one in which the entire boundary region is needed for the CFT, and a second one in terms of two entangled CFTs on just the disjoint boundary regions outside the horizon.

2.4.1 BTZ Boundary as Disconnected Cylinders

We begin by identifying the full boundary region of BTZ, ∂BTZ, within the $\text{AdS}_{\text{Poincaré}}$ realization, regardless of where this takes us with respect to the singularity. Even the simple

identification of ∂BTZ as $z = 0$ is subtle because of the quotienting. Naively this would yield $1 + 1$ Minkowski spacetime with the identification $x^\pm \equiv e^{rs} x^\pm$. Such an identification does not make straightforward sense because rescaling is *not* an isometry of Minkowski space. The subtlety is that the boundary geometry is only determined from the bulk geometry up to a Weyl transformation [6], which conformally invariant dynamics cannot distinguish. Therefore more precisely,

$$ds^2_{\partial\text{BTZ}} = f(x^\pm)dx^+dx^-, \tag{2.22}$$

where f is a Weyl transform of $1 + 1$ Minkowski spacetime, with the identifications $x^\pm \equiv e^{rs} x^\pm$ and hence f-periodicity $f(x^\pm) = e^{2rs} f(e^{rs} x^\pm)$.

Two choices of f will prove insightful. The first is

$$f = \frac{1}{|x^+ x^-|}. \tag{2.23}$$

It is useful to break up the $1 + 1$ Minkowski plane into the four regions,

$$
\begin{aligned}
\text{Right } (R) &\quad x^+ > 0, x^- < 0 \\
\text{Future } (F) &\quad x^\pm > 0 \\
\text{Left } (L) &\quad x^+ < 0, x^- > 0 \\
\text{Past } (P) &\quad x^\pm < 0.
\end{aligned}
\tag{2.24}
$$

We will refer to R, L as Rindler wedges and F, P as Milne wedges. We can adapt

30

Rindler-like coordinates for each wedge,

$$x^{\pm} = \begin{cases} \pm e^{\pm \sigma^{\pm}}, & x \in R \\[2mm] e^{\pm \sigma^{\pm}}, & x \in F \\[2mm] \mp e^{\pm \sigma^{\pm}}, & x \in L \\[2mm] -e^{\pm \sigma^{\pm}}, & x \in P, \end{cases} \qquad \sigma^{\pm} \equiv \tau \pm \sigma \qquad (2.25)$$

so that the quotienting and Weyl transformation take the simple forms

$$\sigma \equiv \sigma + 2\pi r_S$$
$$f = e^{-2\sigma}. \qquad (2.26)$$

We can simply restrict σ to the fundamental region $-\pi r_S \leq \sigma \leq \pi r_S$. We see that ∂BTZ is then given by *four* disjoint spacetime cylinders,

$$ds^2_{\partial \text{BTZ}} = \begin{cases} +d\sigma^+ d\sigma^-, & R, L \quad \text{spacelike circle} \times \text{infinite time} \\[2mm] -d\sigma^+ d\sigma^-, & F, P \quad \text{infinite space} \times \text{timelike circle!} \end{cases} \qquad (2.27)$$

The cylinders in the Rindler wedges are just the boundaries of the $\text{AdS}_{\text{global}}$ asymptotics outside the horizon described above. But the cylinders in the Milne wedges are the boundary region inside the singularity.[3] The Weyl transform maps the cylinders to the four shaded regions of $1 + 1$ Minkowski spacetime in Fig. 2.4a. In this way we can think of the shaded region as a fundamental region for the quotienting procedure on the CFT-side.

---

[3]These four disjoint boundary components are the $\text{AdS}_{\text{Poincaré}}$ subset of the larger set of boundary components arising in the further extension of BTZ as a quotient of $\text{AdS}_{\text{global}}$.

(a) The fundamental region in σ mapped to the Minkowski plane by the Weyl transformation (2.23)

(b) The fundamental region in α mapped to the Minkowski plane by the Weyl transformation (2.28)
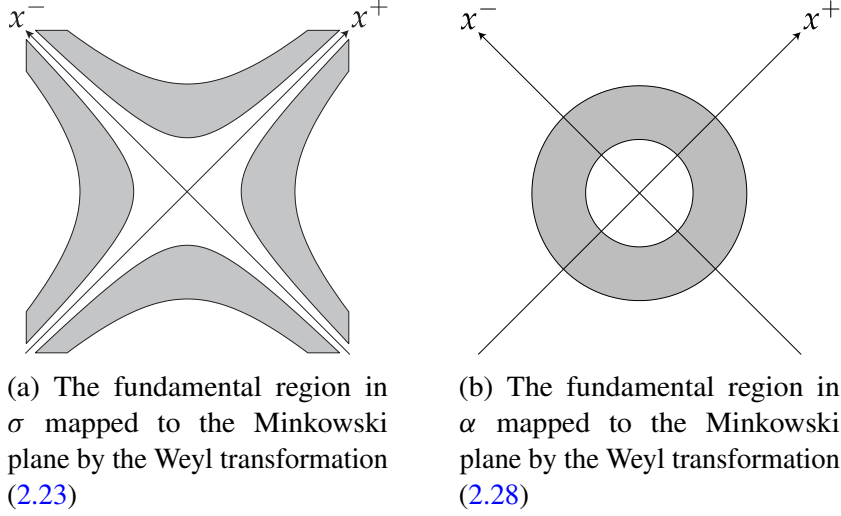
Figure 2.4: Two different choices of fundamental region for the BTZ boundary

We see that the four cylinders present two challenges for hosting a dual CFT. The first is that they remain disjoint and therefore we need some sort of generalization of the thermofield entanglement of two CFTs with which to connect them. For related early work in this direction, see [60]. The second issue is that the Milne wedge cylinders have circular time.

2.4.2   Connected View of ∂BTZ

To guess how to move forward we use a different choice of Weyl transformation, which gives us a different view of ∂BTZ (the CFT being insensitive to such choices),

$$f = \frac{1}{(x^+)^2 + (x^-)^2}.$$

(2.28)

32
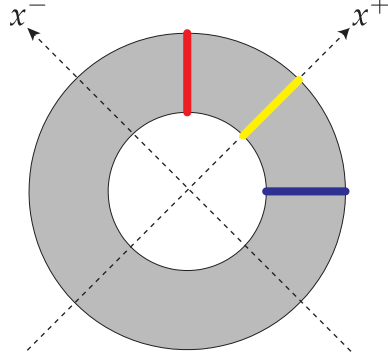
Figure 2.5: The Lorentzian torus contains closed timelike (red), lightlike (yellow), and spacelike (blue) curves. The inner and outer edges of the annulus are identified after Weyl transformation (2.28) to make the Lorentzian torus of (2.30).

Using "polar" coordinates on the Minkowski plane,

$$t = e^\alpha \sin\theta \qquad\qquad x = e^\alpha \cos\theta, \qquad\qquad (2.29)$$

with the usual identification $\theta \equiv \theta + 2\pi$ and the BTZ quotient identification $\alpha \equiv \alpha + 2\pi r_S$, we find (Fig. 2.4b):

$$ds^2_{\partial\text{BTZ}} = \cos 2\theta(d\theta^2 - d\alpha^2) + 2\sin 2\theta \, d\theta d\alpha \qquad\qquad (2.30)$$

$$= \text{Lorentzian Torus!}$$

This geometry [69] is smooth and *connected*, but still contains alarming features (Fig. 2.5). There are still timelike circles in the Milne wedges $\frac{\pi}{4} < \theta < \frac{3\pi}{4}, \frac{-\pi}{4} > \theta > \frac{-3\pi}{4}$, oriented in the α-direction. (There are still only spacelike closed curves in the Rindler wedges.) The "joints", $\theta = \frac{-3\pi}{4}, \frac{-\pi}{4}, \frac{\pi}{4}, \frac{3\pi}{4}$, while smoothly connecting the geometries of the different wedges, are themselves light-like circles in α. So it does not appear that a CFT on this boundary region will allows us to evade the difficult problem of doing field theory

at lightlike circles presented by the BTZ singularity [44] [45]. (For discussion of a very similar $1 + 1$ context see [70]).) If we try to excise these lightlike circles we are left with the disjointedness of the boundary and the CFT living on it.

Before making any interpretation, we will first try to simply define local operator correlators of the CFT on the full ∂BTZ, using the method of images applied to AdS$_{\text{Poincaré}}$ boundary correlators. However, we must check that these are even mathematically well-defined in the face of the BTZ singularity. Therefore we first study simple examples and then general features of how the singularity enters into correlators. We then show that boundary correlators on all of ∂BTZ are mathematically well-defined, although the singularity does represent a breakdown of gravitational EFT.

2.5 Boundary Correlators and the Singularity

In this section we study the simplest examples which illustrate the implications of the singularity for defining correlators within gravitational EFT, and for identifying them with equivalent CFT correlators. For this purpose we will not need to study these BTZ correlators in a UV-complete framework such as string theory, although we assume such a framework exists. We will compute these BTZ correlators using the method of images. It is convenient to define

$$\lambda \equiv e^{rs}, \tag{2.31}$$

so that the quotient identification (2.17) can be written

$$(x^\pm, z) \equiv (\lambda x^\pm, \lambda z).$$

(2.32)

2.5.1 Approaching Singularity from Outside

We start by noting the full $i\epsilon$ structure of the bulk-boundary propagator of AdS$_{\text{Poincaré}}$, which is important for what follows here:

$$K_{\text{AdS}} = \left[\frac{z}{z^2 - (x^+ - y^+)(x^- - y^-) + i\epsilon(x^0 - y^0)^2} \right]^\Delta.$$

(2.33)

This structure for Lorentzian K is most easily derived from the well-known Euclidean K [6] by analytic continuation in time. The boundary point, $x^\pm, z' = 0$ can be in any of the boundary regions, L, R, F, P. The analogous BTZ propagator is given by summing over images of the bulk point, $e^{nrs} y^\pm, e^{nrs} z$, as in (2.21). It is important that the $i\epsilon$ is also thereby imaged. To study the near singularity region it is useful to follow [49] and switch to AdS Schwarzschild coordinates, where the bulk point is at σ, τ, r, and the boundary point is given by $\sigma', \tau', r' = \infty$. We can zoom in on the region where the bulk point approaches the singularity, $r \to 0$, and the image sum divergence for positive large n dominates:

$$\begin{aligned}
K_{\text{BTZ}} \underset{r \to 0,}{\sim} &\sum_{n > 0 \text{ large}} \left(\frac{1}{e^{\sigma'^+} e^{-\tau} - e^{-\sigma'^-} e^\tau + e^\sigma r \lambda^n + i\epsilon \lambda^n} \right)^\Delta \\
\sim &\left(\frac{1}{e^{\sigma'^+} e^{-\tau} - e^{-\sigma'^-} e^\tau} \right)^\Delta \ln \left(e^\sigma r + i\epsilon \right).
\end{aligned}$$

(2.34)

The approximation in the first line is to drop terms even more subdominant for large $n > 0$. In the second line we noted that the λ^n-dependent terms are subdominant for small r for the first $\sim \ln(\lambda/(e^\sigma r))$ terms in $n > 0$, with the sum rapidly converging for larger n. Therefore, the sum is given by the n-independent constant multiplied by $\sim \ln(e^\sigma r)$, for small r. Crucially, the $i\epsilon$ appears inside the logarithm by the first line's analyticity in $e^\sigma r + i\epsilon$.

2.5.2 Flawed attempt to Scatter through Singularity

Let us now explore the possibility that a dual CFT resides on ∂BTZ, as identified in the previous section, by trying to construct the leading in $1/N_{\text{CFT}}$ planar contribution to a 3-point local operator correlator in terms of a tree level BTZ diagram:

$$\langle \tilde{\mathcal{O}}(x_F)\mathcal{O}(x_{R_1})\mathcal{O}(x_{R_2})\rangle_{\text{CFT } \partial\text{BTZ}} \equiv \langle \tilde{\mathcal{O}}(x_F)\mathcal{O}(x_{R_1})\mathcal{O}(x_{R_2})\rangle_{\text{tree BTZ EFT}}, \tag{2.35}$$

where as usual, on the left-hand side the operators are defined operationally as limits of bulk fields,

$$\mathcal{O} = \lim_{z\to 0} \frac{\phi(x^\pm, z)}{z^\Delta}. \tag{2.36}$$

We choose two scalar primary operators to be on the R Rindler wedge, and the remaining operator to be in the F Milne wedge, so that the diagram is forced to pass through the singularity and we can test what difficulties it poses. In this section, we will seek to understand if such a correlator is even mathematically well-defined, not yet addressing its physical interpretation, given that one operator lies inside the singularity where there are

time-like closed curves. In subsection 2.7.2 we will give a physical interpretation of the *F* endpoint as associated to a conceptually straightforward but *non-local* operator in a hot (thermofield) CFT. For convenience, we have chosen the *F* scalar primary to be different from the *R* operators with different scale dimension, $\tilde{\Delta} \neq \Delta$, so that there are two dual scalar fields in BTZ. We consider a typical non-renormalizable interaction term in BTZ EFT,

$$\mathcal{L}_{\text{int}} = \sqrt{g}\,\tilde{\phi}\,g_{\text{BTZ}}^{MN}\,\partial_M\phi\partial_N\phi. \tag{2.37}$$

It is straightforward to then write the resulting 3-point correlator in terms of K_{BTZ} and an integral over a fundamental region of our quotient for the above bulk interaction vertex, and see that it receives divergent contributions as the interaction vertex approaches the singularity (Fig. 2.6),

$$\langle \tilde{\mathcal{O}}_F \mathcal{O}_{R_1} \mathcal{O}_{R_2} \rangle = \int_{\text{fund.}} d^2y\,dz\,\sqrt{g}\,K_{\text{BTZ}}(x_F, y, z)g^{MN}\partial_M K_{\text{BTZ}}(x_1, y, z)\partial_N K_{\text{BTZ}}(x_2, y, z)$$

$$\underset{r \to 0}{\sim} \int_0^\infty dr \int_{-r_S/2}^{r_S/2} d\sigma \int d\tau\,(\text{function of } \sigma, \tau) \times r\,\frac{\ln(r + i\epsilon)}{(r + i\epsilon)^2} \xrightarrow[\epsilon \to 0]{} \infty. \tag{2.38}$$

Ref. [49] earlier worked through a very similar calculation. Naively, this blocks us from defining such correlators. However, this calculation is in error.

2.5.3 Approaching Singularity from Inside

Schwarzschild coordinates are useful for cleanly separating out the direction of approach to the singularity from the direction which is being imaged, but they are restricted to only the outside of the singularity, $z^2 - y^2 > 0$. We should also include the asymptotic contributions

37
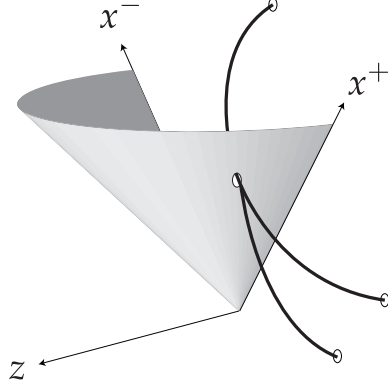
Figure 2.6: Interaction vertex approaching the singularity as seen in the $\text{AdS}_{\text{Poincaré}}$ covering space. The singularity is the half-cone $x^2 + z^2 = t^2$ with $z > 0$. All lines end on the boundary $z = 0$.

as the interaction vertex approaches the singularity from inside it, $z^2 - y^2 < 0$. This requires new Schwarzschild-like coordinates for $z^2 - y^2 < 0$:

$$
\begin{aligned}
y^\pm &= \sqrt{\tfrac{1}{\tilde{r}^2} + 1}\, e^{\pm\sigma^\pm} && (\tilde{r} > 0) \\
z &= \frac{e^\sigma}{\tilde{r}} && (\sigma^\pm \text{ real}) \\
ds^2 &= -(\tilde{r}^2 + 1)d\tau^2 - \frac{d\tilde{r}^2}{\tilde{r}^2 + 1} + \tilde{r}^2 d\sigma^2.
\end{aligned}
\tag{2.39}
$$

Both sets of Schwarzschild coordinates together cover half of $\text{AdS}_{\text{Poincaré}}$, $x^+ > 0$. (We can obviously cover $x^+ < 0$ analogously, but will not need to.)

We can now repeat the analysis of near-singularity asymptotics for K_{BTZ} but approaching from inside. For example, considering the boundary point in K_{BTZ} to be in the R wedge for concreteness (since the asymptotics will not distinguish other choices), we have

$$
\begin{aligned}
K_{\text{BTZ}} &\underset{r\to 0}{\sim} \sum_{n > 0 \text{ large}} \left(\frac{1}{e^{\sigma'^+} e^{-\tau} - e^{-\sigma'^-} e^\tau - e^\sigma \tilde{r}\lambda^n + i\epsilon\lambda^n} \right)^\Delta \\
&\sim \left(\frac{1}{e^{\sigma'^+} e^{-\tau} - e^{-\sigma'^-} e^\tau} \right)^\Delta \ln\left(-e^\sigma \tilde{r} + i\epsilon \right).
\end{aligned}
\tag{2.40}
$$

38

2.5.4 Proper account of Scattering through Singularity

Putting this together with the near-singularity asymptotics from the outside, we obtain the correct behavior,

$$
\begin{aligned}
\langle \tilde{\mathcal{O}}_F \mathcal{O}_{R_1} \mathcal{O}_{R_2} \rangle &= \int_{\text{fund.}} d^2 y \, dz \, \sqrt{g} \, K_{\text{BTZ}}(x_F, y, z) g^{MN} \partial_M K_{\text{BTZ}}(x_1, y, z) \partial_N K_{\text{BTZ}}(x_2, y, z) \\
&\underset{r \to 0}{\sim} \int_0^\infty dr \int d\sigma d\tau \, r \, \frac{\ln(r + i\epsilon)}{(r + i\epsilon)^2} - \int_0^\infty d\tilde{r} \int d\sigma d\tau \, \tilde{r} \, \frac{\ln(-\tilde{r} + i\epsilon)}{(-\tilde{r} + i\epsilon)^2} \\
&\underset{r \equiv -\tilde{r}}{=} \int_{-r_0}^{r_0} dr \int d\sigma d\tau \, r \, \frac{\ln(r + i\epsilon)}{(r + i\epsilon)^2},
\end{aligned}
\tag{2.41}
$$

where we have defined $r \equiv -\tilde{r}$ for $r < 0$, and r_0 is small enough that we trust our asymptotics. It is straightforward to see that the r integral converges near the singularity, $r \sim 0$. For example, the integral can clearly be deformed into the upper half complex r-plane, completely avoiding $r = 0$. In this way, our 3-point correlator is mathematically well-defined despite having to traverse the singularity. (As mentioned earlier, we will give a physical interpretation in subsection 2.7.2.) For a similar BTZ correlator, [49] found a similar cancellation of divergence from positive and negative r, although the $r < 0$ region in this case arose from the past singularity, so that the cancellation was non-local in spacetime. For us however, the cancellation is local, just from the two sides very close to the future singularity surface.

In fact, there is a technically simpler way, directly in Poincaré coordinates, to see the above finiteness. It is not quite as physically transparent as the local and Lorentzian account above, but it will generalize to other correlators, and it will arise very naturally in our final dual CFT construction. The trick is to note that one can rotate the interaction z coordinate

in the complex plane whenever $y^\pm$ is in the F, P wedges, *before* doing the image sums. In

our example,

$$
\langle \tilde{\mathcal{O}}(x_F) \mathcal{O}(x_{R_1}) \mathcal{O}(x_{R_2}) \rangle = \sum_{k,m,n} \int_{F \text{ fund.}} d^2 y \, dz \, \frac{1}{z} \left[\frac{z \lambda^k}{z^2 \lambda^{2k} - (x_F - \lambda^k y)^2 + i\epsilon} \right]^{\tilde{\Delta}}
$$

$$
\times \eta^{MN} \partial_M \left[\frac{z \lambda^m}{z^2 \lambda^{2m} - (x_{R_1} - \lambda^m y)^2 + i\epsilon} \right]^{\Delta} \partial_N \left[\frac{z \lambda^n}{z^2 \lambda^{2n} - (x_{R_2} - \lambda^n y)^2 + i\epsilon} \right]^{\Delta}
$$

$$
+ \text{ other wedges}, \quad (2.42)
$$

where we integrate over a fundamental region in (y, z) for each wedge, and η_{MN} is the $2+1$

Minkowski metric. We can combine one sum, say $\sum_k$, and $\int_{\text{fund.}}$ into $\int$ over all AdS$_{\text{Poincaré}}$,

so that after re-naming the other image indices, $m \to m + k, n \to n + k$,

$$
\langle \tilde{\mathcal{O}}_F \mathcal{O}_1 \mathcal{O}_2 \rangle_{\text{BTZ}} = \sum_{m,n} \int_{\text{AdS}_{\text{Poincaré}} \, F\text{-wedge}} d^2 y \, dz \, \frac{1}{z} \left[\frac{z}{z^2 - (x_F - y)^2 + i\epsilon} \right]^{\tilde{\Delta}}
$$

$$
\times \eta^{MN} \partial_M \left[\frac{z \lambda^m}{z^2 \lambda^{2m} - (x_{R_1} - \lambda^m y)^2 + i\epsilon} \right]^{\Delta} \partial_N \left[\frac{z \lambda^n}{z^2 \lambda^{2n} - (x_{R_2} - \lambda^n y)^2 + i\epsilon} \right]^{\Delta}
$$

$$
+ \text{ other wedges}. \quad (2.43)
$$

Note the m, n summand is analytic in z for $\text{Re}\, z, \text{Im}\, z > 0$ so that we can rotate the z

contour to the imaginary axis. In general we do this only in the F, P wedges, *but not* in

the L, R wedges. Here, we just track the F wedge integration region explicitly for the

interaction vertex:

$$\langle \tilde{\mathcal{O}}_F \mathcal{O}_1 \mathcal{O}_2 \rangle_{\text{BTZ}} = \sum_{m,n} \int_F d^2 y \int_0^\infty dz \frac{1}{z} \left[\frac{iz}{-z^2 - (x_F - y)^2 + i\epsilon} \right]^{\tilde{\Delta}}$$

$$\times \eta^{MN} \partial_M \left[\frac{iz\lambda^m}{-z^2\lambda^{2m} - (x_{R_1} - \lambda^m y)^2 + i\epsilon} \right]^{\Delta} \partial_N \left[\frac{iz\lambda^n}{-z^2\lambda^{2n} - (x_{R_2} - \lambda^n y)^2 + i\epsilon} \right]^{\Delta}$$

$$+ \text{ other wedges.} \quad (2.44)$$

With this rotated z, it is straightforward to see that $y^2 + z^2 \neq 0$ since $y^2 > 0$ in F, so the image sums can now be safely performed and will converge.

The finiteness of correlators with endpoints at the BTZ boundary generalizes to finiteness of *bulk* correlators with endpoints away from the singular surface. The deeper reason for such finiteness will emerge in Section 2.9. This does not mean the singularity has disappeared. As we saw straightforwardly in the discussion of (2.21), there are divergences when correlators end *on* the singularity. Furthermore, we will demonstrate in Section 2.10 one can isolate UV-sensitive effects even at significant distances/times away from the singular surface (but $< R_{\text{AdS}} \equiv 1$).

In [48], we will give a more detailed account of $2 \rightarrow 2$ "scattering" through the singularity into the whisker region, in a manner that allows more direct comparison with related studies in the literature, in string theory and EFT (reviewed in [46]). We will reproduce the pathologies in the literature related to the singularity, but also point out how the whisker regions play an important role in resolving them.

2.5.5 Matching to CFT on ∂BTZ

In the above sequence of operations, rotating the z contours before doing the sum over two of the images, the method of images applied to AdS$_{\text{Poincaré}}$ correlators does seem to provide us with well-defined boundary correlators in BTZ, which in turn can be interpreted as defining local primary correlators for a dual CFT "living" on the Lorentzian torus ∂BTZ. Indeed if one were to directly define a CFT 3-point correlator on the Lorentzian torus by viewing it as a quotient of $1+1$ Minkowski spacetime, it would be given in planar approximation by the analogous correlator in Minkowski space, but with image sums over two of the positions of the three local operators, with one position kept fixed. One can then use AdS$_{\text{Poincaré}}$ tree diagrams to compute these Minkowski correlators. Eqs. (2.43) and (2.44) can be put in precisely this form by dividing imaged numerators and denominators by λ^{2m} or λ^{2n}. This gives

$$
\langle \tilde{\mathcal{O}}_F \mathcal{O}_1 \mathcal{O}_2 \rangle_{\text{BTZ}} = \sum_{m,n} \int_{\text{AdS}_{\text{Poincaré}} \; F\text{-wedge}} d^2 y \, dz \, \frac{1}{z} \lambda^{m\Delta} \lambda^{n\Delta} \left[\frac{z}{z^2 - (x_F - y)^2 + i\epsilon} \right]^{\tilde{\Delta}}
$$

$$
\times \eta^{MN} \partial_M \left[\frac{z}{z^2 - (\lambda^m x_{R_1} - y)^2 + i\epsilon} \right]^{\Delta} \partial_N \left[\frac{z}{z^2 - (\lambda^n x_{R_2} - y)^2 + i\epsilon} \right]^{\Delta}
$$

$$
+ \text{ other wedges,} \quad (2.45)
$$

before rotating z, and

$$\langle \tilde{\mathcal{O}}_F \mathcal{O}_1 \mathcal{O}_2 \rangle_{\text{BTZ}} = \sum_{m,n} \int_F d^2 y \int_0^\infty dz \, \frac{1}{z} \lambda^{m\Delta} \lambda^{n\Delta} \left[\frac{iz}{-z^2 - (x_F - y)^2 + i\epsilon} \right]^{\tilde{\Delta}}$$

$$\times \eta^{MN} \partial_M \left[\frac{iz}{-z^2 - (\lambda^m x_{R_1} - y)^2 + i\epsilon} \right]^\Delta \partial_N \left[\frac{iz}{-z^2 - (\lambda^n x_{R_2} - y)^2 + i\epsilon} \right]^\Delta$$

$$+ \text{ other wedges}, \quad (2.46)$$

after rotating z into the manifestly summable form. We have also re-defined $m, n \to -m, -n$

above.

The summands now have the forms of $1 + 1$ Minkowski CFT correlators computed

by AdS/CFT, at images of the operator positions, x. The x themselves are chosen from a

fundamental region. Given the universal form of these 3-point CFT correlators, we have

$$\langle \tilde{\mathcal{O}}_F \mathcal{O}_1 \mathcal{O}_2 \rangle_{\text{BTZ}} = \sum_{m,n} \frac{\lambda^{m\Delta} \lambda^{n\Delta}}{(\lambda^m x_{R_1} - \lambda^n x_{R_2})^{2\Delta - \tilde{\Delta}} (\lambda^m x_{R_1} - x_F)^{\tilde{\Delta}} (\lambda^n x_{R_2} - x_F)^{\tilde{\Delta}}}. \quad (2.47)$$

This has precisely the form of a correlator for a CFT "living" on the boundary of BTZ,

computed in the planar limit of a $1/N_{\text{CFT}}$ expansion using the method of images, where

Minkowski spacetime is interpreted as the covering space of the BTZ boundary modulo

a Weyl transformation as discussed in subsection 2.4.1. The powers of $\lambda^{m\Delta}, \lambda^{n\Delta}$ in the

numerator are accounted for now as the local primary operator responses to this Weyl-

rescaling. In this form, it is straightforward to check that the sums over images converge as

long as the CFT local operators do not lie exactly on the lightlike circles of ∂BTZ.

We could proceed to generalize in this direction but instead prefer to first reformulate

our whole problem in a way that makes the non-perturbative (in $1/N_{CFT}$) structure clear.

2.6 Space $\leftrightarrow$ Time Inside the Horizon

We now describe a strategy for making sense of the boundary regions and their inter-connections, and thereby framing the CFT dual non-perturbatively. The central observation is that in $1 + 1$ dimensions, and in particular in conformal field theory, there is very little to distinguish "time" from "space". Indeed we can view the switch $x \leftrightarrow t$, or equivalently $x^{\pm} \rightarrow \pm x^{\pm}$, as an "improper" conformal transformation, in that it changes the metric only by an overall factor (the defining feature of conformal transformations), but that factor is -1:

$$ds^2 = dt^2 - dx^2 \rightarrow dx^2 - dt^2 = -(dt^2 - dx^2). \tag{2.48}$$

This makes it a plausible symmetry of CFT. If we can make the switch $x \leftrightarrow t$ in just the Milne wedges, then the timelike circles would be turned into ordinary spacelike circles, as already the case in the Rindler wedges.

2.6.1 $x \leftrightarrow t$ in Free CFT

Eventually, we will have to check this proposition for CFTs with good AdS duals, but let us first gain intuition by studying *free* scalar CFT and seeing in what concrete sense $x \leftrightarrow t$ is a symmetry of the theory. Let us focus on the path integral for correlators in $1 + 1$ Minkowski spacetime for the primary operators of the form $e^{iq\chi(x^{\pm})}$, with scaling dimension $\Delta = q^2/2$, and scalar field χ. If these operators transform as "primaries" with

respect to the improper conformal transformation, $x^\pm \to \pm x^\pm$, then we expect that

$$\int \mathcal{D}\chi e^{i \int dt dx \, (\partial_t \chi)^2 - (\partial_x \chi)^2} e^{i q_1 \chi(x_1^\pm)} \cdots e^{i q_n \chi(x_n^\pm)}$$

$$= \int \mathcal{D}\hat{\chi} e^{i \int dt dx \, (\partial_x \hat{\chi})^2 - (\partial_t \hat{\chi})^2} (-1)^{\frac{\Delta_1}{2}} e^{i q_1 \hat{\chi}(\pm x_1^\pm)} \cdots (-1)^{\frac{\Delta_n}{2}} e^{i q_n \hat{\chi}(\pm x_n^\pm)} \qquad (2.49)$$

$$= \int \mathcal{D}\hat{\chi} e^{-i \int dt dx \, (\partial_t \hat{\chi})^2 - (\partial_x \hat{\chi})^2} e^{i q_1 \hat{\chi}(\pm x_1^\pm)} \cdots e^{i q_n \hat{\chi}(\pm x_n^\pm)} (-1)^{\frac{\Delta_n + \cdots + \Delta_n}{2}},$$

where $\chi(x^\pm) \equiv \hat{\chi}(\pm x^\pm)$ and the q_j satisfy charge conservation, $\sum_j q_j = 0$. Formally, the

powers of -1 are the standard powers of $\partial \hat{x}_-/\partial x^-$ for scalar primaries, although here there

is clearly an ambiguity in how to take fractional powers. Comparing the first and last lines

we arrive at the equivalent statement for the n-point Greens function,

$$G_{q_1, \cdots, q_n}(x_1^\pm, \cdots, x_n^\pm) = (-1)^{\frac{\Delta_n + \cdots + \Delta_n}{2}} G^*_{-q_1, \cdots, -q_n}(\pm x_1^\pm, \cdots, \pm x_n^\pm). \qquad (2.50)$$

It is straightforward to check this guess, since G is known explicitly (reviewed in [71]):

$$G = \prod_{i>j} \left[\frac{1}{(x_i^+ - x_j^+)(x_i^- - x_j^-) + i\epsilon(t_i - t_j)^2} \right]^{\frac{q_i q_j}{2}}$$

$$= \prod_{i>j} e^{\frac{-i\pi q_i q_j}{2}} \left[\frac{1}{(x_i^+ - x_j^+)(-x_i^- - (-x_j^-)) - i\epsilon(x_i - x_j)^2} \right]^{\frac{(-q_i)(-q_j)}{2}} \qquad (2.51)$$

$$= \prod_k e^{\frac{i\pi \Delta_k}{2}} G^*_{-q_1, \cdots, -q_n}(\pm x_1^\pm, \cdots, \pm x_n^\pm).$$

The trade of $(x_i - x_j)^2$ for $(t_i - t_j)^2$ in the second line follows because the $i\epsilon$ only matters

when the rest of the denominator vanishes, which is where these two expressions coincide.

The product of phase factors in the second and third lines coincide by charge conservation,

$$0 = \left(\sum_i q_i \right)^2 = \sum_{ij} q_i q_j = 2 \sum_{i>j} q_i q_j + \sum_k q_k^2$$

$$\implies \sum_k q_k^2 = \sum_k 2\Delta_k = -2 \sum_{i>j} q_i q_j .$$

(2.52)

We see that this resolves the ambiguity of fractional powers of -1 in our formal derivations,
$e^{\frac{i\pi\Delta_k}{2}} \equiv (-1)^{\frac{\Delta_k}{2}}$.

In [72], we will prove the $x \leftrightarrow t$ property for time-ordered correlators with up to four external points for a general $1 + 1$ CFT, using the conformal bootstrap approach. In Section 2.8 of this chapter, we prove (a refinement of) this property on the dual AdS side within EFT for any number of external points.

2.6.2 $x \leftrightarrow t$ in Milne Wedges and Reconnecting to Rindler Wedges

Having made this plausible case for $x \leftrightarrow t$ symmetry, we will apply the transformation on the F Milne wedge to make it more R-Rindlerlike. More generally, we also compound it with $x^\pm \to -x^\pm$ as required to make all four wedges appear R-Rindlerlike, so that we can use R-Rindler coordinates in all of them:

$$\pm e^{\pm\sigma^\pm} = e^\alpha (\sin\theta \pm \cos\theta) = \begin{cases} x_R'^\pm = x_R^\pm & \\ x_F'^\pm = \pm x_F^\pm & x \leftrightarrow t \\ x_L'^\pm = -x_L^\pm & x, t, \leftrightarrow -x, -t \\ x_P'^\pm = \mp x_P^\pm & x \leftrightarrow -t, \end{cases}$$

(2.53)

where $|\theta| \le \frac{\pi}{4}$. Now let us take seriously that the dual CFT lives on the Lorentzian torus, say as prescribed by a CFT path integral on this spacetime. After the above space/time interchanges, the path integral on each wedge *separately* corresponds to a canonical quantum mechanical time evolution (in θ) for the CFT on a spacelike circle (in α). Tentatively, the overall connected toroidal structure suggests that the initial and final states of each wedge evolution are to be identified with those of adjacent wedges, and then summed over. (This neglects any concern that the joints themselves are lightlike circles where field theory is expected to be pathological, but we will be more careful about this below.)

It thereby appears that the full torus path integral is the *CFT-trace* of the product of quantum evolution operators for the four separate wedges, akin to the thermal trace structure of finite temperature field theory and its equivalence to the thermal path integral in cyclic Euclidean time. However, we have neglected to take into account that adjacent wedges have differing space/time interchanges, so that the initial/final state of a particular wedge has to be reinterpreted before being "handed off" to an adjacent wedge. For example, consider the $x^- \to -x^-$ transformation in passing from the R to F wedge. Noting that under the standard CFT symmetry operator $e^{i\beta(S-K)}$, where S, K are the generators of $x^\pm$ dilations and boosts respectively,

$$x^- \to e^{2\beta} x^-$$
$$x^+ \to x^+,$$

(2.54)

it is natural to guess that under $e^{\frac{\pi}{2}(S-K)}$,

$$x^- \to e^{i\pi} x^- = -x^-$$
$$x^+ \to x^+.$$

(2.55)

It has the form of an analytic continuation [60] around the complex x^- plane (by π) and therefore makes sense if the $x^\pm$ dependence in states/amplitudes is analytic enough at the "joints" of the torus. Let us continue to hope for the best and take $e^{\frac{\pi}{2}(S-K)}$ as the requisite operator to reinterpret states at the hand-off between the R and F wedges. Similar operators can be constructed to act at the other "joints" of the torus.

Although we are inspired by the connectedness of the Lorentzian torus, and could proceed directly in this language, it is more convenient to implement the above insights using our first realization of ∂BTZ as four disjoint cylindrical spacetimes, with the standard Rindler coordinates, $\sigma^\pm$. The CFT should be indifferent to these different realizations by different Weyl transformations. We do this for three reasons. Firstly, after the space/time exchanges above, all the four cylindrical spacetimes have the same very simple geometry, $ds^2 = d\sigma^+ d\sigma^-$, with circular σ and infinite time. Secondly, this form of R and L wedges is just the standard home of the CFTs in the thermofield proposal for the black hole dual, so it will make translation of our results into thermofield language easier. Thirdly, the CFT operators involved in the hand-off of states between wedges are simply energy and momentum in Rindler coordinates,

$$P_\pm^{(\sigma)} \equiv \frac{H^{(\tau)} \mp P^{(\sigma)}}{2} = \frac{K^{(x)} \pm S^{(x)}}{2}, \tag{2.56}$$

where the K, S are to be interpreted here as (consistently) restricted to the R wedge.
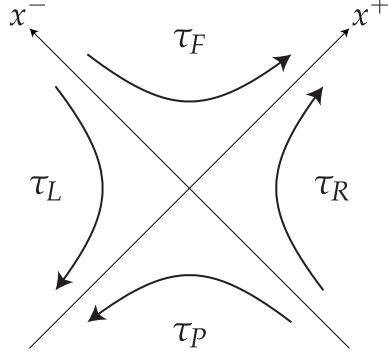
Figure 2.7: The direction of τ in each wedge with respect to Minkowski $x^\pm$ as given in (2.53).

2.6.3 CFT on ∂BTZ as a Trace

We thereby arrive at a precise and well-defined CFT proposal for interpreting the torus path integral, as the dual of BTZ quantum gravity:

$$Z[J_{L,R,F,P}] = \lim_{\mathcal{T}\to\infty} \text{tr} \left\{ U_P^\dagger e^{-\pi P_-} U_L e^{-\pi P_+} U_F^\dagger e^{-\pi P_-} U_R e^{-\pi P_+} \right\}$$
$$\text{where} \quad U = \text{T}_\tau\, e^{-i \int_{-\mathcal{T}}^{\mathcal{T}} d\tau\, (H_{\text{CFT}} - J\mathcal{O})}. \tag{2.57}$$

Here, each U is the time evolution operator within each wedge, with possible source terms for CFT operators $\mathcal{O}$ in any wedge. T_τ denotes time-ordering with respect to τ (Fig. 2.7). In order to be careful about the joins between wedges we regulate the evolutions to finite but very large final/initial times $\tau = \pm\mathcal{T}$, and assume that sources, J, vanish outside these times. We then take the limit as $\mathcal{T} \to \infty$ in order to obtain the Weyl-equivalent of the full torus path integral, except that (just) the lightlike circles have been delicately excised (Fig. 2.8). It is straightforward to see that this limit exists once we write the Dyson series expansion for the source terms, since all $e^{\pm i H_{\text{CFT}}\mathcal{T}}$ factors cancel between the different wedges (using the
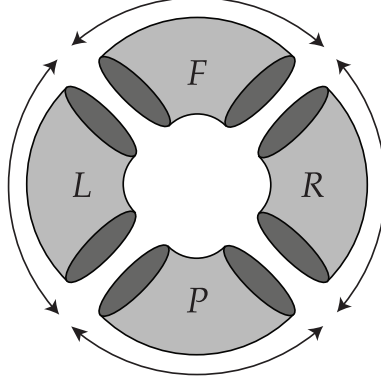
Figure 2.8: Closed lightlike curves are avoided by a limiting process indicated by the arrows. Closed timelike curves are avoided by formally transforming $t \leftrightarrow x$ in the F and P wedges.

fact that H and P commute for the CFT on the cylinder):

$$Z = \text{tr}(\text{T}_\tau \, \hat{U}_P)^\dagger e^{-\pi P_-}(\text{T}_\tau \, \hat{U}_L)e^{-\pi P_+}(\text{T}_\tau \, \hat{U}_F)^\dagger e^{-\pi P_-}(\text{T}_\tau \, \hat{U}_R)e^{-\pi P_+}$$

$$\hat{U} \equiv e^{-i \int_{-\infty}^{\infty} d\tau d\sigma \, J \mathcal{O}^H}. \tag{2.58}$$

Here $\mathcal{O}^H$ is the Heisenberg operator (with respect to H_{CFT}) related to the Schrödinger operator $\mathcal{O}$.

Finally, notice that we have chosen specific signs for our exponents in the $e^{-\pi P_\pm}$ operators, even though formally rotations by π and $-\pi$ are equivalent in the $x^\pm$ complex planes. These choices ensure convergence of the sum over CFT states implied by the trace, in the face of these exponential weights. To see this, note that

$$e^{-\pi P_\pm} = \sum_n e^{-\frac{\pi}{2}(E^n \mp p^n)}|n\rangle\langle n|, \tag{2.59}$$

for a complete set of energy-momentum CFT eigenstates. We expect $E^n > |p^n|$ for such states, and this certainly follows if the CFT is supersymmetric. Therefore we always have exponential damping of excited states in the trace formula, equation (2.58).

We have arrived at a *non-perturbatively* well-defined formulation of a partition functional in terms of a CFT living on a spatial circle × time. It remains to show that it is a hologram of the extended BTZ black hole if the same CFT on Minkowski space has a low-curvature AdS dual. If so, it necessarily must UV complete the approach to the BTZ singularity and gravitational EFT.

2.7 CFT Dual in Thermofield Form

In this section we translate the trace form of the CFT partition functional motivated above into the thermofield language of two entangled CFTs. This will be useful for proving that its large-N_{CFT} diagrammatic expansion reproduces the tree-level (classical) BTZ EFT diagrammatics, and in making contact with the standard framework outside the horizon.

2.7.1 Special Case of Purely Rindler Wedge Sources

Let us first restrict our sources to local operators in the Rindler wedges, L and R, which corresponds to the part of the BTZ boundary lying outside the horizon. We check that the standard picture [23] emerges straightforwardly from our trace formula.

In this special case, $J_{F,P} = 0$ and (2.58) becomes

$$
\begin{aligned}
Z &= \operatorname{tr} e^{-\pi H}(\mathrm{T}\,\hat{U}_L) e^{-\pi H}(T\hat{U}_R) \\
&= \sum_{n,m} e^{-\pi(E_n + E_m)} \langle n|\,\mathrm{T}\,\hat{U}_L|m\rangle \langle m|\,\mathrm{T}\,\hat{U}_R|n\rangle \\
&= \sum_{n,m} e^{-\pi(E_n + E_m)} \langle \bar{m}|\,\mathrm{T}\,\hat{U}_L|\bar{n}\rangle \langle m|\,\mathrm{T}\,\hat{U}_R|n\rangle,
\end{aligned}
\tag{2.60}
$$

where $|\bar{\chi}\rangle \equiv \text{CPT}\,|\chi\rangle$ for arbitrary ket $|\chi\rangle$. Note that $\langle \bar{m}|\,\text{T}\,\hat{U}_L|\bar{n}\rangle$ is still T-ordered with respect to the argument of $\mathcal{O}$, since (taking $x_1^0 \geq x_2^0 \geq \cdots \geq x_n^0$ without loss of generality),

$$
\begin{aligned}
\langle \psi | \,\text{T}\,\mathcal{O}_1(x_1)\cdots\mathcal{O}_n(x_n)|\chi\rangle &= \langle \psi | \mathcal{O}_1(x_1)\cdots\mathcal{O}_n(x_n)|\chi\rangle \\
&= \langle \bar{\chi}|\,\text{CPT}\big[\mathcal{O}_1(x_1)\cdots\mathcal{O}_n(x_n)\big]^\dagger \text{CPT}^{-1}\,|\bar{\psi}\rangle \\
&= \langle \bar{\chi}|\,\text{CPT}\,\mathcal{O}_n^\dagger(x_n)\,\text{CPT}^{-1}\cdots\text{CPT}\,\mathcal{O}_1^\dagger(x_1)\,\text{CPT}^{-1}\,|\bar{\psi}\rangle \\
&= \langle \bar{\chi}|\mathcal{O}_n(-x_n)\cdots\mathcal{O}_1(-x_1)|\bar{\psi}\rangle \\
&= \langle \bar{\chi}|\,\text{T}\,\mathcal{O}_n(-x_n)\cdots\mathcal{O}_1(-x_1)|\bar{\psi}\rangle.
\end{aligned}
$$

$$(2.61)$$

The second line is true for any antiunitary operator, while the second-to-last line is how $\mathcal{O}$, which we take as Lorentz scalar (primary) for simplicity, transforms under CPT. (A more general irreducible representation of the Lorentz group simply receives additional factors of (-1).)

Thus we arrive at standard thermofield form,

$$
Z = \langle \Psi | T\hat{U}_L \otimes \text{T}\,\hat{U}_R|\Psi\rangle, \tag{2.62}
$$

with

$$
|\Psi\rangle \equiv \sum_n e^{-\pi E_n}|\bar{n}\rangle \otimes |n\rangle \tag{2.63}
$$

being an entangled state of two otherwise decoupled CFTs on a spatial circle.

2.7.2   General Case of Arbitrary Sources

Having warmed up as above, let us move to the general case of sources $J_{L,R,F,P} \neq 0$, and even possibly non-local sources in these wedges. By inserting complete sets of energy-momentum eigenstates again, we can translate our trace formula,

$$
\begin{aligned}
Z &= \operatorname{tr} e^{-\pi H} e^{\pi P_-} (\mathrm{T}\,\hat{U}_P)^\dagger e^{-\pi P_-} (\mathrm{T}\,\hat{U}_L) e^{-\pi H} e^{\pi P_-} (\mathrm{T}\,\hat{U}_F)^\dagger e^{-\pi P_-} (\mathrm{T}\,\hat{U}_R) \\
&= \sum_{n,m} e^{-\pi(E_n + E_m)} \langle \bar{m}|(\mathrm{T}\,\hat{U}_L) e^{-\pi P_-} (\mathrm{T}\,\hat{U}_P)^\dagger e^{\pi P_-}|\bar{n}\rangle \langle m|e^{\pi P_-} (\mathrm{T}\,\hat{U}_F)^\dagger e^{-\pi P_-} (\mathrm{T}\,\hat{U}_R)|n\rangle \\
&= \langle \Psi|(\mathrm{T}\,\hat{U}_L) e^{-\pi P_-} (\mathrm{T}\,\hat{U}_P)^\dagger e^{\pi P_-} \otimes e^{\pi P_-} (\mathrm{T}\,\hat{U}_F)^\dagger e^{-\pi P_-} (\mathrm{T}\,\hat{U}_R)|\Psi\rangle,
\end{aligned}
\tag{2.64}
$$

using $P_\pm|\bar{n}\rangle = P_\pm|n\rangle = p_\pm^n|n\rangle$, which follows from CPT $\mathcal{O}$ CPT^{-1} rules. Note that even if the source terms consist of products of local CFT operators, the terms,

$$
e^{-\pi P_-} (\mathrm{T}\,\hat{U}_P)^\dagger e^{\pi P_-} \equiv \left(\mathrm{T}\, e^{-i \int \mathcal{J} e^{\pi P_-} \mathcal{O}^H e^{-\pi P_-}}\right)^\dagger
\tag{2.65}
$$

will be products of non-local operators, $e^{\pi P_-} \mathcal{O}^H e^{-\pi P_-}$, since $e^{-\pi P_-}$ is non-local. Nevertheless, the general partition functional has now been put into thermofield form.

In order to verify that this CFT formula reproduces BTZ gravitational EFT, it is very useful to separate the Rindler wedges from the F and P wedges by insertions of a complete set of states, $|N\rangle$, of $\overline{\text{CFT}} \otimes \text{CFT}$ (in contrast to states $|n\rangle$ of a single CFT). We do this as follows. First we write our thermofield formula in the (obviously equivalent) factorized

form,

$$Z = \langle\Psi|\left[\mathbb{1} \otimes e^{\pi P_-}(\mathrm{T}\,\hat{U}_F)^\dagger e^{-\pi P_-}\right]\left[(\mathrm{T}\,\hat{U}_L) \otimes (\mathrm{T}\,\hat{U}_R)\right]\left[e^{-\pi P_-}(\mathrm{T}\,\hat{U}_P)^\dagger e^{\pi P_-} \otimes \mathbb{1}\right]|\Psi\rangle.$$

(2.66)

We insert the resolution of the identity,

$$\mathbb{1} = \sum_N \left[e^{iH\mathcal{T}} \otimes e^{-iH\mathcal{T}}\right]|N\rangle\langle N|\left[e^{-iH\mathcal{T}} \otimes e^{iH\mathcal{T}}\right],$$

(2.67)

between the first pair of square brackets, and again between the second pair of (2.66). Note that the $e^{iH\mathcal{T}} \otimes e^{-iH\mathcal{T}}|N\rangle$ form a complete orthonormal basis of $\overline{\mathrm{CFT}} \otimes \mathrm{CFT}$ if the $|N\rangle$ do because $e^{iH\mathcal{T}} \otimes e^{-iH\mathcal{T}}$ is unitary (and just the boost symmetry operation in Minkowski spacetime language). We thereby get

$$\begin{aligned}
Z = \sum_{N,M} &\langle\Psi|\left[\mathbb{1} \otimes e^{\pi P_-}(\mathrm{T}\,\hat{U}_F)^\dagger e^{-\pi P_-}\right]\left[e^{iH\mathcal{T}} \otimes e^{-iH\mathcal{T}}\right]|N\rangle \\
&\langle N|\left[e^{-iH\mathcal{T}} \otimes e^{iH\mathcal{T}}\right]\left[(\mathrm{T}\,\hat{U}_L) \otimes (\mathrm{T}\,\hat{U}_R)\right]\left[e^{iH\mathcal{T}} \otimes e^{-iH\mathcal{T}}\right]|M\rangle \\
&\langle M|\left[e^{-iH\mathcal{T}} \otimes e^{iH\mathcal{T}}\right]\left[e^{-\pi P_-}(\mathrm{T}\,\hat{U}_P)^\dagger e^{\pi P_-} \otimes \mathbb{1}\right]|\Psi\rangle.
\end{aligned}$$

(2.68)

We can view the states $|N\rangle, |M\rangle$ as being located on the spacelike hypersurface shown in Fig. 2.9.

Finally, we massage the exponential weights for our later convenience using $\mathbb{1} =$
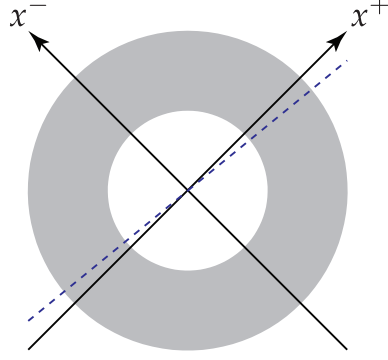
Figure 2.9: Spacelike hypersurface (blue dashed line) where $|N\rangle$ and $|M\rangle$ are located.

$$e^{-\pi P_-}e^{\pi P_-} = e^{\pi P_-}e^{-\pi P_-},$$

$$
\begin{aligned}
Z &= \sum_{N,M} \langle\Psi| \left[e^{-\pi P_-}e^{\pi P_-} \otimes e^{\pi P_-}(\mathrm{T}\,\hat{U}_F)^\dagger e^{-\pi P_-} \right] \left[e^{iH\mathcal{T}} \otimes e^{-iH\mathcal{T}} \right] |N\rangle \\
&\quad \langle N| \left[e^{-iH\mathcal{T}} \otimes e^{iH\mathcal{T}} \right] \left[(\mathrm{T}\,\hat{U}_L) \otimes (\mathrm{T}\,\hat{U}_R) \right] \left[e^{iH\mathcal{T}} \otimes e^{-iH\mathcal{T}} \right] |M\rangle \\
&\quad \langle M| \left[e^{-iH\mathcal{T}} \otimes e^{iH\mathcal{T}} \right] \left[e^{-\pi P_-}(\mathrm{T}\,\hat{U}_P)^\dagger e^{\pi P_-} \otimes e^{\pi P_-}e^{-\pi P_-} \right] |\Psi\rangle \\
&= \sum_{N,M} \langle\Psi| \left[\mathbb{1} \otimes (\mathrm{T}\,\hat{U}_F)^\dagger \right] \left[e^{\pi P_-} \otimes e^{-\pi P_-} \right] \left[e^{iH\mathcal{T}} \otimes e^{-iH\mathcal{T}} \right] |N\rangle \\
&\quad \langle N| \left[e^{-iH\mathcal{T}} \otimes e^{iH\mathcal{T}} \right] \left[(\mathrm{T}\,\hat{U}_L) \otimes (\mathrm{T}\,\hat{U}_R) \right] \left[e^{iH\mathcal{T}} \otimes e^{-iH\mathcal{T}} \right] |M\rangle \\
&\quad \langle M| \left[e^{-iH\mathcal{T}} \otimes e^{iH\mathcal{T}} \right] \left[e^{-\pi P_-} \otimes e^{\pi P_-} \right] \left[(\mathrm{T}\,\hat{U}_P)^\dagger \otimes \mathbb{1} \right] |\Psi\rangle,
\end{aligned}
$$
(2.69)

where to get the last equality we have used

$$e^{\pi P_-} \otimes e^{-\pi P_-}|\Psi\rangle = \sum_n e^{\pi p_-^n}e^{-\pi p_-^n}|\bar{n}\rangle \otimes |n\rangle = |\Psi\rangle. \qquad (2.70)$$

Note that the above invariance of $|\Psi\rangle$ can just be thought of as the repeated application

of the infinitesimal symmetry invariances of $\overline{\text{CFT}} \otimes \text{CFT}$,

$$(\mathbb{1} \otimes P_\pm - P_\pm \otimes \mathbb{1}) \, |\Psi\rangle = 0,$$

$$\mathbb{1} \otimes H - H \otimes \mathbb{1} \equiv \text{Minkowski Boost} \equiv K \qquad (2.71)$$

$$\mathbb{1} \otimes P - P \otimes \mathbb{1} \equiv \text{Minkowski Dilatation} \equiv S.$$

Time and space translations in $\sigma^\pm$-space correspond to boosts and dilatations in $x^\pm$-space. The negative sign on the second P is due to the parity operation in CPT. Even though we are compactifying Minkowski spacetime, we are doing it by quotienting by a discrete dilatation (after a Weyl transformation), which does not break these boost and dilatation symmetries.

In this section and the last, we have made a series of natural guesses to frame the trace formula (2.57), (2.58) for the partition functional. In the next sections we use bulk diagrammatics for explicit verification, beginning with the non-quotiented limit, $r_S \to \infty$.

2.8 $r_S = \infty$: Rindler AdS/CFT

In the limiting case of $r_S = \infty$, we are no longer quotienting AdS to get BTZ, we simply have AdS. In this case we know that there is a CFT dual on $1 + 1$ Minkowski spacetime. Nevertheless all our considerations and derivations above apply for any r_S, including $r_S = \infty$, and therefore (2.69) should give us a second, very different looking, dual description. It is a non-trivial check of our proposal for these two dual descriptions to agree and holographically "project" quantum gravity and matter on AdS. In this section, we verify this at EFT tree level.

We begin with AdS EFT, with bulk sources,

$$\text{Sources} = \int d^2x dz \sqrt{g_{\text{AdS}}}\, \mathcal{J}(x^\pm, z)\phi(x^\pm, z). \qquad (2.72)$$

For simplicity, we consider AdS scalar fields explicitly, but we can clearly generalize our discussion to higher spin fields, including gravitational fluctuations about AdS (as long as we do this in the context of diffeomorphism gauge-fixing, as discussed in the Introduction). We can break up AdS into four wedges, F, P, R, L, just based on $x^\pm$ and extending for all z.

2.8.1 Special Case of Purely Rindler Wedge Sources

We will warm up with the special case of only Rindler wedge sources, $\mathcal{J}_{F,P} = 0$. The usual Rindler construction for any field theory on a spacetime containing a (warped) $1 + 1$ Minkowski spacetime factor implies [73, 74] [75, 76] [77]

$$
\begin{aligned}
Z &= \langle 0 |\, \text{T}\, \hat{U}_L \hat{U}_R | 0 \rangle \\
&= \langle \Psi |\, \text{T}_\tau\, \hat{U}_L\, \text{T}_\tau\, \hat{U}_R | \Psi \rangle.
\end{aligned}
\qquad (2.73)
$$

On the first line we just have correlators for the Dyson series in the source perturbations in the AdS vacuum, where

$$\hat{U} = e^{i \int d^2x dz \sqrt{g_{\text{AdS}}}\, \mathcal{J}\phi}. \qquad (2.74)$$

On the second line, we have replaced the AdS vacuum by its Rindler description (for a general non-conformal field theory),

$$|\Psi\rangle \equiv \sum_k e^{-\pi K_k} |\bar{k}\rangle \otimes |k\rangle = |0\rangle_{\text{AdS}}, \qquad (2.75)$$

where K_k and $|k\rangle$ are boost eigenvalues and eigenstates, respectively. Since $\mathcal{O}_L$ and $\mathcal{O}_R$ commute by their spacelike separation, the T-ordering factorizes into separate T-ordering on the L and R operators. We can take the T-ordering on the second line to be with respect to the Rindler time, τ, since the τ-direction is timelike. We use T_τ to denote ordering with respect to τ and T for time ordering with respect to Minkowski time, t.

We change to coordinates in which the AdS$_{\text{Poincaré}}$ boost symmetry becomes τ-time translation symmetry, and the symmetry of rescaling $x^\pm, z$ becomes a spatial σ translation symmetry,

$$x^\pm = \begin{cases} \mp \sqrt{1 - \frac{1}{r^2}}\, e^{\mp\sigma_\mp}, & x \in L \\[2mm] \pm \sqrt{1 - \frac{1}{r^2}}\, e^{\pm\sigma^\pm}, & x \in R \end{cases} \qquad z = \frac{e^\sigma}{r}, \qquad (r > 1). \qquad (2.76)$$

The new coordinates cover each Rindler wedge, L, R, which now look precisely like the $r_S \to \infty$ limit of the *exterior* of the BTZ black hole in Schwarzschild coordinates (2.19), namely the BTZ black *string* (since σ is not compact now). But it is also just the Rindler coordinate view of the R (or L) wedge of AdS$_{\text{Poincaré}}$. We will refer to the portion of AdS$_{\text{Poincaré}}$ covered by these coordinates for $r > 1$ as "AdS$_{\text{Rindler}}$", and to $r, \sigma^\pm$ as "AdS$_{\text{Rindler}}$

coordinates." We can write the Dyson series for the Rindler wedge source perturbations as

$$\hat{U}_L = e^{i \int d^2\sigma \int_1^\infty dr \sqrt{g_{\text{AdS}_{\text{Rindler}}}} \, \mathcal{J}_L \phi}$$

$$\hat{U}_R = e^{i \int d^2\sigma \int_1^\infty dr \sqrt{g_{\text{AdS}_{\text{Rindler}}}} \, \mathcal{J}_R \phi}.$$

(2.77)

Because $\text{AdS}_{\text{Poincaré}}$ boosts correspond to $\pm \, \text{AdS}_{\text{Rindler}}$ time (τ) translations, we now have

$$|\Psi\rangle = \sum_k e^{-\pi E^k_{\text{AdS}_{\text{Rindler}}}} |\bar{k}\rangle \otimes |k\rangle = |0\rangle_{\text{AdS}_{\text{Poincaré}}},$$

(2.78)

where $E^k_{\text{AdS}_{\text{Rindler}}}$ and $|k\rangle$ are eigenvalues and eigenstates of the $\text{AdS}_{\text{Rindler}}$ Hamiltonian.

2.8.2   Comparison with Dual CFT

Now let us invoke standard AdS/CFT duality. For greater familiarity, first specialize our AdS side further to just boundary sources,

$$\int d^2x dz \sqrt{g} \, \mathcal{J}\phi \rightarrow \int d^2x \, J \lim_{z \to 0} \frac{\phi(x,z)}{z^\Delta} = \int d^2x \, J \mathcal{O}_{\text{primary}}.$$

(2.79)

Comparing with the dual CFT expression,

$$|0\rangle_{\text{AdS}} = \sum_k e^{-\pi E^k_{\text{Rindler}}} |\bar{k}\rangle \otimes |k\rangle$$

$$= \sum_n e^{-\pi E^n_{\text{CFT}}} |\bar{n}\rangle \otimes |n\rangle = |0\rangle_{\text{CFT}},$$

(2.80)

we see that the $\text{AdS}_{\text{Rindler}}$ spacetime must be interpreted as a coarse-grained, classical (planar in large N_{CFT}) description of an excited stationary CFT state which dominates the thermal

sum over states. In the thermofield gravity description, one can think of it as a large excitation of the gravitational field, turning the $AdS_{Poincaré}$ vacuum

$$ds^2 = \frac{1}{z^2}\left[d\tau^2 - d\sigma^2 - dz^2\right] \qquad (z > 0) \tag{2.81}$$

into

$$ds^2 = \frac{1}{z^2}\left[d\tau^2 - (1 + z^2)d\sigma^2 - \frac{dz^2}{1 + z^2}\right], \tag{2.82}$$

where we have rewritten (2.4) using $z \equiv 1/\sqrt{r^2 - 1}$, for $r > 1$. We must also sum over metric and other EFT fluctuations away from this dominant state, and these are dual to the CFT deviations from the dominant CFT state. In the gravity description, these deviations from the $AdS_{Rindler}$ geometry include Unruh radiation (in the language where we are just seeing $AdS_{Poincaré}$ from the Rindler observer viewpoint) or Hawking radiation (in the language where we view the dominant geometry as the BTZ black string with horizon). For simplicity, we are making the following approximations on the gravity side of the duality:

$$\sum_{\substack{\text{quantum} \\ \text{gravity states}}} \approx \sum_{\substack{\text{gravitational} \\ \text{EFT states}}} \approx \sum_{\substack{\text{scalar } \phi \text{ fluctuations on} \\ \text{fixed } AdS_{Rindler} \text{ metric}}} . \tag{2.83}$$

That is, in the sum over metrics we are keeping the dominant $AdS_{Rindler}$ metric but dropping fluctuations of it. Instead, we are keeping just scalar field fluctuations about this geometry as the simplest illustration of how more general fluctuations will work.

2.8.3 General Case of Arbitrary Sources

Having interpreted the special status of the $\text{AdS}_{\text{Rindler}}$ metric, let us return to the case of sources in all regions, $\mathcal{J}_{L,R,F,P} \neq 0$. We now take the gravity dual of our proposed construction of CFT_{Mink} correlators in terms of $|\overline{\text{CFT}_{\text{Rindler}}}\rangle \otimes |\text{CFT}_{\text{Rindler}}\rangle$, and show that there is a perfect and non-trivial match. With $\text{AdS}_{\text{Rindler}}$ as the dominant CFT state in the thermofield sum, the gravity dual of our proposed construction on $|\overline{\text{CFT}_{\text{Rindler}}}\rangle \otimes |\text{CFT}_{\text{Rindler}}\rangle$, (2.69), is given by the analogous construction on $|\Psi\rangle = |0\rangle_{\text{AdS}} \in |\overline{\text{AdS}_{\text{Rindler}}}\rangle \otimes |\text{AdS}_{\text{Rindler}}\rangle$, namely

$$
\begin{aligned}
Z = \sum_{N,M} \langle\Psi| &\left[\mathbb{1} \otimes (\text{T}_\tau \hat{U}_F)^\dagger \right] \left[e^{\pi P_-} \otimes e^{-\pi P_-} \right] \left[e^{iH\mathcal{T}} \otimes e^{-iH\mathcal{T}} \right] |N\rangle \\
&\times \langle N| \left[e^{-iH\mathcal{T}} \otimes e^{iH\mathcal{T}} \right] \left[(\text{T}_\tau \hat{U}_L) \otimes (\text{T}_\tau \hat{U}_R) \right] \left[e^{iH\mathcal{T}} \otimes e^{-iH\mathcal{T}} \right] |M\rangle \qquad (2.84) \\
&\times \langle M| \left[e^{-iH\mathcal{T}} \otimes e^{iH\mathcal{T}} \right] \left[e^{-\pi P_-} \otimes e^{\pi P_-} \right] \left[(\text{T}_\tau \hat{U}_P)^\dagger \otimes \mathbb{1} \right] |\Psi\rangle.
\end{aligned}
$$

Here, $|\Psi\rangle$ is given by (2.78) and all operators relate to excitations on $\text{AdS}_{\text{Rindler}}$. $P_\pm$ are conjugate to $\sigma^\pm$ as before. H refers to the EFT Hamiltonian in the $\text{AdS}_{\text{Rindler}}$ background, $H_{\text{AdS}_{\text{Rindler}}}$.

The $|N\rangle$, $|M\rangle$ are excitations of $|\Psi\rangle$. Converting to $\text{AdS}_{\text{Poincaré}}$ coordinates, the time evolution specified localizes these excitations to the spacelike hypersurface illustrated in Fig. 2.10. We will refer to this as the "$\mathcal{T}$-hypersurface". We can think of $|N\rangle$, $|M\rangle$ as being given by (multiple) scalar field operators on the $\mathcal{T}$-hypersurface acting on $|\Psi\rangle$.

We now massage and reinterpret the various matrix elements in (2.84) in $\text{AdS}_{\text{Poincaré}}$
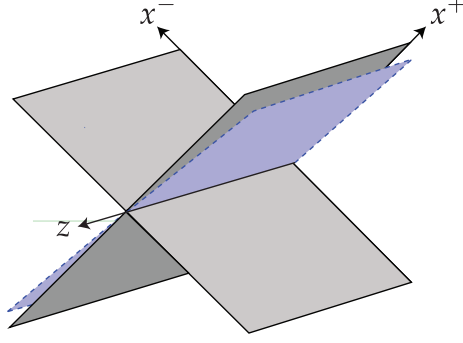
Figure 2.10: Bulk spacelike hypersurface (blue plane) where $|N\rangle$ and $|M\rangle$ are located.

language. Let us first focus on the F matrix element

$$\langle\Psi|\left[\mathbb{1}\otimes(\mathrm{T}_\tau\,\hat{U}_F)^\dagger\right]\left[e^{\pi P_-}\otimes e^{-\pi P_-}\right]\left[e^{iH\mathcal{T}}\otimes e^{-iH\mathcal{T}}\right]|N\rangle$$

$$\equiv\langle N|\left[e^{-iH\mathcal{T}}\otimes e^{iH\mathcal{T}}\right]\left[e^{\pi P_-}\otimes e^{-\pi P_-}\right]\left[\mathbb{1}\otimes(\mathrm{T}_\tau\,\hat{U}_F)\right]|\Psi\rangle^*. \quad (2.85)$$

Note that

$$\mathbb{1}\otimes(\mathrm{T}_\tau\,\hat{U}_F)=\mathbb{1}\otimes\mathrm{T}_\tau\,e^{i\int d\tau d\sigma\,\sqrt{g_{\mathrm{AdS_{Rindler}}}}\,\mathcal{J}_F(\sigma^\pm,\tau)\phi(\sigma^\pm,\tau)}$$

$$=\mathrm{T}\,e^{i\int d^2x dz\,\sqrt{g_{\mathrm{AdS_{Poincaré}}}}\,\mathcal{J}_F(x_F'^\pm,Z)\phi(x_F'^\pm,z)}$$

$$\qquad\qquad\qquad\qquad\qquad\qquad\qquad\qquad\qquad\qquad\qquad\qquad (2.86)$$

$$=\mathrm{T}\,e^{i\int d^2x' dz\,\sqrt{g'_{\mathrm{AdS_{Poincaré}}}}\,\mathcal{J}_F(x_F'^\pm,Z)\phi(x_F'^\pm,z)}$$

$$=\mathrm{T}\,\hat{U}_F.$$

In particular we have replaced Rindler time-ordering by Poincaré time-ordering because these agree up to operators with spacelike separations as usual. In the last two lines we have switched to Poincaré notation rather than the tensor product Rindler^2 notation of the first line. Also note that $\mathcal{J}_F(x'^\pm, z)\neq 0$ only for both $x^\pm > 0$, which is equivalent to $x'^+ > 0$ and $x'^- < 0$. (See x' definition in (2.53)). So we have sources for ϕ in the R-wedge. Of course this better not be the full answer since this source term should be for correlators of points in the F-wedge, and indeed we must still take into account (and translate to Poincaré

62

language) the non-local operation

$$\left[e^{\pi P_-} \otimes e^{-\pi P_-} \right] \equiv e^{\frac{\pi}{2}(S-K)} \qquad (2.87)$$

Using (2.71), (2.86), and (2.87), (2.85) becomes

$$\langle N | \left[e^{-iH\mathcal{T}} \otimes e^{iH\mathcal{T}} \right] \left[e^{\pi P_-} \otimes e^{-\pi P_-} \right] \left[\mathbb{1} \otimes (\mathrm{T}_\tau \, \hat{U}_F) \right] | \Psi \rangle^* = \langle N | e^{-iK\mathcal{T}} e^{\frac{\pi}{2}(S-K)} \, \mathrm{T} \, \hat{U}_F | \Psi \rangle^*$$

$$(2.88)$$

2.8.4 Diagrammatic Analysis of Thermofield Formulation

To get oriented let us first neglect the operation $e^{\frac{\pi}{2}(S-K)}$ in our matrix element (2.88) altogether. Then (2.88) has the following very general $\mathrm{AdS_{Poincaré}}$ diagrammatic form:

$$\langle N | e^{-iK\mathcal{T}} \, \mathrm{T} \, \hat{U}_F | \Psi \rangle^* \rightarrow \int \left[\prod \mathrm{AdS\text{-}Propagators} \times (-i \text{ couplings}) \right]^*, \qquad (2.89)$$

the complex conjugate of AdS diagrams, with external lines ending on the $\mathcal{T}$-hypersurface, corresponding to connecting to the $|N\rangle$ states, or to ϕ in the R-wedge where $\mathcal{J}_F(x', z) \neq 0$. The integral(s) indicated are over internal interaction vertices.

Now consider the effect of $e^{\frac{\pi}{2}(S-K)}$ acting on $|N\rangle$. We can break this up in the form $\left[e^{\frac{\pi}{2k}(S-K)} \right]^k$ for some large number k. Then as long as the above AdS-diagrams (AdS propagators) are analytic enough in their x^-, z dependence for the locations of scalar particles in the $|N\rangle$ state (where external lines attach), the action of each $e^{\frac{\pi}{2k}(S-K)}$ is to just analytically continue the diagram, $x^- \rightarrow e^{\frac{i\pi}{k}} x^-$ and $z \rightarrow e^{\frac{i\pi}{2k}} z$. One can repeat such small

63

analytic continuations many times to analytically continue $x^- \to e^{i\beta} x^-$ and $z \to e^{\frac{i\beta}{2}} z$ as long as the diagram (propagator) remains analytic along the neighborhood of the path traced out thereby in the complex x^-, z planes, ultimately arriving after k iterations to $x^- \to -x^-$ and $z \to iz$.

This is indeed the case, as we now check. The bulk AdS$_{\text{Poincaré}}$ propagator has the form [78] [79],

$$G_{\text{AdS}}(x^\pm, z; y^\pm, z') = \xi^\Delta F(\xi^2), \tag{2.90}$$

where $F(\xi^2) \equiv F(\frac{\Delta}{2}, \frac{\Delta}{2} + \frac{1}{2}; \Delta; \xi^2)$ is a hypergeometric function which is analytic in the complex ξ^2-plane with a cut along $(1, \infty)$, and where

$$\xi \equiv \frac{2zz'}{z^2 + z'^2 - (x^+ - y^+)(x^- - y^-) + i\epsilon(x^0 - y^0)^2}. \tag{2.91}$$

Because of the branch cuts in F and ξ^Δ we must be very careful in any analytic continuations we perform. Our first step will be to simply rotate *all* z coordinates in the diagrams of (2.89),

$$z \to e^{\frac{i\beta}{2}} z, \quad \text{from } \beta = 0 \text{ to } \beta = \pi - \epsilon. \tag{2.92}$$

It is straightforward to check that ξ never passes through a branch cut of G_{AdS} in such a rotation.

Let us interpret this move. If z corresponds to a point on the $\mathcal{T}$-hypersurface, then this rotation is just part of the action of $e^{\frac{\pi}{2}(S-K)}$ acting on $|N\rangle$, as discussed above. The $e^{\frac{\pi}{2}(S-K)}$ is also supposed to rotate the associated x^-, but since we are taking $\mathcal{T}$ very large,

and well to the future/past of our sources, $x^- \approx 0$ along this hypersurface. Therefore the action of $e^{\frac{\pi}{2}(S-K)}$ on it is trivial. If instead, z corresponds to an interaction vertex, then this move corresponds to a (passive) contour rotation of the integral over the interaction vertex location. The only other possibility is that z corresponds to a source point, where $\mathcal{J} \neq 0$. For a source localized to the AdS boundary, necessarily $z = 0$, which is insensitive to the rotation. For a bulk source which is analytic enough in z, the above move would again correspond to (passively) rotating the contour of the z-integral over the source region. We will discuss subtleties of boundary and bulk source terms further in subsections 2.8.5 and 2.8.6, respectively, but proceed with allowing rotation of source points for these broad reasons.

After completing the above rotation of all z coordinates in the diagrams of (2.89), at $\beta = \pi - \epsilon$ it is straightforward to check that we end up with

$$\xi(x^\pm, e^{\frac{i(\pi-\epsilon)}{2}} z; y^\pm, e^{\frac{i(\pi-\epsilon)}{2}} z') = \frac{2zz'}{z^2 + z'^2 + (x^+ - y^+)(x^- - y^-) - i\epsilon(x^1 - y^1)^2}$$

$$= \xi^*(\pm x^\pm, z; \pm y^\pm, z').$$

$$(2.93)$$

From this, and the fact that the hypergeometric function in terms of which G is given satisfies $F(\xi^{*2}) = F^*(\xi^2)$, we obtain the simple but non-trivial identity,

$$G\left(x^\pm, e^{\frac{i(\pi-\epsilon)}{2}} z; y^\pm, e^{\frac{i(\pi-\epsilon)}{2}} z'\right) = G^*(\pm x^\pm, z; \pm y^\pm, z'). \qquad (2.94)$$

The contour rotations of interaction vertices for real to (nearly) imaginary z results in the

65

change of integration measure,

$$\int d^2x \int_0^\infty \frac{dz}{z^3} \cdots \rightarrow i \int d^2x \int_0^\infty \frac{dz}{i^3 z^3} \cdots \,, \tag{2.95}$$

resulting in the replacement in diagrams

$$(-i \text{ couplings}) \rightarrow (+i \text{ couplings}). \tag{2.96}$$

We see that both propagators and interactions are thereby complex-conjugated, and the sign of every x^- is flipped in the diagrams corresponding to (2.89). This all happened as a consequence of a single active move, namely to act with $e^{\frac{\pi}{2}(S-K)}$ on the points ending on the $\mathcal{T}$-hypersurface. The complex conjugation simply undoes the conjugation already appearing in (2.89). For interaction vertices $x^- \rightarrow -x^-$ is clearly irrelevant since it is integrated, and for points ending on the $\mathcal{T}$-hypersurface we are insensitive to $x^- \rightarrow -x^-$ because $x^- \approx 0$ there. Therefore, $x^- \rightarrow -x^-$ is only significant for source points. This now corrects the naive "wrong", that we started with F-wedge sources for ϕ in the R-wedge, as noted below (2.86). The action of $e^{\frac{\pi}{2}(S-K)}$ has performed this "correction".

We are now poised to recover all AdS$_{\text{Poincaré}}$ correlators from our thermofield formula, but must carefully consider boundary versus bulk source options.

2.8.5 Testing Boundary Localized Correlators (in all regions)

Let us first study the familiar case of sources localized to ∂AdS. Since

$$\mathcal{O} = \lim_{z \to 0} \frac{\phi(x^\pm, z)}{z^\Delta}, \tag{2.97}$$

we are not integrating z. Therefore rotating such z as we prescribe in the previous subsection will not be a passive move, but will result in an extra factor of $1/i^\Delta$ from the above limit. This is easily corrected by multiplying the correlator from the trace formula by i^Δ for each external boundary point in the F (P) region. Then, for boundary sources, the diagrammatic analysis of the previous subsection proves that (2.88) is

$$\langle N | e^{-iK\mathcal{T}} e^{\frac{\pi}{2}(S-K)} \, \mathrm{T} \, \hat{U}_F | \Psi \rangle^* = \langle \Psi | \left(\mathrm{T} \, \hat{U}_F \Big|_{x^- \to -x^-} \right) e^{iK\mathcal{T}} | N \rangle. \tag{2.98}$$

As discussed below (2.96), the $x^- \to -x^-$ applies to all source points in $\hat{U}_F$, correcting the naive "wrong" of starting with F-wedge sources for ϕ in the R-wedge. A completely

analogous analysis can be made for the P wedge. Eq. (2.84) thereby takes the form,

$$
\begin{aligned}
Z_{\text{Rindler Thermofield}} &= \sum_{N,M} \langle \Psi | \left(\mathrm{T}\, \hat{U}_F \Big|_{x^- \to -x^-} \right) e^{iK\mathcal{T}} | N \rangle \\
&\quad \times \langle N | e^{-iK\mathcal{T}}\, \mathrm{T}\, \hat{U}_L \hat{U}_R e^{iK\mathcal{T}} | M \rangle \\
&\quad \times \langle M | e^{-iK\mathcal{T}} \left(\mathrm{T}\, \hat{U}_P \Big|_{x^- \to -x^-} \right) | \Psi \rangle \\
&= \langle \Psi | \left(\mathrm{T}\, \hat{U}_F \Big|_{x^- \to -x^-} \right) \mathrm{T}\, \hat{U}_L \hat{U}_R \left(\mathrm{T}\, \hat{U}_P \Big|_{x^- \to -x^-} \right) | \Psi \rangle \\
&= \langle \Psi | \mathrm{T}\{ \hat{U}_F \hat{U}_L \hat{U}_R \hat{U}_P \} | \Psi \rangle \Big|_{\{x_F^-, x_P^-\} \to \{-x_F^-, -x_P^-\}} \\
&= Z_{\text{Poincaré}},
\end{aligned}
\tag{2.99}
$$

where we used the orthonormality of $|N\rangle$ to get to the second equality, and the fact that all future and past operators lie to the future and past of the L, R wedges respectively, and that L wedge operators commute with those of the R wedge, to get to the third equality. Again, the $\{x_F^-, x_P^-\} \to \{-x_F^-, -x_P^-\}$ applies only to source points in $\hat{U}_F$ and $\hat{U}_P$, correcting the naive "wrong." We have thereby demonstrated that our trace formula and its thermofield equivalent correctly reproduce arbitrary (local) CFT correlators in Minkowski space as captured by the dual AdS EFT.

The i^Δ factors needed to achieve the above agreement may seem unusual, but they are just what one should expect of a conformal transformation law of a scalar primary $\mathcal{O}$, given our *improper* conformal transformation,

$$
\mathcal{O}' = \left(\frac{dx^+}{dx'^+} \right)^{\frac{\Delta}{2}} \left(\frac{dx^-}{dx'^-} \right)^{\frac{\Delta}{2}} \mathcal{O},
\tag{2.100}
$$

$x' = t, t' = x$ or $x'^+ = x^+, x'^- = -x^-$. Equivalently, in the F wedge, local operators $\mathcal{O}$

in the trace formula are reinterpreted as

$$e^{\frac{\pi}{2}(K-S)}\mathcal{O}(x^{\pm})e^{\frac{\pi}{2}(S-K)} = e^{-\frac{i\pi\Delta}{2}}\mathcal{O}(\pm x^{\pm}), \tag{2.101}$$

inside T-ordered matrix elements. Therefore there is a perfect match between our trace formula and the Minkowski/Poincaré formulation once these transformation factors are included.

In detail, we see that the F, P source terms in the trace formula must have extra i^{Δ} factors in order to yield a desired set of AdS$_{\text{Poincaré}}$ source terms. If we think of source terms as perturbations of the CFT Hamiltonian, then hermiticity of such perturbations implies that $\mathcal{J}$ is real for hermitian $\mathcal{O}$. Clearly, to get such sources for the AdS$_{\text{Poincaré}}$ correlators, we must start with *complex* sources ($i^{\Delta} \times$ real) in the trace formula, corresponding to *non-hermitian* CFT perturbations there. This appears to be an essential part of our construction following from the improper nature of the conformal transformation switching x and t. We will see a generalization of this feature for bulk sources.

2.8.6 Testing General Bulk Correlators

Finally, consider *bulk* source terms in F. As mentioned in subsection 2.8.4, this case is easiest if we have a bulk source which is analytic in z. Suppose our goal is to end up with a bulk correlator with a F region source

$$\int \frac{d^2x\,dy}{z^3}\mathcal{J}\phi = \int_0^{\infty} \frac{dz}{z}e^{-\frac{1}{a^2}(\log z - \log \bar{z})^2}\phi(t = \bar{t}, x = \bar{x}, z) \tag{2.102}$$

69

where

$$\mathcal{J}(t, x, z) = \delta(t - \bar{t})\delta(x - \bar{x})z^2 e^{-\frac{1}{a^2}(\log z - \log \bar{z})^2} \tag{2.103}$$

This is a nice Gaussian function of proper distance in the z direction, with size set by a, which can be as small as desired. Note that this source term is analytic in z throughout the set of rotated values in (2.92), and falls off rapidly as $|z| \to 0, \infty$. To obtain such a source for our AdS$_{\text{Poincaré}}$ correlator, we have seen in subsection 2.8.4 that we must begin in the trace formula with a source which analytically continues to the target source above, as $z \to iz$. That is, in the trace formula we must begin with

$$\int \frac{d^2x\, dy}{z^3}\mathcal{J}\phi = \int_0^\infty \frac{dz}{z} e^{-\frac{1}{a^2}\left(\log z - \log \bar{z} - i\frac{\pi}{2}\right)^2} \phi(t = \bar{x}, x = \bar{t}, z) \tag{2.104}$$

where

$$\mathcal{J}(t, x, z) = \delta(t - \bar{x})\delta(x - \bar{t})z^2 e^{-\frac{1}{a^2}\left(\log z - \log \bar{z} - i\frac{\pi}{2}\right)^2} \tag{2.105}$$

As discussed earlier, the trading of $\bar{x}$ and $\bar{t}$ will be fixed by the action of $e^{\frac{\pi}{2}(S-K)}$. The analytic z integrand clearly becomes the target source integrand upon performing the $z \to iz$ move of (2.92).

Again, what is unusual about such a source term for a real bulk field ϕ is that it is not real, and therefore corresponds to a non-hermitian perturbation of a (diffeomorphism gauge-fixed) bulk Hamiltonian. Of course, one can break up such complex sources into real and imaginary parts, so that we reproduce our target AdS$_{\text{Poincaré}}$ correlators/sources by taking straightforward complex linear combintations of the corresponding trace formula correlators. With this slightly non-trivial matching of source terms, the results of subsection 2.8.4 again

70

translate into the trace formula reproducing the $\text{AdS}_{\text{Poincaré}}$ correlators (integrated against the target sources).

The non-trivial matching of sources is to be expected once we take into account that the trace formula reinterprets $x \leftrightarrow t$ in the CFT in the F region (and similarly for P), the result of $e^{\frac{\pi}{2}(K-S)} \mathcal{O}(x^{\pm}) e^{\frac{\pi}{2}(S-K)}$ for any operator $\mathcal{O}$ whether local or non-local. When a bulk field operator (in some diffeomorphism gauge-fixed formulation of quantum gravity), $\phi(x^{\pm}, z)$, corresponds to *some* kind of non-local CFT operator by AdS/CFT duality, it should be reinterpreted in the trace formula as

$$e^{\frac{\pi}{2}(K-S)} \phi(x^{\pm}, z) e^{\frac{\pi}{2}(S-K)} = \phi(\pm x^{\pm}, iz), \qquad (2.106)$$

if it lies in F, inside T-ordered matrix elements. Of course the bulk field for imaginary z on the right-hand side is not *a priori* well-defined, so this equation should be thought of as a short-hand for our main result: for analytic sources the $\text{AdS}_{\text{Poincaré}}$ sources match the trace formula sources via continuation $z \to -iz$ for F/P regions.

2.9 Finite r_S: BTZ/CFT

2.9.1 Finiteness of BTZ EFT correlators

We consider bulk or boundary correlators of the BTZ black hole, with sources anywhere in the *extended spacetime* (including inside the horizon, or even beyond the singularity in the whiskers), as long as bulk sources are analytic in z in the manner discussed in subsection 2.8.6. In the gravitational EFT these BTZ correlators are obtained by the method

of images applied to AdS$_{\text{Poincaré}}$, in particular the (scalar) propagator in BTZ has the form,

$$
\begin{aligned}
G_{BTZ}(x^\pm, z; y^\pm, z') &= \sum_{n=-\infty}^{\infty} G_{AdS}(\lambda^n x^\pm, \lambda^n z; y^\pm, z') \\
&= \sum_{n=-\infty}^{\infty} \xi_n^\Delta F(\xi_n^2),
\end{aligned}
\tag{2.107}
$$

where, as in Section 2.5, we define for convenience

$$
\lambda \equiv e^{rs}.
\tag{2.108}
$$

The second line of (2.107) follows from (2.90) and (2.91), where

$$
\xi_n \equiv \frac{2\lambda^n z z'}{\lambda^{2n} z^2 + z'^2 - (\lambda^n x^+ - y^+)(\lambda^n x^- - y^-) + i\epsilon(\lambda^n x^0 - y^0)^2}.
\tag{2.109}
$$

A central question is the mathematical finiteness of such EFT correlators, given that the associated Feynman diagrams generally traverse the singularity. This can be understood by looking at the large image-number contributions in the above sum, where

$$
\xi_n \xrightarrow[n\to\infty]{} \frac{2zz'}{\lambda^n(z^2 - x^+ x^- + i\epsilon(x^0)^2) + \mathcal{O}(1)}
\tag{2.110}
$$

implies that for generic points the summand $\propto \lambda^{-n\Delta} F(0)$ for large n and hence the sum converges rapidly. However, at the singular surface, $z^2 - x^+ x^- = 0$, *if* we neglect the $i\epsilon$, we see that ξ_n and hence the summand, become n-independent for large n, and the sum diverges. This is the diagrammatic root of the singularity. Once we take into account the $i\epsilon$ term we see that we always get a convergent sum again, but for diagrams to remain finite

after the ultimate $\epsilon \to 0$ requires major cancellations before that limit is taken. We studied the simplest examples of this situation and such cancellations in Section 2.5, but in general correlators the requisite cancellations are not immediately apparent. Nevertheless they do take place, as we now show in a simple and general way.

Let us again perform the complex rotation of all z coordinates as we did in (2.92), but now stopping at an intermediate value of $\beta = \pi/2$,

$$z \to \frac{1+i}{\sqrt{2}} z, \quad z > 0. \tag{2.111}$$

As discussed in Section 2.8, this simply represents a passive deformation of z-integration contours in the complex plane for interaction vertices and bulk endpoints (with analytic sources as in subsection 2.8.6), and multiplication by some phases for boundary endpoints. Therefore this "move" does not affect the finiteness of the correlator. But now we see that for *all* points in BTZ, we have

$$\xi_n \xrightarrow[n \to \infty]{} \frac{2izz'}{\lambda^n(iz^2 - x^+x^-) + \mathcal{O}(1)}, \tag{2.112}$$

so that the propagator summand $\propto \lambda^{-n\Delta} F(0)$ always for large n, the sum converges, and the correlator is indeed finite (even as $\epsilon \to 0$). It is crucial to note that this finiteness required integrating over all $z > 0$ in the first place, so that inside the horizon we are integrating both inside and outside the singularity. Therefore finiteness required inclusion of the whisker regions.

The relationship between BTZ and the covering spacetime AdS$_{\text{Poincaré}}$ diagrammatics

is most straightforwardly seen in the (leading) tree-level diagrams of EFT, as illustrated in Fig. 2.11. We draw the BTZ spacetime as filling in the Lorentzian torus, to topologically make a *solid* torus with the Lorentzian torus surface as its boundary. In order to view BTZ like this we have switched the roles of the two circles of the Lorentzian torus with respect to Fig. 2.4. Specifically, we generalize (2.29) to the bulk,

$$t = e^\alpha \sin\zeta \sin\theta \qquad x = e^\alpha \sin\zeta \cos\theta \qquad z = e^\alpha \cos\zeta \qquad \left(0 \le \zeta \le \tfrac{\pi}{2}\right). \qquad (2.113)$$

We compare diagrams in the solid torus with diagrams in $\text{AdS}_{\text{Poincaré}}$, which we view in the above coordinates as a solid Lorentzian cylinder by first removing the origin. Its boundary, the surface of that cylinder, is interpreted as $1 + 1$ Minkowski spacetime with the origin removed in α, θ coordinate space. In this representation, the solid torus is simply the quotient of the solid cylinder by a discrete α translation, periodizing the direction along the cylinder's length. Figs. 2.11b and 2.11d show tree diagrams on $\text{AdS}_{\text{Poincaré}}$ (as the solid cylinder) where the endpoints of both diagrams are (examples of) images of the same set of endpoints for a BTZ (solid torus) correlator. Wrapping the AdS diagrams onto BTZ in Figs. 2.11a and 2.11c, the two $\text{AdS}_{\text{Poincaré}}$ diagrams appear as different contributions to the same BTZ correlator, but with different image terms for one of the propagators. In this way, by adding up all connected tree $\text{AdS}_{\text{Poincaré}}$ diagrams with end points being images of the desired BTZ correlator, we get the tree-level BTZ diagram, where every BTZ propagator is a sum over AdS image propagators.
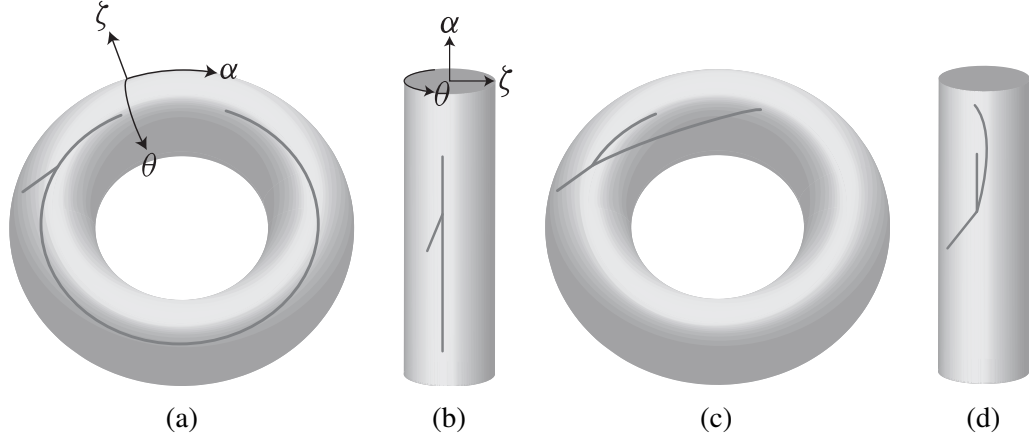
Figure 2.11: Relationship between bulk tree level BTZ diagrams and the corresponding diagrams on the AdS$_{\text{Poincaré}}$ covering space. The dark gray lines are to be interpreted as propagators inside the gray solids (although they may end on the surface).

2.9.2 Local boundary correlators: EFT dominance and scattering behind the horizon

While EFT correlators are finite in BTZ, as described above, this in itself does not prove that these finite correlators dominate the true correlators, which may also include the contributions of heavy states of the UV complete quantum gravity. It is also not immediately obvious that these BTZ correlators sharply probe scattering processes inside the horizon in the same way that AdS$_{\text{Poincaré}}$ correlators probe scattering behind the Rindler horizon. However, both these properties are indeed true of the "protected" set of local boundary correlators of BTZ realized as a quotient of AdS$_{\text{Poincaré}}$. (Bulk correlators contain extra UV sensitivity, as do the more general boundary correlators in the BTZ realization as a quotient of AdS$_{\text{global}}$ [48].)

We first demonstrate that for $\lambda \equiv e^{rs} \gg 1$, local boundary EFT correlators are dominated by $n = 0$ in the sum over images in each propagator, (2.107). This follows after

75

rotating z by $\beta = \pi/2$ in the complex plane, (2.111), so that for large λ and $x^{\pm}, z, y^{\pm}, z' \sim$ $\mathcal{O}(1)$ in propagators, all other terms are $\sim \mathcal{O}(\lambda^{-|n|\Delta})$. The scaling, $x^{\pm}, z, y^{\pm}, z' \sim \mathcal{O}(1)$ in λ follows, even though these arguments are being integrated, if the boundary endpoints $x_i^{\pm}$ (which determine the region of convergence of the integrals) are chosen $\mathcal{O}(1)$. That is, after rotation of z, it is as if there were no singularity, just a very large but compact σ direction, and the resulting diagrams are *dominated by the equivalent un-imaged diagrams in the covering* $AdS_{Poincaré}$ *spacetime*. In particular, since these un-imaged diagrams describe scattering behind the Rindler horizon, the BTZ correlators must describe scattering behind the quotient of the Rindler horizon, namely the black hole horizon.

Because we are limiting ourselves to the Poincaré patch of AdS and its quotient, we are restricted in how "sharp" scattering processes can be when initiated and detected from the boundary. The reason is that we have to send and receive scattering waves from the boundary at $z = 0$, naively suggesting a violation of z-momentum conservation. Indeed, z-translation invariance is broken by warping but this does not allow us to scatter waves with z-wavelengths much smaller than the AdS radius of curvature using boundary correlators. On the other hand, there is no similar obstruction to how small the x-wavelength can be. Wavepackets with z-wavelengths of order R_{AdS} and much smaller x-wavelengths can be aimed so that scattering definitely only takes place inside the horizon, and predominantly away from the singularity. They thereby give us access to reasonably sharp probes of inside-horizon scattering, but obviously not the most general scattering processes. In short, the sharpness of BTZ boundary correlators is the same as for $AdS_{Poincare}$ boundary correlators.

Since we are dominated by the un-imaged $AdS_{Poincaré}$ correlators, with $\mathcal{O}(e^{-|n|r_S\Delta})$ corrections to ensure BTZ compactness (in σ), it follows that EFT dominates the boundary

76

correlators as it does in AdS$_{\text{Poincaré}}$. Even if we included a very heavy particle into the Feynman rules, it can be integrated out in the leading $n = 0$ contribution as in AdS, inducing only contact effective interactions among the light EFT states. We will see that this UV-insensitivity is not the case for the subleading $\mathcal{O}(e^{-|n|r_S\Delta})$ effects in Section 2.10, and that the effects of large cosmological blueshifts near the singularity are indeed present.

It may appear that *bulk* correlators are similarly protected by the above reasoning, but it is important to understand why this is not the case. The subtlety is that the above analysis required first performing the complex rotation of (2.111). As we have seen, this only changes Witten diagram contributions to boundary correlators by complex phase factors, so that estimates for the magnitudes of different contributions apply straightforwardly to the original correlator before rotation. However, this is not the case for bulk correlators, where bulk sources have to be analytically continued to accomplish (2.111), as discussed in subsection 2.8.6. In general, such analytic continuations will completely change the magnitudes of different contributions. Therefore estimates performed after (2.112) do not apply to the original BTZ correlators before (2.112). Indeed we will give an example of bulk correlator UV sensitivity in Section 2.10.

If the σ circle were always very large there would be no surprise that the correlators approximate those of non-compact σ, namely AdS$_{\text{Poincaré}}$. But it is at first surprising here that the $n \neq 0$ corrections are small even for Witten diagrams passing through the singularity, where the physical size of the σ circle is going to zero, as seen in the Schwarzchild metric of (2.4). We will see the deeper reason for this in subsection 2.9.5.

2.9.3 Method of Images applied to Rindler AdS/CFT

We now use the method of images to go to the finite r_S (compact σ direction) analog of (2.84), relating local EFT correlators anywhere in BTZ to (non-local) EFT correlators in two copies of the outside-horizon BTZ with thermofield entanglement:

$$Z_{\text{BTZ}} = {}_{\text{HH}}\langle\Psi| \left[\mathbb{1} \otimes (\text{T}_\tau \, \hat{U}_F)^\dagger \right] \left[e^{\pi P_-} \otimes e^{-\pi P_-} \right]$$

$$\times \left[(\text{T}_\tau \, \hat{U}_L) \otimes (\text{T}_\tau \, \hat{U}_R) \right] \left[e^{-\pi P_-} \otimes e^{\pi P_-} \right] \left[(\text{T}_\tau \, \hat{U}_P)^\dagger \otimes \mathbb{1} \right] |\Psi\rangle_{\text{HH}}. \quad (2.114)$$

The left-hand side is the generating functional of the bulk or boundary correlators of the BTZ black hole discussed above, with any bulk sources being analytic in z. The right-hand side is written in terms of the thermofield state formed by two copies of the *outside-horizon* ($r > 1$) portion of the Schwarzschild view of the BTZ black hole. (Of course these two copies can then be thought of as the outside-horizon portions of a single extended BTZ black hole.) This outside-horizon geometry is just the quotient of the AdS$_{\text{Rindler}}$ wedge of AdS$_{\text{Poincaré}}$. The time and space translation generators on the right-hand side are with respect to the τ, σ directions of the Schwarzschild coordinates for the BTZ black hole, and the fields in all source terms on the right-hand side live only outside the horizon.

The derivation of (2.114) from (2.84) is more transparent when the right-hand side is written in trace form,

$$Z_{\text{BTZ}} = \text{tr}_{\text{outside}}(\text{T}_\tau \, \hat{U}_L) e^{-\pi P_+} (\text{T}_\tau \, \hat{U}_F)^\dagger e^{-\pi P_-} (\text{T}_\tau \, \hat{U}_R) e^{-\pi P_+} (\text{T}_\tau \, \hat{U}_P)^\dagger e^{-\pi P_-}, \quad (2.115)$$

where the trace is over the Hilbert space on one copy of the outside-horizon region. This equation is just the quotient of the analogous non-compact statement, where the left-hand side is the generating functional for AdS$_{\text{Poincaré}}$ correlators and the right-hand side is a trace over the Hilbert space on AdS$_{\text{Rindler}}$. On both sides, the compact result follows by imaging the relevant type of propagator and keeping coordinates within a fundamental region. As pointed in the discussion below (2.59), the exponential weights in (2.115) are a net suppression of high energy excitations of the Schwarzchild spacetime (outside the horizon), and therefore the right-hand sides of (2.114) and (2.115) are mathematically well-defined, matching the good behavior we have found for the left-hand side.

As discussed below (2.64), one can think of local correlators ending inside the horizon (including whiskers) on the left-hand side of (2.114) as being equal to correlators outside the horizon for non-local operators of the form $e^{\pi P_-}\mathcal{O}_{\text{local}}e^{-\pi P_-}$ on the right-hand side. So far we have established that local boundary correlators in BTZ are EFT-dominated and finite, but we still have not given a physical interpretation of such correlators when they end in the whiskers, problematic due to the time-like closed curves. However, for local boundary correlators, the right-hand side of (2.114) gives such a simple interpretation. Defining states,

$$|\Psi_P\rangle_{\text{outside}} \equiv \left[e^{-\pi P_-} \otimes e^{\pi P_-}\right]\left[(\mathrm{T}_\tau \, \hat{U}_P)^\dagger \otimes \mathbb{1}\right]|\Psi\rangle_{\text{outside}}$$
$$|\Psi_F\rangle_{\text{outside}} \equiv \left[e^{-\pi P_-} \otimes e^{\pi P_-}\right]\left[(\mathrm{T}_\tau \, \hat{U}_P)^\dagger \otimes \mathbb{1}\right]|\Psi\rangle_{\text{outside}},$$

(2.116)

Eq. (2.114) can be re-written

$$Z_{\text{BTZ}} = \langle\Psi_F|(\mathrm{T}_\tau \, \hat{U}_L) \otimes (\mathrm{T}_\tau \, \hat{U}_R)|\Psi_L\rangle$$

(2.117)

That is, the correlators including possible endpoints in the whisker boundaries are equal to correlators with endpoints only on the boundaries outside the horizon, but with the thermofield state being replaced by the modified $|\Psi_{P,F}\rangle$ states. Given that we have established that such correlators are dominated by the non-compact $\text{AdS}_{\text{Poincaré}}$ EFT correlators (image terms being subdominant), we can readily interpret these new states. In non-compact correlators, endpoints in the F (say) boundary just act to "detect" the results of earlier scattering inside the Rindler horizon, or evolving backwards, they set up "out" states, $|\Psi_F\rangle$ which sharply probe the results of the scattering process. The same must therefore be true after quotienting to BTZ, where the F boundary is the whisker boundary. In summary, the whisker regions can be thought of as an auxiliary spacetime in which the local boundary correlator endpoints encode non-local operators that sculpt the thermofield state into a variety of "in" and "out" states that probe the results of scattering inside the horizon, very much as do F/P boundary correlators in $\text{AdS}_{\text{Poincaré}}$. Furthermore, the local boundary correlators of BTZ are diffeomorphism invariants of quantum gravity.

2.9.4   Connecting to CFT Dual on ∂BTZ

It remains to connect (2.114) to the CFT thermofield form of (2.64), (2.69), or equivalently the CFT on the Lorentzian torus $\equiv \partial BTZ$. The diagrammatic expansion in the bulk theory is dual to a large-N_{CFT} expansion in a CFT gauge theory. At infinite r_S, tree diagrams such as Fig. 2.11b capture the same physics as the planar diagrams of Fig. 2.12b in the dual CFT, by standard AdS/CFT duality. Just as Fig. 2.11b maps to contributions to BTZ correlators for specific fixed images in Fig. 2.11a, Fig. 2.12b maps to planar diagrams of
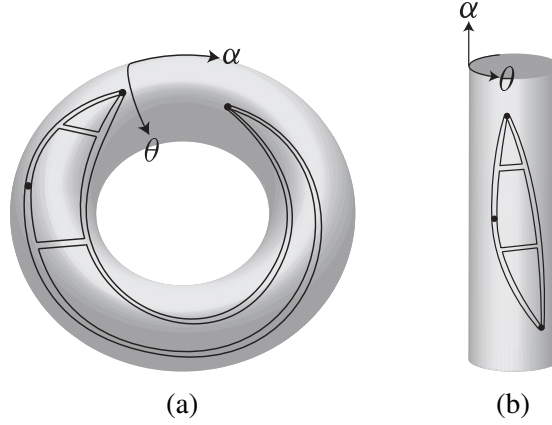
Figure 2.12: Relationship between planar CFT diagrams in double-line notation (reviewed in [1]) on the Lorentzian torus and its covering space, the Lorentzian cylinder. These CFT "gluon" lines are to be interpreted as propagating on the boundary surfaces of the gray solids in Fig. 2.11. The black dots represent local CFT operators.

the CFT on the Lorentzian torus in Fig. 2.12a , as discussed in more detail for the example of subsection 2.5.5. Equivalently, we have seen that we can use the right-hand side of (2.114) for BTZ tree amplitudes, and these are then identified with the careful construction of (2.57), (2.58) for the CFT on the Lorentzian torus at planar order. That is, the method of images straightforwardly identifies the bulk tree amplitudes to planar CFT amplitudes, either directly on (∂)BTZ or in equivalent thermofield form. The value in the CFT construction of (2.57), (2.58) however is that it includes a UV-complete and non-perturbative (in $1/N_{\text{CFT}}$) description of the approach to the singularity, even when bulk EFT eventually completely breaks down.

Naively, at the same planar order in the CFT there are also diagrams which "wrap" around the torus in the α direction, such as Fig. 2.13a, which do not descend from cylinder (Minkowski) planar diagrams by the method of images, and yet are of the same order in N_{CFT}. These diagrams necessarily break up a minimal color singlet combination of "gluons" and send some of them to an operator and the remainder to its image (Fig. 2.13b).

(a)   (b)
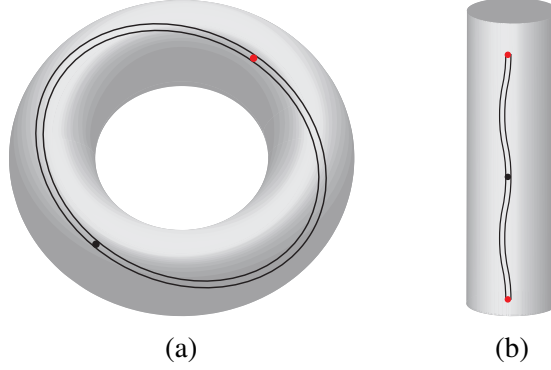
Figure 2.13: Naively, there are diagrams at leading order in N_{CFT}, such as (a), but which unwrap to diagrams in Minkowski space, such as (b), which violate gauge invariance (for example, gauge non-singlets are created by different images of the same operator). Such contributions vanish by gauge invariance.

But in the full gauge-invariant path integral on the torus such diagrams are constrained to vanish. This is a familiar fact if we think of the α direction as "time" (now that we are acclimatized to choosing the "time" direction for our convenience): the non-abelian Gauss Law constraint says that only gauge-invariant states propagating around the α direction are physical, whereas any part of of a minimal color singlet cannot be gauge-invariant. Closely analogous to this, in equilibrium thermal gauge theory it is the Gauss Law constraint that enforces that only gauge invariant states can circle around compact imaginary time (equivalently, the thermal trace is only over gauge-invariant states).

At nonplanar order in the CFT, there are subleading diagrams that can be identified with the loop-level bulk diagrams that unitarize the tree-level contributions. But there are also new CFT contributions not of this form, namely creation and destruction of finite-energy Wilson-loop states winding around the compact σ direction. These have no analog in the non-compact case. In BTZ, these are dual to quantum gravity states, generically finite-energy "strings", that wind around the bulk σ circle, but which have no analog in non-compact AdS$_{\text{Poincaré}}$. The effects of such extended objects cannot be captured by the simple

82

diagrammatic method of images we have followed for BTZ. If the extended objects have tension then the winding states will ordinarily be extremely heavy for large r_S, and thereby give exponentially suppressed virtual contributions to correlators between well-separated source points. But approaching the singularity, the physical σ-circumference approaches zero, as seen in the Schwarzchild metric, (2.4), and the winding states can become light. They are then part of the normally-UV physics which becomes important near the singularity. See [47] for discussion within string theory. We expect this physics to be contained in our CFT proposal for the non-perturbative BTZ dual, but not part of the EFT checks we have performed in the regime where we argued EFT should dominate.

Finally, beyond any order in $1/N_{\mathrm{CFT}}$, the CFT correlators will have effects, not matching bulk EFT or even perturbative string theory. They may well play an important role near the singularity.

2.9.5 Deeper reason for insensitivity to singularity

Our diagrammatic derivations have non-trivially confirmed our formal CFT expectations for local correlators set forth in (2.64). But this does not explain *why* EFT is well-behaved despite the singularity, why technically there was a way to deform the contour for interaction vertex integrals so as to avoid the perturbative face of the singularity in image sums, and for boundary correlators why these image sums converge so rapidly. We might also worry that EFT misses important UV physics near the singularity, such as heavy particles or the winding states mentioned above. In general, we therefore want to understand whether to trust EFT at all for boundary correlators, especially when some endpoints are in the whiskers.
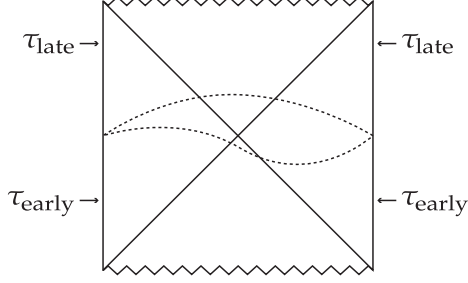
Figure 2.14: The dashed curves represent two spacelike hypersurfaces that are related by bulk diffeomorphisms.

We begin with non-compact AdS$_{\text{Poincaré}}$ where we understand the diagrammatic expansion. We have formally motivated and then diagrammatically derived the Rindler AdS/CFT result of (2.84) and more compactly, (2.64). The typical local boundary correlator of AdS$_{\text{Poincaré}}$ is thereby re-expressed on the right-hand sides using (2.65),

$$\langle\Psi|\{\mathbb{1}\otimes\overline{T}_\tau[(e^{\pi P_-}\mathcal{O}_1^F e^{-\pi P_-})....(e^{\pi P_-}\mathcal{O}_{n_F}^F e^{-\pi P_-})]\}$$

$$\times\{T_\tau[\mathcal{O}_1^L....\mathcal{O}_{n_L}^L]\otimes T_\tau[\mathcal{O}_1^R....\mathcal{O}_{n_R}^R]\}\{\mathbb{1}\otimes\overline{T}_\tau[(e^{\pi P_-}\mathcal{O}_1^P e^{-\pi P_-})....(e^{\pi P_-}\mathcal{O}_{n_P}^F e^{-\pi P_-})]\}|\Psi\rangle,$$

$$(2.118)$$

where the $\mathcal{O}$ are local Heisenberg operators of the CFT or local boundary operators of AdS. The operators of the form $e^{\pi P_-}\mathcal{O}e^{-\pi P_-}$ are then non-local, but only in the spatial sense. Time evolution, implicit in the Heisenberg operators, ranges between the earliest and latest times that appear in any of the $\mathcal{O}$ operators above, τ_{early}, τ_{late}, say. It is important to note that this time evolution does not go all the way from $\tau = -\infty$ to $\tau = +\infty$. This is no surprise because we have a (generalized) in-in formalism [50, 51] (see [52] for a modern discussion and review) in the thermofield form for correlators. We represent this situation in the Penrose diagram of Fig. 2.14, where the symmetry σ direction is omitted, but is now non-

compact $-\infty < \sigma < \infty$. The spacelike hypersurfaces are pinned on the boundary by the boundary time evolution, but their form in the bulk is otherwise arbitrary by diffeomorphism invariance. What is not immediately obvious from the figure, but straightforwardly verified by the AdS$_{\text{Poincaré}}$ metric, is that all such hypersurfaces pinned to the boundary outside the (Rindler) horizon cannot go beyond the jagged lines at any point. This is the only significance of the jagged lines in Fig. 2.14 since there is of course no singularity in AdS. We have depicted the simplest choice of such hypersurfaces.

The central point when we move to the compact BTZ case for such correlators, as in (2.114), is that Fig. 2.14 still holds, but now with the omitted σ direction of course being compact, and the jagged lines depicting the location of the singularity. What we see is that in deriving (2.114) from (2.84) we are only trusting the diagrammatic expansion and the method of images to compactify σ *away from the singularity*. As long as $\tau_{\text{early/late}}$ are not too early or late, the physical circumference of the σ circle can be taken to be large throughout the time evolution and it is not surprising if our correlators are dominated by the non-compact limit and insensitive to the UV physics of the singularity. In particular, winding states will be very massive throughout this evolution.

2.10   Sensing Near-Singularity Physics

A good part of this chapter has been concerned with the validity and use of bulk EFT and the diagrammatic expansion in order to capture scattering processes behind the BTZ horizon. This has allowed us to test our proposed non-perturbative CFT formulation under conditions where we already know what to expect. However, the real importance of such a

CFT formulation is that it allows us to study processes close to the singularity, where large cosmological blue-shifts make the physics very UV sensitive and EFT breaks down. In this section, we want to demonstrate that the UV-sensitive physics near the singularity is certainly present in the BTZ quantum gravity and that whisker correlators and their CFT duals can detect this. To do this, we will show under what circumstances we become sensitive to heavy states beyond EFT, and yet without such sensitivity invalidating our derivations.

We know that we see divergences if correlator endpoints are right on the singularity, as simply illustrated just by (2.21). But EFT should come with some effective cutoff length, below which we do not ask questions. If we simply move correlator endpoints more than the cutoff length away from the singularity they are finite and the cosmological blueshifts are more modest. But mathematical finiteness is not necessarily the same as insensitivity to heavy states. We begin by demonstrating that even at distances/times of order R_{AdS} away from the singularity, correlators are sensitive to the UV heavy states outside BTZ EFT. To do this we move the point in the F wedge of our Section 2.5 example correlator from the boundary to the interior and consider

$$
\langle \tilde{\phi}_F(x_F, z') \mathcal{O}(x_{R_1}) \mathcal{O}(x_{R_2}) \rangle_{\text{tree BTZ}}
$$
$$
= \int_{\text{fund.}} d^2 y \, dz \, \sqrt{g} \, \tilde{G}_{\text{BTZ}}(x_F, z'; y, z) g^{MN} \partial_M K(x_{R_1}; y, z) \partial_N K(x_{R_2}; y, z). \quad (2.119)
$$

We assume from now on that $\tilde{\Delta} \gg 1$ and corresponds (via $\tilde{m}^2 = \tilde{\Delta}(\tilde{\Delta} - 2)$) to some heavy particle of BTZ quantum gravity that is more massive than the cutoff of BTZ EFT ("string excitations"). We are going to show that we are sensitive to such states at order R_{AdS} separations from the singularity.

Choose x_F, z' to have timelike geodesic to some points on the singularity, with proper times to these points $< R_{\text{AdS}}(\equiv 1)$, but much larger than the cutoff length. For example, $x_F^\pm = \pm(z' - \delta)$, $\delta < 1$ and near-singularity points ($y^\pm \sim \pm z', z \sim z'$) are related in this way. For such small separations, the bulk propagator can be approximated by its $2 + 1$ local Minkowski equivalent,

$$\tilde{G}_{\text{AdS}} \approx \frac{z' e^{i \frac{\tilde{\Delta}}{z'} \sqrt{(x_F - y)^2 - (z - z')^2 - i\epsilon(x_F^0 - y^0)^2}}}{\sqrt{(x_F - y)^2 - (z - z')^2 - i\epsilon(x_F^0 - y^0)^2}}, \qquad (2.120)$$

where z' is the approximately constant redshift of the inertial $2 + 1$ Minkowski patch. $\tilde{G}_{\text{BTZ}}$ is of course obtained by images of (y, z) from $\tilde{G}_{\text{AdS}}$. Combining this sum with integration of interaction points over the fundamental region to get integration over all $\text{AdS}_{\text{Poincaré}}$, similarly to (2.43),

$$\langle \tilde{\phi} \mathcal{O}_1 \mathcal{O}_2 \rangle \sim \int_{\text{AdS}} d^2 y\, dz \sqrt{g} \, \frac{z' e^{i \frac{\tilde{\Delta}}{z'} \sqrt{(x_F - y)^2 - (z - z')^2 - i\epsilon(x_F^0 - y^0)^2}}}{\sqrt{(x_F - y)^2 - (z - z')^2 - i\epsilon(x_F^0 - y^0)^2}} g^{MN} \partial_M K_1 \partial_N K_2 + \cdots .$$

$$(2.121)$$

The ellipsis corresponds to integration over interaction points outside R_{AdS} of $(x_F^\pm, z)$ and interaction points spacelike separated from $(x_F^\pm, z)$. For either of these, the Minkowski-dominance approximation breaks down, but precisely so as to suppress these contributions for very large $\tilde{\Delta}$. We are therefore correctly focused on the small timelike separation region.

We again zoom in on the contribution from (y, z) near the singularity and switch to

Schwarzschild coordinates:

$$\langle \tilde{\phi} \mathcal{O}_1 \mathcal{O}_2 \rangle \underset{r \to 0}{\sim} \int_{-r_0}^{r_0} \frac{dr d\sigma d\tau \, r}{(r + i\epsilon)^2} \frac{e^{i\tilde{\Delta}\sqrt{2 - 2rr'\cosh(\sigma - \sigma') + (r^2 + r'^2 - 2)\cosh(\tau - \tau')}}}{\sqrt{2 - 2rr'\cosh(\sigma - \sigma') + (r^2 + r'^2 - 2)\cosh(\tau - \tau')}}$$

$$\sim \int_{-r_0}^{r_0} \frac{dr d\sigma d\tau \, r}{(r + i\epsilon)^2} \frac{e^{i\tilde{\Delta}\sqrt{(r'-r)^2 - (\tau - \tau')^2}}}{\sqrt{(r' - r)^2 - (\tau - \tau')^2}},$$

$$(2.122)$$

with $(\sigma - \sigma')$, $(\tau - \tau')$, r, r' all small, but only $r \to 0$. As $r \to 0$, timelike separation to

(x_F, z) requires $r'^2 > (\tau - \tau')^2$, so

$$\langle \tilde{\phi} \mathcal{O}_1 \mathcal{O}_2 \rangle_{\text{BTZ}} \sim \int_{-r_0}^{r_0} \frac{dr d\sigma d\tau}{r + i\epsilon} e^{\pm i\tilde{\Delta}(r - r')}. \tag{2.123}$$

The behavior at $\pm r_0$ is smooth so we are basically computing the Fourier transform of $\frac{1}{r + i\epsilon}$.

As $\epsilon \to 0$, we have unsuppressed Fourier components and there is no suppression for large

$\tilde{\Delta}$. In other words the particles sent in from the R wedge are able to produce cutoff scale

heavy particles that can propagate far away from singularity. Therefore these heavy states

cannot simply be integrated out by r', even though $l_{\text{cutoff}} \sim \frac{1}{\tilde{\Delta}} \ll r' < 1$. So EFT cannot be

trusted at r'.

We can contrast this situation with with the analogous $\text{AdS}_{\text{Poincaré}}$ correlators (not BTZ):

$$\langle \tilde{\phi}(x_F, z') \mathcal{O}_{R_1} \mathcal{O}_{R_2} \rangle_{\text{AdS}} = \int d^2 y \, dz \sqrt{g} \, \tilde{G}_{\text{AdS}} g_{\text{AdS}}^{MN} \partial_M K_1^{\text{AdS}} \partial_N K_2^{\text{AdS}}. \tag{2.124}$$

Without any infinite image sums, the K's are smoothly varying on $R_{\text{AdS}} \equiv 1$ length scales,

except on light cones from $x_{1,2}$. We take $(x_F^{\pm}, z')$ to be away from these lightcones. For

$\tilde{\Delta} \gg 1$ not to be the exponent of a suppression, (y, z) must be timelike separated with

separation $< R_{\text{AdS}}$. Therefore in looking for unsuppressed contributions, (y, z) can also be taken away from $x_{1,2}$ lightcones. But then $\tilde{G}$ rapidly oscillates on $\frac{1}{\Delta}$ lengths, so its integral with the smooth $\partial K \partial K$ is highly suppressed. This is the standard reason for why we can integrate out heavy $\tilde{\phi}$ in long-wavelength processes. In AdS$_{\text{Poincaré}}$ we do not see the kind of breakdown of gravitational EFT that we see in BTZ.

It is important to note that the BTZ sensitivity to heavy particles, just illustrated, takes place in a correlator with one *bulk* endpoint. Thus it is not in contradiction with our general observation that the purely local boundary correlators are dominated by EFT. But it is the local boundary correlators that are most straightforwardly matched non-perturbatively to CFT correlators and ideally we want to use just these to detect the UV physics near the singularity. Fortunately, while we have shown that EFT dominates local boundary correlators, and even more strongly that the non-compact limit (AdS$_{\text{Poincaré}}$) dominates, this does not preclude the UV physics from residing in the small corrections to these leading approximations. The key then is to look at boundary correlators that vanish at the leading approximation, so that the small UV-sensitive effects dominate.

In the process we have considered that creates a heavy particle near the singularity using the large cosmological blueshift there, and propagates it into the whisker, the obvious way to get a purely local boundary correlator is to attach two light particle lines to the bulk point in Fig. 2.15a and then connect these to the whisker boundary, as in Fig. 2.15b. Using the ability to choose the boundary sources for the four boundary points, we can insist that the incoming beams are softer than the threshold for heavy particle production *unless* one takes into account the cosmological blueshifts, that is unless one looks at large image numbers in the propagators and not just $n = 0$ in the notation of (2.107). Similarly, we can choose sources
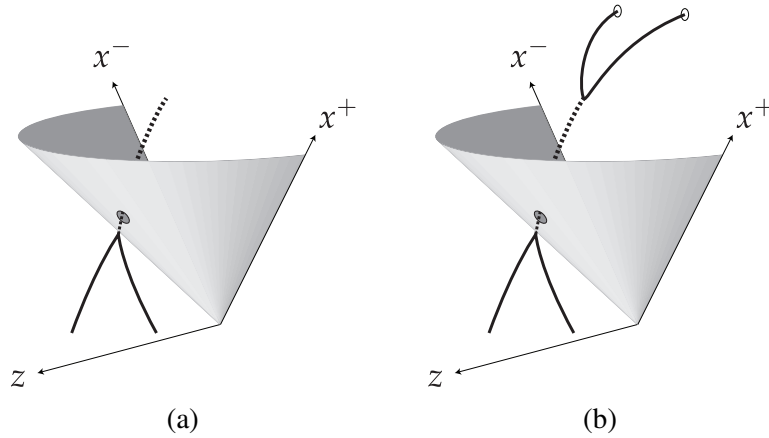
Figure 2.15: Sensitivity to the singularity. The cone marks the location of the singularity and the dashed line represents a heavy particle. The lower black lines represent two incoming particles that are initially subthreshold. The heavy particle can be produced due to blueshifting as the singularity is approached. In (b), the heavy particle subsequently decays and its decay products are received at the boundary.

for the boundary whisker points to be "looking" for hard particles coming from a point away from the singularity. In this way, we have chosen the boundary correlator to vanish at the usual leading approximation of the non-compact limit, but clearly the full correlator captures the heavy particle production near the singularity and its distant propagation. In fact it might seem that this UV sensitive BTZ boundary correlator is order one, in violation of our general result. But it is easy to see the source of suppression: if it were not for the warp factor we would expect z-momentum to be conserved, in which case the heavy particle produced from light particle beams originating at $z = 0$ would not "decay" into light particle beams which return to $z = 0$. Instead we would expect the final light particle beams to escape to large z and not contribute to this purely boundary correlator. The warp factor can indeed violate z-momentum conservation, but it is a very mild effect for hard incoming beams. This is the source of suppression of the boundary correlator that is in keeping with our general result. Therefore, the four-point correlator depicted in Fig. 2.15b is small, but the UV-sensitivity

dominates this small correlator. Using (2.64) and (2.114), we can write this correlator as a non-perturbatively well-defined CFT thermofield correlator. Of course there might be other UV physics which is harder to model, which would be picked up in similar fashion by our non-perturbative formulation. This is the central payoff of our work.

2.11 Comments and Conclusions

We have made a precise proposal for the non-perturbative CFT dual of quantum gravity and matter on a BTZ black hole, in terms of $1 + 1$ Minkowski CFTs with weakly-coupled, low-curvature $\text{AdS}_{\text{Poincaré}}$ duals, and provided several non-trivial checks. It extends the now-standard duality by making sense of a CFT "living" on the full BTZ boundary realized as a quotient of $\text{AdS}_{\text{Poincaré}}$, which includes "whisker regions" beyond the singularity containing timelike closed curves. We did this by observing that there are well-defined non-local generalizations, $e^{-\pi P_\pm}$, of the familiar Boltzmann weight, $e^{-\beta H}$, which effectively switch the roles of space and time inside the horizon, and turn the timelike circles into familiar spacelike circles. We then gave an equivalent thermofield construction of our CFT dual in which non-local correlators in the entangled CFTs are responsible for capturing the results of scattering inside the horizon, giving a concrete realization of complementarity.

We chose to realize BTZ as a quotient of $\text{AdS}_{\text{Poincaré}}$, rather than of $\text{AdS}_{\text{global}}$, based on its greater technical simplicity, and because the set of local boundary correlators in this smaller spacetime are "protected", in the sense of being dominated by gravitational effective field theory even when the contributing Witten diagrams traverse the singularity. This construction gave us the minimal extension of BTZ beyond the singularity to make contact

91

with boundary components within and to explore the role they play, even in just ensuring the mathematical finiteness of bulk amplitudes. But both $\text{AdS}_{\text{Poincaré}}$, and the portion of the extended BTZ spacetime it covers, are geodesically incomplete. Our CFT proposal "projects" this geodesically incomplete portion of BTZ in an analogous manner to the way in which CFT on Minkowski spacetime "projects" quantum gravity on geodesically incomplete $\text{AdS}_{\text{Poincaré}}$. Our CFT dual of BTZ lives on the Lorentzian torus, which is also incomplete because of geodesics that can "escape" by passing close to the lightlike circles. But in our careful construction we are cutting out thin wedges around the lightlike circles so this does not arise. Alternatively phrased, in our final construction we only use CFT on spacetime "pieces" of the cylindrical form circle $\times$ time. We will address the maximally extended BTZ spacetime arising from the quotient of $\text{AdS}_{\text{global}}$ in future work.

While analytic continuation played a role in this chapter, we believe it was a matter of calculational efficiency, rather than as a conceptual tool. For example, in subsection 2.5.4 studying scattering through the singularity, we arrived at the same conclusion by direct computation of BTZ diagrams and by rotating the interaction integral contour of the z-coordinate. In Section 2.8, we used analytic continuations as the simplest way of computing the non-local consequence of the $e^{-\pi P_\pm}$ "generalized Boltzmann weights". In principle one could directly do the integral over such weights without any continuations but it would be technically much harder. We have checked that the direct computation in *free* CFT gives the same result as analytic continuation.

We believe our approach should be closely generalizable to quotients of higher-dimensional AdS spacetimes [80] [81] [82]. These yield interesting black objects with horizons and singularities. Of course it would be a greater technical feat to obtain the dual of higher-

dimensional black holes or higher-dimensional cosmologies, without the advantage of a quotient construction from AdS, and with even worse (looking) singularities. It remains of great interest to understand the dual of evaporating black holes. We hope that the "Ising model" of black holes, BTZ, shares enough in common with other systems with horizons and singularities to provide hints on how to proceed.

In the chapter, we have viewed the whisker regions, in particular their boundary, as an auxiliary spacetime grafted onto the physical spacetime which is useful in defining states on the physical region, much as Euclidean spacetime grafts are useful in defining Hartle-Hawking states on physical spacetime. However, since the whiskers do have Lorentzian signature, it is intriguing to also see if they can be accorded any more direct physical reality. Once the whisker boundaries are added to the usual boundary regions outside the horizon, we saw that we arrive at a Lorentzian torus. Because of the existence of circular time in the whisker boundaries, the CFT path integral does not have a canonical quantum mechanical interpretation, in that we cannot simply specify any initial state in a Hilbert space and let it evolve. Instead the path integral gives us an entire quantum spacetime which we can ask questions of, in the form of correlations of Hermitian observables. In this sense, it has the form of a kind of wavefunction of the Universe.

Alternatively, we can think of our results as simply demonstrating that the extended black hole is a *robust emergent phenomenon* within a (single) "hot" CFT. For instance, we saw in subsection 2.7.1 that with sources restricted to being *outside* the horizon, in either exterior region L or R, our trace formula reduces to (2.60), which is equivalent to the standard thermofield description, (2.62), (2.63). Local sources in L can be thought of as

specific non-local sources in R, so that there is a single CFT in a thermal heat bath,

$$Z[J_{L,R}] = \text{tr}\left\{e^{-\beta H}\left[e^{\pi H}U_L e^{-\pi H}\right]U_R\right\}$$

(2.125)

where $\beta \equiv 2\pi$.

This is just a re-writing of the thermofield description as a thermal trace in a single CFT, rather than pure quantum mechanical evolution in two copies of the CFT. To describe observables in L, we see we have to take standard observables and "smear" them between $e^{\pi H}$ and $e^{-\pi H}$. In other words, local L observables are secretly just non-local observables in R. In this view there is only the R CFT in a heat bath, and the L is an "emergent" description to track certain non-local correlators. This is related to the discussion of the emergence of "doubling" of CFTs in subsection 5.1 of [59]. Now, the results of our chapter, in particular the last line of (2.64), has shown that the $U_{F,P}$ probes of the inside-horizon F, P regions can be thought of as "emerging" from non-local probes in the outside-horizon R and L regions, arising from "smearing" standard R, L observables between $e^{\pi P_-}$ and $e^{-\pi P_-}$. Putting all these observations together, we can think of probes anywhere in the extended black hole spacetime as emerging from non-local correlators in a single CFT with thermal density-matrix: Eq. (2.57) can be re-expressed as

$$Z[J_{L,R,F,P}] = \text{tr}\left\{e^{-\beta H}\left[e^{\pi H}(e^{\pi P_-}U_P^\dagger e^{-\pi P_-})U_L e^{-\pi H}\right](e^{\pi P_-}U_F^\dagger e^{-\pi P_-})U_R\right\}$$

(2.126)

where $\beta \equiv 2\pi$.

Non-local correlators in the thermal density matrix "project" the extended black hole, including the singularity. This follows from our results. In this way, there is a modest

"landscape" of regimes of the gravitational dual, connected by horizons. Possibly other

non-local operators, not of the forms above, may project other parts of the "landscape" of

the quantum gravity dual.

Chapter 3:   Natural Inflation and Quantum Gravity

3.1   Introduction

The success of modern cosmology is founded on the simplifying features of homogeneity, isotropy and spatial flatness of the Universe on the largest distances. In this limit, spacetime evolution is given in terms of a single scale-factor, $a(t)$, and its Hubble expansion rate, $H \equiv \dot{a}/a$. Homogeneity and flatness are themselves puzzling, constituting very special "initial" conditions from the viewpoint of the Hot Big Bang (HBB). But they become more robust if the HBB is preceded by an even earlier era of Cosmic Inflation, exponential expansion of the Universe driven by the dynamics of a scalar field ϕ (the "inflaton") coupled to General Relativity (see [83] for a review):

$$H^2 = \frac{8\pi G_N}{3} \left[\tfrac{1}{2}\dot{\phi}^2 + V(\phi) \right]$$

$$\ddot{\phi} + 3H\dot{\phi} + V' = 0. \tag{3.1}$$

(We work in fundamental units in which $\hbar = c = 1$. G_N is Newton's constant.) If "slow roll" is achieved for a period of time, $\dot{\phi}$ subdominant and $V(\phi) \approx$ constant, we get $a \propto e^{Ht}$, $H \approx$ constant, after which the potential energy is released, "reheating" the Universe to the HBB. Phenomenologically, $\mathcal{N}_{\text{e-folds}} > 40 - 60$ are required to understand

the degree of homogeneity/flatness we see today.

Remarkably, quantum fluctuations during inflation can seed the inhomogeneities in the distribution of galaxies and in the Cosmic Microwave Background (CMB). In particular, the CMB temperature-fluctuation power-spectrum,

$$\Delta_S(k) \propto k^{n_s(k)}, k \equiv \text{wavenumber}, n_s \equiv \text{spectral index}, \tag{3.2}$$

is generically predicted by inflation to be approximately scale-invariant, $n_s \approx 1$, and is measured to be $n_s \approx 0.96$ [84, 85].

Slow roll itself requires an unusually flat potential, suggesting that the inflaton ϕ is a pseudo-Nambu-Goldstone boson of a spontaneously broken global $U(1)$ symmetry, an "axion". If there is a weak coupling that *explicitly* violates $U(1)$ symmetry by a definite amount of charge, one can generate a potential,

$$V(\phi) = V_0 \left(1 - \cos \frac{\phi}{f} \right), \tag{3.3}$$

where f is a constant determined by the spontaneous breaking dynamics, while V_0 is a constant proportional to the weak coupling. This is the model of "Natural Inflation" [86].[1] It can be successfully fit to data, and in particular for $\mathcal{N}_{\text{e-folds}} > 50, n_s \approx 0.96$, one finds [85]

$$f > 2 \times 10^{19} \, \text{GeV} \approx 10 M_{\text{pl}}$$
$$\tag{3.4}$$
$$V_0 > (2 \times 10^{16} \, \text{GeV})^4 \approx (10^{-2} M_{\text{pl}})^4.$$

---

[1]The fine-tuning of the two terms in Eq. (3.3) to obtain a (nearly) vanishing vacuum energy relates to the notorious Cosmological Constant Problem [87], which we do not address here.

The Planck scale $M_{\rm pl} \equiv 1/\sqrt{8\pi G_N} = 2 \times 10^{18}\,{\rm GeV}$ is the energy scale above which Quantum Gravity (QG) effects become strong, and effective field theory (EFT) must break down in favor of a more fundamental description such as superstring theory [88].

The very high energy scale $V_0^{1/4} \approx 0.01 M_{\rm pl}$ is without precedent in observational physics and implies sensitivity to new exotic phenomena. For such large inflationary energy densities, quantum graviton production during inflation gives rise to a tensor/scalar ratio of the CMB power spectrum of $r \sim 0.1$. Indeed, the BICEP2 CMB experiment has claimed a signal at this sensitivity [89], although there is still serious concern over possible contamination by foreground dust [90, 91]. Regardless, cosmological observations have the potential to provide information about physics at the highest energy scales in the near future.

However, the proximity of the QG scale raises concerns about the validity of effective field theory treatments of inflation and susceptibility to poorly-understood QG effects. There are broadly two approaches to addressing such QG uncertainties in high-scale inflation models. One is to derive inflationary models directly within known superstring constructions, which provide reasonably explicit UV descriptions of QG. Such constructions feature many moduli fields (for example, describing the size and shape of several extra dimensions) which must be stabilized and which also receive time-dependent back-reaction effects during the course of inflation. Consistently constructing and analyzing models of this type can be an involved and difficult task, and there is as yet no fully realistic top-down derivation. Nevertheless, considerable qualitative progress has been made on possible shapes and field-ranges of inflaton potentials in string theory and their effects [92–100].

Alternatively, one can try to construct bottom-up effective field theory models, incorporating simple mechanisms that shield the inflationary structure from unknown QG

corrections, aspects of which have been previously explored in e.g. [101–110]. However, studies of robust quantum properties of large black hole solutions in General Relativity, as well many string theory precedents, strongly suggest that there are non-trivial constraints on effective field theory couplings in order for them to be consistent with *any* UV completion incorporating QG, which make inflationary model-building challenging. In this chapter, we will discuss the impact of such black-hole/QG considerations in the context of Natural Inflation, in particular the role of the Weak Gravity Conjecture (WGC) [111]. While these considerations rule out some inflationary models, we demonstrate for the first time that there do exist simple and predictive effective theories of natural inflation, consistent with the WGC, where the inflaton arises from components of higher-dimensional gauge fields. The advantage of the effective field theory approach is two-fold: (i) the models have relatively few moving parts, whose dynamics can be analyzed quite straightforwardly and comprehensively, and (ii) one can achieve full realism. We believe that such a higher-dimensional realization yields the most attractive framework for cosmic inflation to date. Further elaboration of our work will be presented in [112].

3.2 Quantum Gravity Constraints

Classical black holes can carry gauge charges, observable by their gauge flux outside the horizon, but not global charges. Studies of black hole formation and Hawking evaporation, combined with the statistical interpretation of their entropy, then imply that such quantum processes violate global charge conservation [113, 114]. By the Uncertainty Principle this holds even for virtual black holes, implying that at some level global symmetries such as

those desired for Natural Inflation cannot co-exist with QG. Of course, global symmetries are seen in a variety of experimental phenomena, but these are accidental or emergent at low energies, while Natural Inflation only achieves slow roll for $f > M_{\text{pl}}$! A loop-hole is that $1/f$ may represent a weak coupling and low-scale symmetry breaking rather than very high scale breaking. The mechanism of "Extranatural Inflation" [101] precisely exploits this loop-hole, realizing ϕ as a low-energy remnant of a $U(1)$ *gauge* symmetry. The model is electrodynamics, but in 4+1-dimensional spacetime, with the usual dimensions, $x^{\mu=0-3}$, augmented by a very small extra-dimensional circle, $x^5 \in (-\pi R, \pi R]$. The 3+1-dimensional inflaton is identified with the phase of the gauge-invariant Wilson loop around the circle,

$$\phi(x^\mu) \equiv \frac{1}{2\pi R} \oint dx^5 A_5(x^\mu, x^5). \tag{3.5}$$

Classically, the masslessness of the Maxwell field, $A_{M=\mu,5}$, matches onto $V(\phi) = 0$ in the long distance effective theory $\gg R$. But 4+1D charged matter, with charge g_5, mass m_5, and spin S, corrects the quantum effective potential [115, 116],

$$\delta V(\phi) = \frac{3(-1)^S}{4\pi^2} \frac{1}{(2\pi R)^4} \sum_{n \in \mathbb{Z}} c_n e^{-2\pi n R m_5} \operatorname{Re} e^{in\phi/f}$$
$$c_n(2\pi R m_5) = \frac{(2\pi R m_5)^2}{3n^3} + \frac{2\pi R m_5}{n^4} + \frac{1}{n^5}, \tag{3.6}$$

where $(e^{-2\pi R m_5})/R^4$ is a typical (Yukawa-suppressed) extra-dimensional Casimir energy density, and the phase captures an Aharonov-Bohm effect around the circle. We have written

this in terms of the emergent scale,

$$f \equiv \frac{1}{2\pi R g},$$

(3.7)

where g is the effective 3+1 coupling which matches onto g_5 in the UV. We see that Natural Inflation structure (with innocuous harmonics), with $f > M_{\mathrm{pl}}$, can emerge at a sub-Planckian compactification scale, $1/R \ll M_{\mathrm{pl}}$, by choosing weak gauge coupling $g \ll 1$. After reaching the minimum of its potential the inflaton can "reheat" the Universe to a radiation-dominated phase by decaying into the charged matter.

The requirement $g \ll 1$ seems suspiciously close to $g = 0$, the limit in which the $U(1)$ gauge symmetry effectively reverts to an exact global symmetry, at odds with QG. Indeed, Extranatural Inflation runs afoul of a subtle QG criterion known as the Weak Gravity Conjecture [111]. (For related work see e.g. [117–123].) The WGC again uses universal features of black holes to provide insights into QG constraints on EFT. In brief, one argument is as follows. (We will discuss this and other motivations for the WGC at greater length in [112].) Ref. [114] has shown that in EFTs containing both a Maxwell gauge field and General Relativity, the associated gauge group must be *compact $U(1)$*, in the sense that electric charges must be quantized in integer multiples of the coupling g, in order to avoid other exact *global* symmetries and related negative consequences. Then, there exist large black hole solutions to the Einstein-Maxwell Equations carrying both electric and magnetic charges. These solutions are quantum-mechanically consistent if they obey the Dirac quantization condition, whereby magnetic charges are quantized in units of $2\pi/g$.

All precedent in General Relativity and string theory research (e.g. [7,124–126]) suggests

that black holes are themselves coarse-grained EFT descriptions of gravitational bound states of more basic components (see [127, 128] for reviews). In particular, magnetically charged black holes should be "made out of" fundamental magnetic charges which are themselves not black holes. And yet, this is impossible for sufficiently small $g \ll 1$. The reason is that Maxwell EFT cannot describe electric and magnetic charges which are both light and pointlike. Instead, the magnetic charges must be heavy solitons, with a size $1/\Lambda$, where $\Lambda < M_{\mathrm{pl}}$ is the UV energy cutoff of the EFT. The magnetostatic self-energy in the region outside the $1/\Lambda$-sized "core", where EFT applies, is then $\pi\Lambda/(2g^2) \gg \Lambda$; [2] the mass m_{core} within the core is expected to be at least comparable to this. In order for the soliton to be larger than its horizon radius $2G_N m_{\mathrm{core}}$, to avoid being a black hole itself, we must have

$$\Lambda \lesssim 2\sqrt{2}g M_{\mathrm{pl}}. \tag{3.8}$$

Here the "$\lesssim$" reminds us of the $\mathcal{O}(1)$ uncertainties in this argument. This is the WGC. When testing theories of inflation for *parametric control* these $\mathcal{O}(1)$ uncertainties will be irrelevant, but we will be subject to them when fitting models to precision data.

Requiring the compactification scale to be below the EFT cutoff, $1/R < \Lambda$, then implies $f < M_{\mathrm{pl}}$, by Eq. (3.7), spoiling minimal Extranatural Inflation [111, 129]. Note that even with the $\mathcal{O}(1)$ uncertainty in the WGC, we cannot get parametrically large f/M_{pl} (ie. large $\mathcal{N}_{\mathrm{e-folds}}$).

---

[2]By comparison, for weakly coupled electrically-charged point particles, the length scale that sets the electrostatic self-energy is played by the Compton wavelength, which is then a small perturbation of the mass, $g^2 m/(8\pi) \ll m$.

3.3 Bi-Axion Models

We now show that we can achieve inflation subject to the constraints of the WGC by generalizing to bi-axion (extra-)natural inflation, with two axions, A, B [130–135]. Consider the potential

$$V = V_0 \left[1 - \cos \frac{A}{f_A} \right] + \tilde{V}_0 \left[1 - \cos \left(\frac{NA}{f_A} + \frac{B}{f_B} \right) \right], \qquad (3.9)$$

where $N \in \mathbb{Z}$ by A-periodicity, following from its Nambu-Goldstone status. For sufficiently large $N \gg 1$, we get two hierarchical eigenmodes. At lower energies than the higher mass, the second term enforces the constraint

$$\frac{NA}{f_A} + \frac{B}{f_B} \approx 0. \qquad (3.10)$$

Plugging back into V gives an effective potential for the light mode, $\phi \approx B$,

$$V_{\text{eff}}(\phi) = V_0 \left(1 - \cos \frac{\phi}{f_{\text{eff}}} \right), \quad f_{\text{eff}} = N f_B. \qquad (3.11)$$

This model is straightforwardly realized from 4+1 electrodynamics of two $U(1)$ gauge fields [135], A_M, B_M, [3] with charges $(N, 1)$ and $(1, 0)$, and 4+1 masses less than $1/R$. Aharonov-Bohm effects analogous to (3.6) then give rise to (3.9), for effective 3+1 scalars, A, B defined analogously to (3.5), with $V_0 \sim \tilde{V}_0$ and $f_A = 1/(2\pi R g_A)$, $f_B = 1/(2\pi R g_B)$. It is clear that the WGC, (3.8), can be satisfied for both gauge interactions, with $f_A, f_B \ll$

---

[3]Ref. [122] claims that there are additional constraints from the WGC in theories with multiple $U(1)$ fields, though this does not follow from our arguments. If there are n $U(1)$'s all with a common coupling, then [122] claims that WGC bounds become stronger by a factor of $\sqrt{n}$, which is $O(1)$ in our examples.

M_{pl}, while still obtaining $f_{\text{eff}} \gg M_{\text{pl}}$, provided N is large enough. Large N also ensures that quantum tunneling of the fields through the potential barrier from the second term of Eq. (3.9) is extremely suppressed.

But in non-renormalizable 4+1D QED, the UV scale of strong coupling (and EFT breakdown), Λ_{gauge}, falls rapidly as N increases,

$$\Lambda_{\text{gauge}} = \frac{8\pi}{N^2 g^2} \frac{1}{R}. \tag{3.12}$$

Minimally, both this cutoff and the WGC cutoff should be above the compactification scale, $1/R$, to remain in theoretical control. Given that for Natural Inflation, $f_{\text{eff}} \gtrsim \sqrt{\mathcal{N}_{\text{e-folds}}} M_{\text{pl}}$, it is easy to check that the bi-axion model can give parametrically large $\mathcal{N}_{\text{e-folds}}$ provided N and $M_{\text{pl}}R$ are taken sufficiently large while keeping Ng fixed.

3.4   Radius Stabilization

When 4+1 General Relativity is taken into account, R is not an input parameter, but rather the expectation of a dynamical effective 3+1 ("radion") field, $\sigma(x^\mu)$,

$$R = M_{\text{pl}} e^{\sqrt{\frac{2}{3}} \langle \sigma(x) \rangle / M_{\text{pl}}}. \tag{3.13}$$

We show that $M_{\text{pl}}R \gg 1$ can arise naturally, and that the extra dimension is effectively rigid during inflation. A suitable σ potential can arise simply via Goldberger-Wise stabilization [136], in the case where the extra-dimensional circle is further "orbifolded" in half, down to an interval. (This has the added benefit of projecting out the unnecessary 3+1 vector

components of the gauge field, without otherwise affecting our earlier discussion.) The stabilization mechanism requires adding a 4+1 neutral scalar field, χ. The energy in this field depends on R, providing an effective potential for σ,

$$V_{\text{radion}} \sim m_\chi^2 M_5^3 \left(c_1 e^{2\pi R m_\chi} + c_2 e^{-2\pi R m_\chi}\right)$$
$$\implies 2\pi R \sim \frac{1}{m_\chi}, \tag{3.14}$$

where $c_{1,2} \sim \mathcal{O}(1)$ are determined by χ boundary conditions at the ends of the interval, and M_5 is the 4+1 Planck scale. Large R clearly requires small m_χ. This (and the small 4+1 cosmological constant that has been neglected above) can both be natural if the 4+1 "bulk" spacetime preserves supersymmetry (to a high degree). The potential also gives the radion a mass,

$$m_\sigma^2 \sim \frac{1}{(2\pi R)^2} \gg H^2, \tag{3.15}$$

so that it is not excited during and after inflation.

3.5 Precision CMB Observables

CMB observables are sensitive to even small corrections to the inflationary potential. An attractive feature of the extra-dimensional realizations are that the structure of subleading corrections is controlled by the higher gauge symmetry. Eq. (3.6) shows that massive charges decouple exponentially from the potential, with the extra dimension effectively acting as a "filter" of unknown UV physics, but they can have observable effects if not too heavy. Since

our effective theory has cutoffs on its validity given by the WGC, (3.8), and strong coupling in the UV, (3.12), in general new physics will appear by (the lower of) these cutoffs, $\equiv \Lambda$. This may include new particles with 5D mass $M \approx \Lambda$ carrying charges (n_A, n_B), where each charge is plausibly in the range $|n| \lesssim N$. Such charges will create an Aharonov-Bohm correction to the potential, which after imposing the IR constraint, (3.10), yields

$$\delta V \sim V_0 \frac{(2\pi R M)^2}{3} e^{-2\pi R M} \cos\left(N n_B - n_A\right) \frac{\phi}{f_{\text{eff}}}. \tag{3.16}$$

If $N n_B - n_A \gg 1$, this "higher harmonic" gives a modulating correction to the slow-roll parameter $\epsilon \equiv \frac{M_{\text{pl}}^2}{2} \left(\frac{V'}{V}\right)^2$,

$$\frac{\delta \epsilon}{\epsilon} = 2(N n_B - n_A) \frac{(2\pi R M)^2}{3} e^{-2\pi R M} \sin(N n_B - n_A) \frac{\phi}{f_{\text{eff}}}. \tag{3.17}$$

For this to not obstruct inflation itself requires $\delta\epsilon/\epsilon < 1$. However, the parameter $\delta\epsilon/\epsilon$ also controls corrections to the temperature power-spectrum in the slow-roll limit, where the modulating part of the potential is almost constant during a Hubble time. Such periodic modulations of the inflationary potential have been searched for in the CMB data [137–142], most recently motivated by the possibility of such signals in axion monodromy inflation [93, 139,142]. These results place more stringent bounds, requiring $\delta\epsilon/\epsilon \lesssim 1-5\%$, for $N n_B - n_A$ in a realistic range of $\sim \mathcal{O}(10 - 100)$.

Parametrically, it is easy to check that $\delta\epsilon/\epsilon$ can be made arbitrarily small while still satisfying theoretical constraints, and consistent with large $\mathcal{N}_{\text{e-folds}}$. But this is accomplished at the expense of taking $M_{\text{pl}} R$ parametrically large. However, as seen in (3.6), $1/R$ sets the

scale of V_0 in Natural Inflation, which is bounded by current observations. For example, we can fit the data, (3.4), with $N = 42$, $g = 0.08$, $M_{pl}R = 8$. Then if we have new particles at the cutoff, $M = \Lambda$ and charges ($n_A \sim \mathcal{O}(N)$, $n_B \sim \mathcal{O}(1)$), we have $\delta\epsilon/\epsilon \sim 3\%$. Of course, the charges at the cutoff may have a different pattern, and from (3.17), we are exponentially sensitive to order one uncertainties in determining Λ from (3.8) and (3.12), but we see that our parametric success is also numerically plausible in the real world. Our estimates clearly motivate searching for such modulation in the CMB power spectrum.

3.6 Tri-Axion Models

Our discussion can be straightforwardly extended to tri-axion models [131, 135, 143], where smaller charge ratios are possible in the extranatural realization [135]. We find that such models can also satisfy the WGC, both parametrically and numerically in realistic models, with a higher and safer EFT cutoff. Consider 3 gauge fields A, B, C and 3 particles with charges $(1, 0, 0)$, $(N_A, 1, 0)$, $(0, N_B, 1)$. $N_A, N_B \gg 1$ implies only one light field, ϕ, with

$$f_{\text{eff}} = \frac{N_A N_B}{2\pi R g_C}. \tag{3.18}$$

We can now fit the data with smaller charges and lower corrections to the slow-roll parameter; e.g. taking $N_{A,B} = 8$, $g_{A,B,C} = 0.12$, $M_{pl}R = 8$ we obtain $\delta\epsilon/\epsilon \sim 3 \times 10^{-4}$.

3.7 Chern-Simons Model

The need for specific, large charges for light 4+1 matter may seem somewhat contrived. Arbitrary light charges would have effects similar in form to (3.16) but without Yukawa

suppression, spoiling inflation. To explore this issue we modify our extra-dimensional approach so that these large quantum numbers become outputs of the model rather than fixed input parameters. For simplicity, we first focus on the single Maxwell field, A_M, and replace its coupling to explicit light charged matter by a Chern-Simons coupling to a non-abelian Yang-Mills (YM) gauge sector (say with $SU(2)$ gauge group),

$$\delta\mathcal{L}_{\text{CS, 4+1}} = \frac{N}{64\pi^2}\epsilon^{LMNPQ}G^a_{LM}G^a_{NP}A_Q.$$

(3.19)

At this stage N is still an input parameter, its quantization enforced now by invariance under *large* gauge transformations. In general, Chern-Simons couplings allow gauge fluxes to play the role of gauge currents; in this case YM fluxes act as an A_M current. YM instantons can then replace the role of virtual Aharonov-Bohm effects. This is best seen by first passing to the 3+1 effective theory,

$$\delta\mathcal{L}_{\text{CS, 3+1}} = \frac{N}{64\pi^2}\frac{A}{f}\epsilon^{\mu\nu\rho\sigma}G^a_{\mu\nu}G^a_{\rho\sigma}.$$

(3.20)

This is very similar to the coupling of the Peccei-Quinn axion to QCD in order to solve the Strong CP Problem: upon YM confinement [144] we obtain

$$\delta\mathcal{L}_{4D\text{ eff}} = \hat{V}_0\mathcal{F}\left(\frac{NA}{f}\right),$$

(3.21)

where $\mathcal{F}$ is an order-one 2π-periodic function replacing the second cosine in (3.9), and $\hat{V}_0$ is set by the YM confinement scale. Similar generalizations $\mathcal{F}(NA) \rightarrow \mathcal{F}(NA + B)$ can replace (3.9). In this way, we recover Natural Inflation via bi-axion or tri-axion models.

A virtue of the 4+1 Chern-Simons model is that it can be extended to 6+1 field theory with a Chern-Simons coupling, which may be written compactly in differential form notation as

$$\delta \mathcal{L}_{CS,7D} = \frac{1}{32\pi^2} dA \wedge A \wedge G \wedge G, \qquad (3.22)$$

such that N does not appear as an input coupling. Instead, we take the 6th, 7th dimensions to form a small 2-sphere, on which quantized $F = dA$ gauge flux can be trapped. We will quantize about classical solutions with N flux quanta,

$$\oint_{S^2} F = \frac{N}{2\pi}. \qquad (3.23)$$

In this way, N defines discrete selection sectors of the 6+1 theory, a "landscape" of perturbatively stable vacuua. Plugging this condition into (3.22) reduces it to the 4+1 model, (3.19).

This basic mechanism can be extended to bi-/tri-axion models. For example, the second term of (3.9) can be produced if the A field has a 6+1 Chern-Simons coupling as in (3.22) while the B field has only a 4+1 coupling of the form in (3.19) to the same YM gauge sector. This could occur e.g. if the B field is localized to a 4-brane defect. In [112] we will demonstrate that these 6+1 models are also parametrically controlled while being consistent with the WGC and $\mathcal{N}_{\text{e-folds}} \gg 1$. A key new feature in the analysis is the dynamical role N plays in stabilizing the size of the 6-7 sphere. Note that obtaining many e-foldings of inflation does not require a very specific, "tuned" choice of N; large $\mathcal{N}_{\text{e-folds}}$ can in fact be

generic within this landscape of solutions.

Let us summarize. Black hole processes and properties provide a unique window into quantum gravity, placing tight constraints, such as the Weak Gravity Conjecture, on effective field theories of inflation. We have demonstrated that a parametrically large number of e-foldings of high-scale inflation can be realized by simple multi-axion generalizations of Extranatural Inflation, consistent with these constraints. The resulting models achieve large gravitational wave signals of $r \sim 0.1$ while remaining realistic and theoretically controlled, and predict potentially observable modulations of the scalar power spectrum.

Chapter 4:   The Conformal Bootstrap and Critical Universality

4.1   Introduction

Consider the phase diagram of water shown in figure 4.1. The curve separating the liquid and gas phases ends at a critical point. Beyond that point, there is no longer any distinction between the two phases. The modern form of the renormalization group was developed by Ken Wilson [145–147] in order to understand these critical points, and he was awarded the Nobel Prize for this work. One may wonder why such points are so interesting. This has to do with the concept of universality.

Near the critical temperature T_c of water, the specific heat C_V behaves as

$$C_V \propto |T - T_c|^{-\alpha}, \tag{4.1}$$
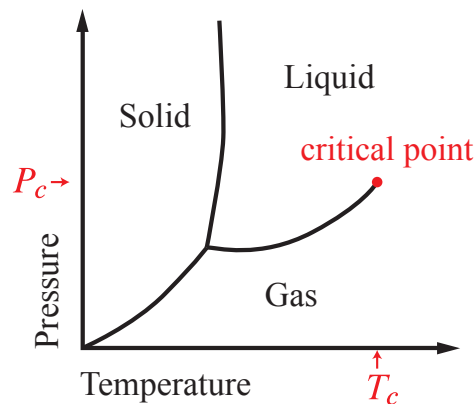

Figure 4.1: Phase diagram of water

where $\alpha \approx 0.11$. Similarly, the compressibility χ_T also exhibits power-law behavior:

$$\chi_T \propto |T - T_c|^{-\gamma} \tag{4.2}$$

where $\gamma \approx 1.22$. In fact, many other quantities exhibit power-law behavior as well, and their exponents are called critical exponents.

Besides water, there are obviously many other substances that can undergo a liquid-gas phase transition, and a corresponding set of critical exponents can also be defined. The remarkable thing is that every such substance has the same set of critical exponents ($\alpha \approx 0.11$, $\gamma \approx 1.22$, etc.). Even more remarkable is that systems with phase transitions that are completely unrelated to liquid/gas can also exhibit the same set of critical exponents. For example, magnets have a phase transition in which they lose their magnetization at a high enough temperature. In the specific case of a uniaxial ferromagnet, the critical exponents match those of water. This phenomena of universal behavior is called universality, and systems that have the same set of critical exponents are said to be in the same universality class.

In the language of the renormalization group (RG), a universality class is associated with a fixed point of the RG flow. The fixed point has a basin of attraction. Tuning a system to its critical point means that its RG initial condition lies in the basin of attraction (figure 4.2). Different members of the universality class, when tuned to their critical points, will start their RG at different points in the basin of attraction. However, all these different initial conditions flow to the same point, and therefore they describe the same long-distance physics. This is the explanation of universality. For reviews, see [148, 149]

(a) View of flows on the basin
of attraction.

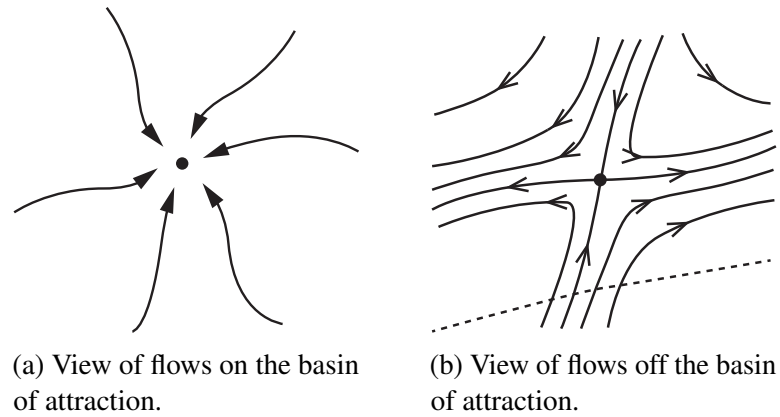(b) View of flows off the basin
of attraction.

Figure 4.2: Renormalization group flows near a critical point. The dotted line in B represents different initial conditions as an external parameter is tuned.

Each step of the RG consists of a course-graining in which short distance degrees of freedom are integrated over, followed by a rescaling so that the "grains" return back to their previous size. As a result, any intrinsic length scale of the system, such as a correlation length, shrinks on each RG step. However, at the fixed point, the system is invariant under the RG, and hence any length scale must be such that it remains the same after a rescaling. Of course, this is impossible unless the length scale is either zero or infinity. Therefore, the fixed point theory actually has no length scales, and is thus a scale-invariant theory. Now, in a wide variety of cases, it turns out that scale-invariant theories also happen to be invariant under RG transformations that are non-uniform in space. In other words, the course graining is finer in some places and courser in others. Such a theory is called a conformal field theory (CFT).

All properties of a universality class are encoded in its corresponding scale-invariant fixed point theory. In this chapter, we will only deal with scale-invariant theories that are also conformal. Because of this, recently developed tools in conformal field theory can be used to understand an unexplained but striking feature about universality: there are only

very few universality classes. Specifically, the classes are generally distinguished by only three properties: the number of dimensions, the global symmetry group of the Hamiltonian, and the number of experimental "knobs" that need to be tuned to reach the critical point. A priori, the RG would allow multiple universality classes with those same three properties, but that is not what is found in nature. A CFT explanation for this striking feature has been suggested by the work of [150–153]. They present evidence that in three dimensions, there is only one theoretically consistent CFT with a specified global symmetry group and number of relevant operators.[1] In this chapter, we extend their results on the Ising universality class to two dimensions. Specifically, we give evidence that the CFT describing the 2D Ising universality class is the only $\mathbb{Z}_2$-symmetric unitary CFT in two dimensions with exactly two relevant operators.

In this chapter, we give a review of conformal field theory and the conformal bootstrap, independent of its relation to critical phenomena. For more detailed reviews and references to the literature, see [154, 155]. We then apply the conformal bootstrap to the concept of universality as just reviewed. The sections are organized as follows. In section 4.2, we define a CFT in terms of the behavior of its correlation functions under Weyl transformations. In section 4.3, we argue that a CFT has a convergent operator product expansion. In section 4.4, we describe how all local correlators can be determined by a CFT's conformal data, which are the set of numbers that determine the 2-point and 3-point functions. In section 4.5, we derive the conformal bootstrap equations, which are the severe consistency conditions that the conformal data must satisfy . In section 4.6, we derive additional constraints on the

_____

[1]The relevant operators correspond to directions away from the fixed point's basin of attraction, which correspond to experimental knobs that need to be tuned.

conformal data imposed by unitarity. In section 4.7, we show how numerical methods can efficiently identify large regions in the space of putative conformal data that are inconsistent with the bootstrap equations. In section 4.8, we improve the numerical methods. In section 4.9, we return to the concept of universality. In section 4.10, we present the new 2D Ising results.

The main novelty of the conformal bootstrap is the use of computers to prove rigorous theorems in conformal field theory. The author acknowledges the University of Maryland supercomputing resources (http://www.it.umd.edu/hpcc) made available for conducting the research reported in this chapter.

4.2 Conformal Field Theory

In this section, we define conformal field theory (CFT), being careful to explain the relationship between scale transformations, Weyl transformations, conformal transformations, and diffeomorphisms. We also derive the exact 2-point and 3-point correlation functions in a CFT.

As mentioned in the introduction, at a fixed point of the RG, the theory is scale invariant. This means that correlation functions behave very simply under a uniform rescaling of positions:

$$\langle \mathcal{O}_1(\lambda x_1) \cdots \mathcal{O}_n(\lambda x_n) \rangle = \lambda^{-\Delta_1} \cdots \lambda^{-\Delta_n} \langle \mathcal{O}_1(x_1) \cdots \mathcal{O}_n(x_n) \rangle. \tag{4.3}$$

We can always choose a basis of operators so that this equation is true. Operators in this basis are called scaling operators, and we will work exclusively with them. The number Δ_i is an

intrinsic property of $\mathcal{O}_i$ called its scaling dimension (or simply "dimension"). Furthermore, $\mathcal{O}_i$ can transform under a finite dimensional representation of the Lorentz group, though we will mostly consider scalars for simplicity.

Now, instead of rescaling all positions $x \to \lambda x$, we could equally well keep the positions fixed and rescale the background flat space metric $\eta_{\mu\nu} \to \lambda^2 \eta_{\mu\nu}$:

$$\langle \mathcal{O}_1(\lambda x_1) \cdots \mathcal{O}_n(\lambda x_n) \rangle_\eta = \langle \mathcal{O}_1(x_1) \cdots \mathcal{O}_n(x_n) \rangle_{\lambda^2 \eta}. \tag{4.4}$$

Here $\langle \cdots \rangle_g$ denotes the correlator calculated in the background metric g. Therefore, scale invariance can be phrased as

$$\langle \mathcal{O}_1(x_1) \cdots \mathcal{O}_n(x_n) \rangle_{\lambda^2 \eta} = \lambda^{-\Delta_1} \cdots \lambda^{-\Delta_n} \langle \mathcal{O}_1(x_1) \cdots \mathcal{O}_n(x_n) \rangle_\eta. \tag{4.5}$$

Remarkably, for reasons still not fully understood [156–159], scale invariance is very often enhanced to Weyl invariance. This means that for a certain class of operators, the constant scale factor λ in (4.5) can be replaced by an arbitrary function of position $\lambda \to \Omega(x)$:

$$\langle \mathcal{O}_1(x_1) \cdots \mathcal{O}_n(x_n) \rangle_{\Omega(x)^2 \eta} = \Omega(x_1)^{-\Delta_1} \cdots \Omega(x_n)^{-\Delta_n} \langle \mathcal{O}_1(x_1) \cdots \mathcal{O}_n(x_n) \rangle_\eta. \tag{4.6}$$

This is the defining property of a conformal field theory.[2] The operators for which (4.6) is true are called primary operators. In flat space, these are the set of operators that are not

---

[2]In even dimensions there is a Weyl anomaly. However, it cancels out in correlation functions provided correlators are normalized by the partition function. We will take this to be the case.

total derivatives. Total derivatives are called descendants, and their correlators can be simply found by taking appropriate derivatives of the correlators of primary operators. We will therefore now use $\mathcal{O}$ to denote primary operators only.

A Weyl transformation generally transforms a flat manifold into a curved one. However, we often want to remain in flat space and instead have relations between correlators evaluated at different points. We will now show how Weyl invariance combined with diffeomorphism invariance allows us to obtain powerful transformation properties of flat space correlators. By diffeomorphism invariance, we mean that correlation functions are invariant under diffeomorphisms of the background spacetime manifold.[3] Specifically, under the combined replacement,

$$x^\mu \to \tilde{x}^\mu(x) \tag{4.7}$$

$$\eta_{\mu\nu} \to \tilde{g}_{\mu\nu}(\tilde{x}) = \frac{\partial x^\alpha}{\partial \tilde{x}^\mu} \frac{\partial x^\beta}{\partial \tilde{x}^\nu} \eta_{\alpha\beta} \tag{4.8}$$

correlators are invariant for arbitrary $\tilde{x}^\mu(x)$:

$$\langle \mathcal{O}_1(x_1) \cdots \mathcal{O}_n(x_n) \rangle_\eta = \langle \mathcal{O}_1(\tilde{x}_1) \cdots \mathcal{O}_n(\tilde{x}_n) \rangle_{\tilde{g}}. \tag{4.9}$$

Now, there is a restricted class of diffeomorphisms $x \to \tilde{x}(x)$ that leave the metric $\eta_{\mu\nu}$ invariant up to an overall multiplicative factor:

$$\frac{\partial \tilde{x}^\alpha}{\partial x^\mu} \frac{\partial \tilde{x}^\beta}{\partial x^\nu} \eta_{\alpha\beta} = \Omega(x)^2 \eta_{\mu\nu}. \tag{4.10}$$

---

[3]Diffeomorphism invariance can be used to derive the Ward Identity for the conservation of the stress tensor.

These are called conformal transformations. We see from (4.8), that for conformal transformations, $\tilde{g}_{\mu\nu}(\tilde{x}) = \Omega(x)^{-2}\eta_{\mu\nu}$.[4] Thus, (4.9) becomes

$$\langle \mathcal{O}_1(x_1)\cdots\mathcal{O}_n(x_n)\rangle_\eta = \langle \mathcal{O}_1(\tilde{x}_1)\cdots\mathcal{O}_n(\tilde{x}_n)\rangle_{\Omega(x)^{-2}\eta} \tag{4.11}$$

$$= \Omega(x_1)^{\Delta_1}\cdots\Omega(x_n)^{\Delta_n}\langle \mathcal{O}_1(\tilde{x}_1)\cdots\mathcal{O}_n(\tilde{x}_n)\rangle_\eta, \tag{4.12}$$

where we then used the defining Weyl invariance of the CFT (4.6) in the last line to return the metric back to $\eta_{\mu\nu}$. Therefore,

$$\langle \mathcal{O}_1(\tilde{x}_1)\cdots\mathcal{O}_n(\tilde{x}_n)\rangle = \Omega(x_1)^{-\Delta_1}\cdots\Omega(x_n)^{-\Delta_n}\langle \mathcal{O}_1(x_1)\cdots\mathcal{O}_n(x_n)\rangle. \tag{4.13}$$

These are the powerful transformation properties of flat space correlators (with background metric $\eta_{\mu\nu}$) mentioned earlier. To summarize, we arrived at (4.13) by using the subgroup of Weyl and diffeomorphism transformations that leaves the metric $\eta_{\mu\nu}$ invariant.

We will now use (4.13) to completely fix the form of 2-point and 3-point functions. The defining property of conformal transformations is (4.10). Clearly, Poincaré and scale transformations are of this form. In dimensions $d > 2$, there is actually only one other independent conformal transformation.[5] These are inversions:

$$\tilde{x}^\mu = \frac{x^\mu}{x^2}. \tag{4.14}$$

All conformal transformations can be obtained by composing Poincaré transformations with

---

[4]Note the minus sign in the exponent. The conventions were arranged to give a Weyl factor of $\Omega = \lambda$ under $x \to \lambda x$.

[5]In $d = 2$, there are an infinite number of independent conformal transformations.

inversions.

Using conformal transformations, we can fix three points to have whatever value we want. To see this, we will move an arbitrary configuration of three points x_1, x_2, and x_3 to the points 0, 1, and ∞ along some arbitrarily chosen axis. First, translate x_3 to the origin, followed by an inversion to move it to infinity. Next, translate x_1 to the origin. Finally, use rotations and scale transformations to move x_2 to the point 1. Therefore, the 2-point and 3-point functions are completely determined by (4.13) and their values at any one point. We will write the explicit expressions for primaries since correlators of descendents are just derivatives of these expressions as already mentioned. For the 2-point function of scalar primaries, we find

$$
\langle \mathcal{O}_i(x_1)\mathcal{O}_j(x_2) \rangle =
\begin{cases}
0, & \text{if } \Delta_i \neq \Delta_j \\[2mm]
\dfrac{Z_{ij}}{x_{12}^{2\Delta}} & \text{if } \Delta_i = \Delta_j \equiv \Delta
\end{cases}
\tag{4.15}
$$

where $x_{ij}^p \equiv \left[(x_i - x_j)^2\right]^{p/2}$. In section 4.6, we will see that the symmetric matrix Z_{ij} is positive definite in a unitary theory. Therefore, we can always choose a basis of operators such that $Z_{ij} = \delta_{ij}$. We will also need the 2-point function of operators with spin-l (i.e. traceless symmetric tensors of rank l):

$$
\langle \mathcal{O}^{\mu_1 \cdots \mu_l}(x)\mathcal{O}_{\nu_1 \cdots \nu_l}(0) \rangle = \frac{I^{(\mu_1}{}_{\nu_1}(x) \cdots I^{\mu_l)}{}_{\nu_l}(x)}{x^{2\Delta}} - \text{traces,}
\tag{4.16}
$$

where

$$
I^{\mu}{}_{\nu}(x) = \delta^{\mu}_{\nu} - 2\frac{x^{\mu}x_{\nu}}{x^2}.
\tag{4.17}
$$

119

Moving on to the 3-point function:

$$\langle \mathcal{O}_i(x_1)\mathcal{O}_j(x_2)\mathcal{O}_k(x_3)\rangle = \frac{\lambda_{ijk}}{x_{12}^{\Delta_i+\Delta_j-\Delta_k}\, x_{23}^{\Delta_j+\Delta_k-\Delta_i}\, x_{31}^{\Delta_k+\Delta_i-\Delta_j}}. \tag{4.18}$$

Note that once the 2-point functions has been normalized so that $Z_{ij} = \delta_{ij}$, then the λ_{ijk} are unambiguous data of the CFT. We will also see later that by unitarity they must be real numbers.

Now for the 4-point function. Since we can only fix three points, the 4-point function is not completely fixed by conformal symmetry. In particular, given four points $x_1, \cdots x_4$, the combinations

$$u = \frac{x_{12}^2 x_{34}^2}{x_{13}^2 x_{24}^2} \quad \text{and} \quad v = \frac{x_{14}^2 x_{34}^2}{x_{23}^2 x_{24}^2} \tag{4.19}$$

are invariant under all conformal transformations. Therefore, the 4-point function can naively contain an arbitrary function of u and v:

$$\langle \mathcal{O}_i(x_1)\mathcal{O}_j(x_2)\mathcal{O}_k(x_3)\mathcal{O}_l(x_4)\rangle = \frac{1}{x_{12}^{\Delta_i+\Delta_j}\, x_{34}^{\Delta_k+\Delta_l}}\left(\frac{x_{24}}{x_{14}}\right)^{\Delta_{ij}}\left(\frac{x_{14}}{x_{13}}\right)^{\Delta_{kl}} G_{ijkl}(u,v),$$

$$\tag{4.20}$$

where $\Delta_{ij} \equiv \Delta_i - \Delta_j$ and $G_{ijkl}(u,v)$ is the arbitrary function of u and v. We will see in section 4.4 that G is actually completely fixed if we know the entire spectrum of operators in the CFT plus the complete set of 3-point function coefficients λ_{ijk}.

4.3 Operator Product Expansion

In this section, we will argue that a CFT has an operator product expansion (OPE) that converges at finite separation. We will do this by Weyl transforming from Euclidean $\mathbb{R}^d$ to the cylinder $S^{d-1} \times \mathbb{R}$. The convergent OPE will result from applying the standard rules of quantum mechanics to the CFT on the cylinder. For more details, see [160].

In polar coordinates, the flat space metric is

$$ds^2 = dr^2 + r^2 d\Omega_{d-1}^2 \tag{4.21}$$

$$= e^{2\tau} \left(d\tau^2 + d\Omega_{d-1}^2 \right), \tag{4.22}$$

where $r = e^{\tau}$. In the last line, the term in the parenthesis is the metric for the cylinder $S^{d-1} \times \mathbb{R}$. Thus, we see that flat Euclidean space is Weyl equivalent to the cylinder. Therefore, we can simply map the CFT to the cylinder via transformation (4.6) with $\Omega = e^{-\tau}$. Now, we will assume that after Wick rotating to Lorentzian time on the cylinder, the standard rules of quantum mechanics apply. In particular,

1. There is a complete Hilbert Space of normalizable states.

2. The Hamiltonian is diagonalizable.

3. The energy eigenstates form a basis.

As usual, states on the cylinder can be given a path integral construction. Suppose that our CFT is given by a path integral over the scalar field Φ. Let $\varphi(\vec{x})$ denote field configurations on the sphere S^{d-1}. Then, for example, the ground state wavefunctional
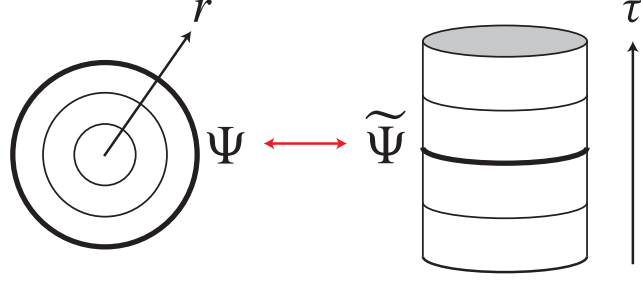
Figure 4.3: There is a one-to-one correspondence between functionals on $\mathbb{R}^d$ and wavefunctionals on the cylinder.

$\Psi_0[\varphi]$ in the basis of field eigenstates $|\varphi\rangle$ can be constructed as

$$\Psi_0[\varphi] \equiv \langle \varphi | 0 \rangle = \int_{\substack{\Phi(\tau, \vec{x}) = \varphi(\vec{x}) \\ \tau \leq 0}} \mathcal{D}\Phi \, e^{-S[\Phi]}. \tag{4.23}$$

This is the Euclidean path integral over the field $\Phi(\tau, \vec{x})$ on the half cylinder ($\tau \leq 0$) with the boundary condition $\Phi(0, \vec{x}) = \varphi(\vec{x})$. Excited states $|\Psi\rangle$ can be constructed by inserting additional operators in the path integral:

$$\Psi[\varphi] \equiv \langle \varphi | \Psi \rangle = \int_{\substack{\Phi(\tau, \vec{x}) = \varphi(\vec{x}) \\ \tau \leq 0}} \mathcal{D}\Phi \, e^{-S[\Phi]} \mathcal{O}_1 \cdots \mathcal{O}_n. \tag{4.24}$$

We can also transform the path integral back to $\mathbb{R}^d$. There, the region of integration is a solid ball with boundary conditions on its S^{d-1} boundary. The path integral over the interior of the ball as a function of its boundary conditions also defines a functional $\widetilde{\Psi}[\varphi]$. There is thus a one-to-one correspondence between this functional $\widetilde{\Psi}[\varphi]$ on $\mathbb{R}^d$ and the wavefunctional $\Psi[\varphi]$ on the cylinder (figure 4.3). We will use this correspondence heavily below.

By assumption, any state $|\Psi\rangle$ on the cylinder can be expanded in a complete set of

122

energy eigenstates $|\Delta_i\rangle$:

$$|\Psi\rangle = \sum_i c_i |\Delta_i\rangle. \tag{4.25}$$

We labeled the energies by Δ since time translations on the cylinder corresponds to scale transformations on $\mathbb{R}^d$ (quantizing this way goes by the name "radial quantization"). Having seen in (4.24) how operators can create states on the cylinder, we will now show that the converse is also true. Namely, for each $|\Delta_i\rangle$ on the cylinder, we can define a local operator $\mathcal{O}_{|\Delta_i\rangle}$ on $\mathbb{R}^d$. We will define $\mathcal{O}_{|\Delta_i\rangle}$ by defining its correlation functions. As argued in the previous paragraph, the wavefunctional $\Psi_{|\Delta_i\rangle}[\varphi] = \langle\varphi|\Delta_i\rangle$ corresponds in $\mathbb{R}^d$ to a functional $\widetilde{\Psi}_{|\Delta_i\rangle}[\varphi]$ defined over a sphere S^{d-1}. Correlators of $\mathcal{O}_{|\Delta_i\rangle}$ can now be defined by cutting a solid ball out of the path integral on $\mathbb{R}^d$ and gluing in the functional $\widetilde{\Psi}_{|\Delta_i\rangle}[\varphi]$. By gluing, we mean do the path integral outside the solid ball with the boundary condition φ on the the boundary. Then integrate over the boundary condition weighted by $\widetilde{\Psi}_{|\Delta_i\rangle}[\varphi]$.

$$\langle \mathcal{O}_{|\Delta\rangle} \mathcal{O}_{|\Delta\rangle} \mathcal{O}_{|\Delta\rangle} \rangle \equiv \qquad\qquad\qquad\qquad\qquad \tag{4.26}$$

We are now ready to derive the OPE. In $\mathbb{R}^d$, consider two operators $\mathcal{O}_i(x)\mathcal{O}_j(0)$ inside a ball. The path integral inside the ball defines a functional $\widetilde{\Psi}$ on the boundary. This functional has a corresponding cylinder wavefunctional $\Psi[\varphi] = \langle\varphi|\Psi\rangle$. Expand the state $|\Psi\rangle = \sum_k c_k |\Delta_k\rangle$. Finally, each $|\Delta_k\rangle$ maps back to an operator $\mathcal{O}_{|\Delta_k\rangle}$ in $\mathbb{R}^d$. In the end,

we have

$$\mathcal{O}_i(x)\mathcal{O}_j(0) = \sum_k c_k(x)\mathcal{O}_{|\Delta_k\rangle}, \qquad (4.27)$$

This is the OPE. Our derivation makes it clear that the OPE converges anytime a sphere can be drawn around two operators with out enclosing any others. Note that neither of the two operators needs to be located at the center of the sphere.

4.4 Conformal Data

The conformal data of a CFT consists of its spectrum of primary operators $\{\Delta_i, l_i\}$, together with the corresponding set of 3-point function coefficients $\{\lambda_{ijk}\}$. In this section, we will show that a CFT's conformal data completely determines all the correlations functions of its local operators.

We begin with the OPE (4.27) from last section, reorganizing it as a sum over only the primaries and writing the sum over the descendants explicitly,

$$\mathcal{O}_i(x)\mathcal{O}_j(0) = \sum_k a_k(x)\mathcal{O}_k(0) + b_k^\mu(x)\partial_\mu\mathcal{O}_k(0) + c_k^{\mu\nu}(x)\partial_\mu\partial_\nu\mathcal{O}_k(0) + \cdots. \quad (4.28)$$

For simplicity, consider only scalar operators in what follows. We will now show that for each k, conformal invariance completely fixes the coefficient functions up to a single

constant. To see this, use the OPE to evaluate the 3-point function:

$$\langle \mathcal{O}_i(x)\mathcal{O}_j(0)\mathcal{O}_k(y)\rangle = \sum_{k'} \left[a_{k'}(x) + b_{k'}^\mu(x)\partial_\mu + c_{k'}^{\mu\nu}(x)\partial_\mu\partial_\nu + \cdots \right] \langle \mathcal{O}_{k'}(0)\mathcal{O}_k(y)\rangle$$

(4.29)

$$= \left[a_k(x) + b_k^\mu(x)\partial_\mu + c_k^{\mu\nu}(x)\partial_\mu\partial_\nu + \cdots \right] \frac{1}{y^{2\Delta_k}}.$$

(4.30)

The sum over k' collapsed due to the orthonormality of the 2-point function. On the other hand, we know the exact form of the 3-point function,

$$\langle \mathcal{O}_i(x)\mathcal{O}_j(0)\mathcal{O}_k(y)\rangle = \frac{\lambda_{ijk}}{x^{\Delta_i+\Delta_j-\Delta_k} y^{\Delta_k+\Delta_j-\Delta_i} |x-y|^{\Delta_k+\Delta_i-\Delta_j}}$$

(4.31)

$$= \frac{\lambda_{ijk}}{x^{\Delta_i+\Delta_j-\Delta_k} y^{2\Delta_k}} \left(1 - \frac{2x\cdot y}{y^2} + \frac{x^2}{y^2} \right)^{\frac{\Delta_j-\Delta_k-\Delta_i}{2}}.$$

(4.32)

By expanding the term in parenthesis for small x and comparing with (4.30), we can determine all the OPE coefficient functions $a_k(x)$, $b_k^\mu(x)$, etc. For example,

$$a_k(x) = \frac{\lambda_{ijk}}{x^{\Delta_i+\Delta_j-\Delta_k}}$$

(4.33)

$$b_k^\mu(x) = \frac{\lambda_{ijk}}{x^{\Delta_i+\Delta_j-\Delta_k}} \frac{\Delta_i - \Delta_j + \Delta_k}{2\Delta_k} x^\mu.$$

(4.34)

Up to the 3-point function constant λ_{ijk}, we see that the OPE coefficient functions are completely fixed by the dimensions (and spins) of the three operators involved. Because of

125

this the, λ_{ijk} are commonly called OPE coefficients. We can now write the OPE as,

$$\mathcal{O}_i(x)\mathcal{O}_j(0) = \sum_k \lambda_{ijk} P_{ijk}(x, \partial)\mathcal{O}_k(0), \tag{4.35}$$

where P is a differential operator completely fixed by conformal symmetry.

The OPE can be used recursively to turn any n-point function into a sum of $(n-1)$-point functions:

$$\langle\mathcal{O}_1(x_1)\mathcal{O}_2(x_2)\mathcal{O}_3(x_3)\cdots\mathcal{O}_n(x_n)\rangle = \sum_k \lambda_{12k} P_{12k}(x_{12}, \partial_2)\langle\mathcal{O}_k(x_2)\mathcal{O}_3(x_3)\cdots\mathcal{O}_n(x_n)\rangle.$$
$$\tag{4.36}$$

We can keep doing this until we are left with a sum of 2-point functions, which we already know.[6] Therefore, by using the OPE, all n-point functions are completely determined once the conformal data is known.

4.5   Conformal Bootstrap Equations

In this section, we derive the conformal bootstrap equations. These are the central equations used in practically all studies of conformal field theory in the last eight years. As we saw in the previous section, the conformal data of a CFT is an efficient way of specifying all its local correlators. In fact, the modern point of view attempts to take the conformal data as an algebraic definition of a CFT. Of course, we are not free to just randomly specify a set of $\{(\Delta_i, l_i), \lambda_{ijk}\}$ and claim that we have defined a CFT. There are severe constraints that this data must satisfy, and these are encapsulated in the conformal bootstrap equations.

---

[6]We could equally well stop at 3-point functions, but we will be stopping at 2-point functions later.

The constraints arise because there are many different ways of pairing together operators when using the OPE to recursively reduce n-point functions down to a convergent sum of 2-point functions. The resulting expressions can look very different, however they must all sum to the same answer. For example, consider one way of pairing a 4-point function of identical scalars ϕ:

$$\langle \overset{\frown}{\phi(x_1) \phi}(x_2) \overset{\frown}{\phi(x_3) \phi}(x_4) \rangle$$

$$= \sum_{\mathcal{O},\mathcal{O}'} \lambda_{\phi\phi\mathcal{O}} \lambda_{\phi\phi\mathcal{O}'} P^a_{\phi\phi\mathcal{O}}(x_{12}, \partial_2) P^b_{\phi\phi\mathcal{O}'}(x_{34}, \partial_4) \langle \mathcal{O}^a(x_2) \mathcal{O}^b(x_3) \rangle \qquad (4.37)$$

$$= \frac{1}{x_{12}^{2\Delta_\phi} x_{34}^{2\Delta_\phi}} \sum_{\mathcal{O}} \lambda_{\phi\phi\mathcal{O}}^2 \left[x_{12}^{2\Delta_\phi} x_{34}^{2\Delta_\phi} P^a_{\phi\phi\mathcal{O}}(x_{12}, \partial_2) P^b_{\phi\phi\mathcal{O}}(x_{34}, \partial_4) \frac{I^{ab}(x_{24})}{x_{24}^{\Delta_\mathcal{O}}} \right],$$

$$(4.38)$$

where a, b are previously suppressed collective spin indices $(\mu_1 \cdots \mu_l)$ and I^{ab} is the tensor from (4.16). Having stripped off the necessary position factors to account for the conformal transformation properties of the 4-point function (compare with (4.19)), the factor in brackets is now only a function of the conformal cross-ratios u and v. As we can see, this factor is completely determined by conformal symmetry and is only a function of the dimensions and spins of the five operators involved. In other words, for each set of dimensions and spins, it only needs to be calculated once and then it can be used for all CFTs. These functions are called conformal blocks and will be denoted by $g_{\Delta,l}(u, v)$,[7] where the Δ and l refer to the exchanged operator while the dependence on the external operators is suppressed.

---

[7]Recombined with the factors of x that were stripped off, they are also called conformal partial waves due to being the conformal group analog of partial waves for the rotation group
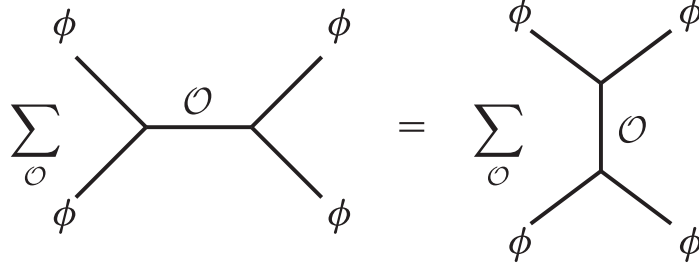
Figure 4.4: The conformal bootstrap equations

Therefore, the 4-point function can be written as

$$\langle \phi(x_1)\phi(x_2)\phi(x_3)\phi(x_4)\rangle = \frac{1}{x_{12}^{2\Delta_\phi} x_{34}^{2\Delta_\phi}} \sum_{\mathcal{O}} \lambda_{\phi\phi\mathcal{O}}^2 g_{\Delta_\mathcal{O},l_\mathcal{O}}(u,v). \tag{4.39}$$

This was just one way of pairing the operators in the 4-point function. By pairing them in a different way, we get a different conformal block expansion of the same 4-point function. Within their overlapping region of convergence, the two expansions must be equal:

$$\overbrace{\langle \phi(x_1)\phi(x_2)}\overbrace{\phi(x_3)\phi(x_4)\rangle} = \overbrace{\langle \phi(x_1)\phi(x_2)\phi(x_3)\phi(x_4)\rangle}. \tag{4.40}$$

The set such equations for all 4-point functions is called the conformal bootstrap equations (figure 4.4).

Note that in our case of four identical scalars, the RHS of (4.40) is simply equal to (4.39) with $x_1 \leftrightarrow x_3$. After a little rearranging, (4.40) becomes

$$v^{\Delta_\phi} \sum_{\mathcal{O}} \lambda_{\phi\phi\mathcal{O}}^2 g_{\Delta_\mathcal{O},l_\mathcal{O}}(u,v) = u^{\Delta_\phi} \sum_{\mathcal{O}} \lambda_{\phi\phi\mathcal{O}}^2 g_{\Delta_\mathcal{O},l_\mathcal{O}}(v,u). \tag{4.41}$$

We will separate out the contribution of the identity operator $\mathbb{1}$ because we know that $\lambda_{\phi\phi\mathbb{1}} = g_{0,0} = 1$. This can be determined by using the OPE to evaluate the 2-point function

$\langle\phi\phi\rangle$. Therefore, (4.41) can be written as

$$1 = \sum_{\mathcal{O}} \lambda_{\phi\phi\mathcal{O}}^2 F_{\phi\phi\mathcal{O}}(u, v), \tag{4.42}$$

where

$$F_{\phi\phi\mathcal{O}}(u, v) \equiv \frac{v^{\Delta_\phi} g_{\Delta_\mathcal{O}, l_\mathcal{O}}(u, v) - u^{\Delta_\phi} g_{\Delta_\mathcal{O}, l_\mathcal{O}}(v, u)}{u^{\Delta_\phi} - v^{\Delta_\phi}}. \tag{4.43}$$

Equation (4.42) is the conformal bootstrap equation for four identical scalar operators.

To be concrete, the closed form expression for the conformal blocks in the (12)(34) channel of $\langle \mathcal{O}_1 \mathcal{O}_2 \mathcal{O}_3 \mathcal{O}_4 \rangle$ is [161]

$$g_{\Delta, l}(u, v)$$
$$= \left[z^h \, _2F_1(h - h_{12}, h + h_{34}; 2h, z) \times \bar{z}^{\bar{h}} \, _2F_1(\bar{h} - \bar{h}_{12}, \bar{h} + \bar{h}_{34}; 2\bar{h}, \bar{z}) \right] + (z \leftrightarrow \bar{z}), \tag{4.44}$$

where $_2F_1$ is the hypergeometric function, $\Delta = h + \bar{h}$, $l = h - \bar{h}$, $u = z\bar{z}$, $v = (1-z)(1-\bar{z})$, $h_{ij} = h_i - h_j$, and $\bar{h}_{ij} = \bar{h}_i - \bar{h}_j$.

Remarkably, once the bootstrap equations are satisfied for all 4-point functions, there are no further consistency conditions imposed by higher point functions. The reason this works is that the ability to arbitrarily pair up operators in a correlation function amounts to requiring that the OPE is associative:

$$\overline{\mathcal{O}_1 \mathcal{O}_2} \mathcal{O}_3 \quad = \quad \mathcal{O}_1 \overline{\mathcal{O}_2 \mathcal{O}_3}. \tag{4.45}$$

Taking the correlator of both sides with a fourth operator $\mathcal{O}_4$ results in the conformal bootstrap equation.

Going back to the modern attempt at an algebraic definition of a CFT mentioned at the beginning of this section: a CFT is defined as a set of conformal data that satisfies OPE associativity. Equivalently, a CFT is a set of conformal data that satisfies the conformal bootstrap equations for all 4-point functions. An ultimate goal would be to classify all CFTs analogously to the way finite-dimensional Lie algebras are classified starting from the Jacobi identity. This algebraic definition of a CFT is still tentative, and there will likely be additional data and new constraints to be discovered.[8] However, for our purposes, we only need the fact that the conformal bootstrap equations are a necessary condition on CFTs.

4.6 Unitarity

In this section, we derive constraints on the conformal data imposed by unitarity. Specifically, we derive lower bounds on operator dimensions as well as the condition that the OPE coefficients λ_{ijk} are real.

In Lorentzian signature, a Heisenberg operator is defined as

$$\mathcal{O}_L(t) = e^{iHt}\mathcal{O}_0 e^{-iHt}, \qquad (4.46)$$

where we suppressed the spatial index. For Hermitian $\mathcal{O}_0$, we thus have $\mathcal{O}_L^\dagger(t) = \mathcal{O}_L(t)$. On the other hand, the Euclidean operator $\mathcal{O}_E(\tau)$ is defined via analytic continuation of

---

[8] For example, there is surely additional data associated with non-local operators, and probably additional constraints from requiring that the CFT be consistent on manifolds that are not conformally flat.

$\mathcal{O}_L(t)$:

$$\mathcal{O}_E(\tau) = \mathcal{O}_L(-i\tau) = e^{H\tau}\mathcal{O}_0 e^{-H\tau}. \tag{4.47}$$

Therefore, we instead have $\mathcal{O}_E^\dagger(\tau) = \mathcal{O}_E(-\tau)$. Conjugation causes a reflection in the Euclidean time direction. Now define the state

$$\langle\psi| = \langle 0|\mathcal{O}(\tau_1)\cdots\mathcal{O}(\tau_n) \tag{4.48}$$

where $\tau_1 \geq \tau_2 \geq \cdots \geq \tau_n$. In order to have a consistent Hilbert space interpretation, $\langle\psi|\psi\rangle \geq 0$. This condition is called unitarity in the literature.[9] Therefore, by (4.48),

$$\langle\psi|\psi\rangle = \langle 0|\mathcal{O}(\tau_1)\cdots\mathcal{O}(\tau_n)\mathcal{O}(-\tau_n)\cdots\mathcal{O}(-\tau_1)|0\rangle \geq 0. \tag{4.49}$$

The correlator is a standard time-ordered correlator. Note that the operators are arranged symmetrically about $\tau = 0$. Conversely, all correlators that are symmetric about an axis can be interpreted as computing the norm of some state and therefore must be positive. This condition is called reflection positivity.

As an example, consider the 2-point function of the operator $\partial^2\mathcal{O}$, where $\mathcal{O}$ is a scalar:

$$\langle\partial^2\mathcal{O}(x)\partial^2\mathcal{O}(y)\rangle = \partial_x^2\partial_y^2\frac{1}{(x-y)^{2\Delta}}. \tag{4.50}$$

Requiring this to be reflection positive gives the constraint $\Delta \geq \frac{d-2}{2}$. Furthermore, by considering the two point function of $\partial_{\mu_1}\mathcal{O}^{\mu_1,\cdots\mu_s}$, where $\mathcal{O}^{\mu_1,\cdots\mu_s}$ is an operator of spin s

---

[9]This meaning of unitarity is a logically distinct and more primitive concept then that of time evolution with a unitary operator.

(a traceless symmetric tensor of rank s), we get bounds for operators with spin. Altogether, the unitarity bounds are

$$s = 0 \quad \Delta \geq \frac{d-2}{2} \tag{4.51}$$

$$s > 0 \quad \Delta \geq s + d - 2. \tag{4.52}$$

Finally, we need to derive the condition that $\lambda_{ijk}^2 \geq 0$. This constraint is extremely crucial for the numerical bootstrap program. Its proof is simple. First, we are always working in a basis in which all operators are Hermitian in Lorentzian signature. Now, consider a Lorentzian correlator of three operators at equal time. Since they commute, we have

$$\langle 0|\mathcal{O}_i(0, x_1)\mathcal{O}_j(0, x_2)\mathcal{O}_k(0, x_3)|0\rangle^* = \langle 0|\mathcal{O}_i(0, x_1)\mathcal{O}_j(0, x_2)\mathcal{O}_k(0, x_3)|0\rangle. \tag{4.53}$$

Using the expression for the 3-point function (4.18), we see that the λ_{ijk} are real and therefore

$$\lambda_{ijk}^2 \geq 0. \tag{4.54}$$

4.7 Numerical Bounds

In this section, we will illustrate how general theorems can be proved about CFTs through the use of numerical methods. The goal is to show that even though the methods are numerical (as opposed to analytical), the results are still rigorous. Currently, the lofty goal of classifying all solutions to the bootstrap equations is completely intractable. There

are an infinite number of equations (one for each 4-point function) and an infinite number of variables (the conformal data). Furthermore, the dimensions and spins enter the equations in a highly nonlinear way. The breakthrough came in 2008 when [162] realized that instead of using the bootstrap to find CFTs, they could instead use it to rule out putative CFTs by showing that their conformal data do not satisfy the bootstrap equations.

As we derived in the last section, the bootstrap equation for four scalars (4.42) is

$$1 = \sum_{\Delta,l} \lambda_{\Delta,l}^2 F_{\Delta,l}(u,v), \tag{4.55}$$

where we rewrote the sum over $\mathcal{O}$ as a sum over the dimensions Δ and spins l of $\mathcal{O}$, and we also suppressed the dependence on the external operators ϕ. In what follows, assume that we have picked a specific numerical value for Δ_ϕ. The numerical analysis must be done separately for each value of Δ_ϕ. We now begin with a very simple algorithm which shows the essential way numerical methods are used.

1. Propose a set of $\{(\Delta, l), \lambda_{\Delta,l}\}$.

2. Pick values of u, v, and numerically evaluate the RHS of (4.55).

3. If the RHS $\neq 1$, then a CFT with such an OPE does not exist.

Numerical methods are used only in evaluating the functions $F_{\Delta,l}$. The situation is like the common algebra homework problem of proving the inequality $\pi^e < e^\pi$. While in this case, there exist analytic proofs using various identities involving e and π, one can also simply cheat and use a calculator to check. Our current situation is like this homework problem but without any known identities that can be used for an analytic proof.

133

Moving on, it would be more powerful if we did not have to specify a given set of conformal data so exclusively. Fortunately, unitarity allows us to inclusively rule out large regions of conformal data parameter space. Specifically, as shown in section 4.6, unitarity requires that the $\lambda_{\Delta,l}$'s are real and therefore $\lambda_{\Delta,l}^2 \geq 0$. We can use this to improve our primitive algorithm so that we don't even have to specify the OPE coefficients.

1. Propose just a spectrum $\{\Delta, l\}$ of operators that can appear in the $\phi \times \phi$ OPE.

2. Pick values of u, v, and numerically evaluate $F_{\Delta,l}(u, v)$.

3. If, for any u, v, we find that $F_{\Delta,l}(u, v) \leq 0$ for all Δ, l in the spectrum, then a CFT with such an OPE does not exist.

By using unitarity, we can thus rule out an operator spectrum regardless of the $\lambda_{\Delta,l}$'s. Note that unitarity allows the $\lambda_{\Delta,l}$'s to vanish. Therefore, the operators in the proposed spectrum do not actually have to appear in the $\phi \times \phi$ OPE. More precisely, this algorithm rules out CFTs whose operators *only* come from the operators in the proposed spectrum. In other words, it rules out CFTs without operators that are not in the proposed spectrum.

By thinking geometrically, we can further improve the previous algorithm. In step (2), pick n values of u, v and label them $u_i, v_i, i = 1, \ldots, n$. Obviously, (4.55) must hold for each i. Arrange the n separate equations into a single vector equation:

$$\begin{pmatrix} 1 \\ 1 \\ \vdots \\ 1 \end{pmatrix} = \sum_{\Delta,l} \lambda_{\Delta,l}^2 \begin{pmatrix} F_{\Delta,l}(u_1, v_1) \\ F_{\Delta,l}(u_2, v_2) \\ \vdots \\ F_{\Delta,l}(u_n, v_n) \end{pmatrix}. \tag{4.56}$$

(a) No solution.   (b) Extremal case.   (c) There exist a solution.
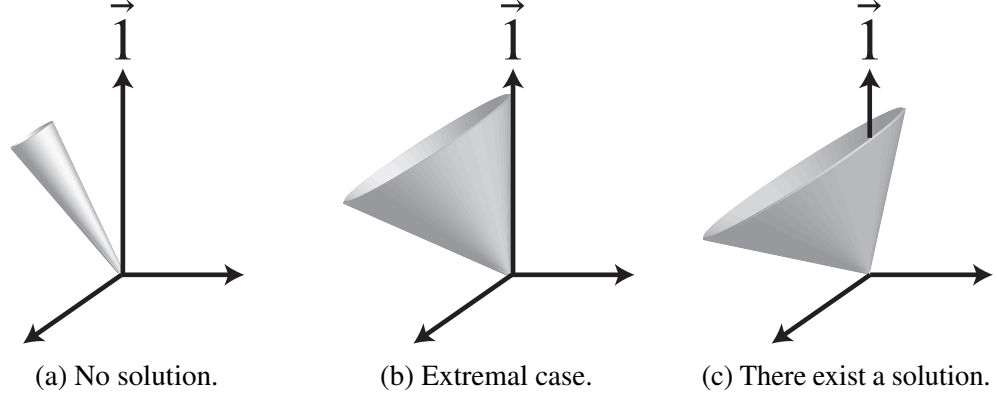
Figure 4.5: Geometry of the conformal bootstrap equations.

Since each $F_{\Delta,l}(u_i, v_i)$ is a known number (found using numerical methods), (4.56) can be viewed as a system of equations for $\lambda_{\Delta,l}^2$. Crucially, since $\lambda_{\Delta,l}^2 \geq 0$, the space of all possible RHS's forms a convex cone in n-dimensions. The question is simply whether the vector of 1's on the LHS falls inside or outside the cone. If it falls inside, then there is a solution, and otherwise, there is not (figure 4.5). In other words, if all the vectors in the sum on the RHS of (4.56) point in one direction, while the vector on the LHS points in the other, then there is no solution. Mathematically, if this is the case, we can then find a vector $\vec{n}$ such that

$$
\vec{n} \cdot \begin{pmatrix} 1 \\ 1 \\ \vdots \\ 1 \end{pmatrix} < 0 \quad \text{and} \quad \vec{n} \cdot \begin{pmatrix} F_{\Delta,l}(u_1, v_1) \\ F_{\Delta,l}(u_2, v_2) \\ \vdots \\ F_{\Delta,l}(u_n, v_n) \end{pmatrix} \geq 0. \tag{4.57}
$$

If we can find such a vector, then the corresponding CFT does not exist.

In practice, instead of evaluating (4.55) at various points, derivatives about $u = v = \frac{1}{4}$

135

are used:

$$
\begin{pmatrix} 1 \\ 0 \\ 0 \\ \vdots \\ 0 \end{pmatrix} = \sum_{\Delta,l} \lambda_{\Delta,l}^2 \begin{pmatrix} F_{\Delta,l} \\ \partial_u F_{\Delta,l} \\ \partial_v F_{\Delta,l} \\ \vdots \\ \partial_u^m \partial_v^n F_{\Delta,l} \end{pmatrix}\Bigg|_{u=v=\frac{1}{4}} , \tag{4.58}
$$

for some chosen m, n. Then, an appropriate vector $\vec{n}$ can again be searched for. In general, both methods can be phrased in terms of a linear functional α acting on both sides of the bootstrap equation (4.55):

$$
\alpha(1) = \sum_{\Delta,l} \lambda_{\Delta,l}^2 \alpha(F_{\Delta,l}). \tag{4.59}
$$

In the case of (4.58), the linear functional is

$$
\alpha(f) = \sum_{m+n \leq \Lambda} a_{mn} \partial_u^m \partial_v^n f |_{u=v=\frac{1}{4}} . \tag{4.60}
$$

Therefore, the final algorithm is:

1. Propose a spectrum of $\{\Delta, l\}$ of operators that can appear in the $\phi \times \phi$ OPE.

2. Search for a linear functional α such that $\alpha(1) < 0$ and $\alpha(F_{\Delta,l}) \geq 0$ for all Δ, l in the proposed spectrum.

3. If such an α is found, then a CFT with such an OPE does not exist.

In practice, the search over linear functionals α amounts to a search for the coefficients a_{mn} in (4.60) satisfying the linear inequalities in step (2) of this final algorithm. This type of

search is a problem in linear algebra called a linear programming problem, and efficient numerical methods exist to solve such problems.

Let us now consider the prototypical example. In the language of perturbation theory, the question is: what is the maximum dimension of the operator ϕ^2 as of function of the dimension of ϕ? In perturbation theory, the answer is always $\Delta_{\phi^2} = 2\Delta_\phi + \text{small corrections}$. However, in a strongly interacting theory, ϕ^2 can obtain a large anomalous dimension. In fact, the operator ϕ^2 really has no a priori meaning. We will simply define it to be the lowest dimension scalar operator in the $\phi \times \phi$ OPE.

Now let us apply the algorithm. The proposed spectrum is:

$l > 0$ all operators consistent with unitarity bounds ($\Delta \geq l + d - 2$)

$l = 0$ all operators with $\Delta > \Delta_{\text{gap}}$

Now, we need to search for an α of the form (4.60) such that $\alpha(1) < 0$ and $\alpha(F_{\Delta,l}) \geq 0$ for all Δ, l in the proposed spectrum.

Unfortunately, before we can put it on a computer, there is one more issue that we need to deal with. Since there are a continuous infinity of Δ, l in the proposed spectrum, the inequalities $\alpha(F_{\Delta,l}) \geq 0$ are a continuously infinite number of inequalities. To make further progress, we simply truncate and discretize the values of Δ and l in the spectrum, leaving us with a finite number of inequalities. However, once a functional is found, we can then verify that the inequalities are satisfied on the remainder of the spectrum. If they are, then the CFT is ruled out. The results for this example in 2D are plotted in figure 4.6.

As an aside, the original motivation of [162] was phenomenological, in which they were
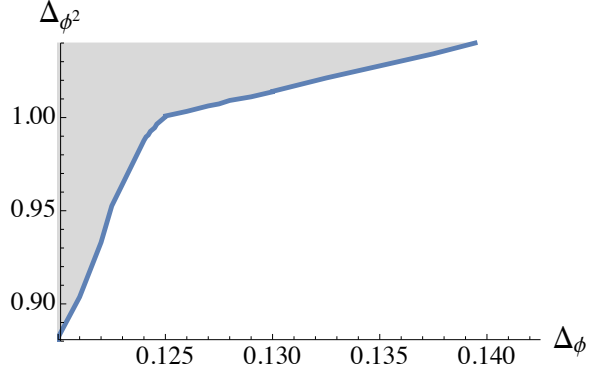
137

Figure 4.6: The maximum value of Δ_{ϕ^2} as a function of Δ_ϕ in two dimensions. The shaded region is ruled out.

attempting to rule out a proposed solution to the hierarchy problem [163]. The hierarchy problem is simply the puzzle as to why the standard model of particle physics appears to be finely tuned extremely close to a critical point. The relevant operator in question is $H^\dagger H$, where H is the Higgs field. Reference [163] proposed that, due to new strongly coupled conformal dynamics, the composite operator $H^\dagger H$ has dimension close to 4, making it much less relevant and thus requiring much less tuning. On the other hand, due to other issues concern flavor physics, the dimension of H needed to be close to 1. Therefore, [162] developed the numerical bootstrap in an attempt to show that such a scenario was impossible. In [164], the simplest "flavor-generic" versions of conformal technicolor was ruled out.

4.8   Multiple Correlators

The results from last section came from analyzing just a single 4-point function. However, the consistency conditions imposed by OPE associativity requires that the infinite set of 4-point functions satisfy the conformal bootstrap equations. In this section, we move a little in that direction by preparing for the analysis of a system of three crossing equations.

To begin, we will need to analyze 4-point functions of non-identical operators. Until now, we have only looked at 4-point functions of the same operator. Naively, 4-point functions of non-identical operators pose problems for the numerical bootstrap. For example, consider the crossing equation for $\langle\sigma\sigma\epsilon\epsilon\rangle$, where σ and ϵ are non-identical scalars:

$$\langle\sigma\sigma\epsilon\epsilon\rangle = \sum_{\mathcal{O}} \quad\quad = \sum_{\mathcal{O}'} \tag{4.61}$$

After some rearranging, the analog of (4.41) is

$$\sum_{\mathcal{O}} \lambda_{\sigma\sigma\mathcal{O}}\lambda_{\epsilon\epsilon\mathcal{O}}\, g_{\mathcal{O}}(u,v) = \sum_{\mathcal{O}'} \lambda^2_{\sigma\epsilon\mathcal{O}'}\tilde{g}_{\mathcal{O}'}(v,u), \tag{4.62}$$

where $g_{\mathcal{O}}$ and $\tilde{g}_{\mathcal{O}}$ are the appropriate conformal blocks after absorbing some additional factors of u and v. The problem is that while $\lambda^2_{\sigma\epsilon\mathcal{O}} \geq 0$, the product of two different OPE coefficients $\lambda_{\sigma\sigma\mathcal{O}}\lambda_{\epsilon\epsilon\mathcal{O}}$ can have either sign. Therefore, we cannot simply apply linear functionals to both sides of (4.62) and derive results as in the last section.

In order to obtain some kind of positivity condition, [150] combined the crossing equation for $\langle\sigma\sigma\epsilon\epsilon\rangle$ with the crossing equations for $\langle\sigma\sigma\sigma\sigma\rangle$ and $\langle\epsilon\epsilon\epsilon\epsilon\rangle$,

$$1 = \sum_{\mathcal{O}} \lambda^2_{\sigma\sigma\mathcal{O}} F_{\mathcal{O}} \tag{4.63}$$

$$1 = \sum_{\mathcal{O}} \lambda^2_{\epsilon\epsilon\mathcal{O}} F_{\mathcal{O}}. \tag{4.64}$$

The combined equation can be written as

$$\sum_{\mathcal{O}} \begin{pmatrix} \lambda_{\sigma\sigma\mathcal{O}} & \lambda_{\epsilon\epsilon\mathcal{O}} \end{pmatrix} \begin{pmatrix} F_{\mathcal{O}} & g_{\mathcal{O}} \\ g_{\mathcal{O}} & F_{\mathcal{O}} \end{pmatrix} \begin{pmatrix} \lambda_{\sigma\sigma\mathcal{O}} \\ \lambda_{\epsilon\epsilon\mathcal{O}} \end{pmatrix} - \sum_{\mathcal{O}'} \lambda^2_{\sigma\epsilon\mathcal{O}'} \tilde{g}_{\mathcal{O}'}(v,u) = 0, \qquad (4.65)$$

where the identity operator $\mathbb{1}$ has been included in the sum. Now consider a linear functional α such that

$$\begin{pmatrix} \alpha(F_{\mathcal{O}}) & \alpha(g_{\mathcal{O}}) \\ \alpha(g_{\mathcal{O}}) & \alpha(F_{\mathcal{O}}) \end{pmatrix} \succeq 0, \qquad (4.66)$$

where $\succeq$ means that the 2×2 matrix is positive semidefinite. By definition, a positive semidefinite matrix satisfies

$$\begin{pmatrix} \lambda_{\sigma\sigma\mathcal{O}} & \lambda_{\epsilon\epsilon\mathcal{O}} \end{pmatrix} \begin{pmatrix} \alpha(F_{\mathcal{O}}) & \alpha(g_{\mathcal{O}}) \\ \alpha(g_{\mathcal{O}}) & \alpha(F_{\mathcal{O}}) \end{pmatrix} \begin{pmatrix} \lambda_{\sigma\sigma\mathcal{O}} \\ \lambda_{\epsilon\epsilon\mathcal{O}} \end{pmatrix} \geq 0 \qquad (4.67)$$

for all $\lambda_{\sigma\sigma\mathcal{O}}$ and $\lambda_{\epsilon\epsilon\mathcal{O}}$. Therefore, by applying α to both sides of (4.65) and also requiring $\alpha(\tilde{g}_{\mathcal{O}'}) \leq 0$, we can again rule out putative CFTs.

Note that searching for α's subject to the positive semidefiniteness constraint (4.66) is no longer a linear programming problem. However, there are still efficient numerical algorithms for such "semidefinite programming" problems. In particular, [151] has been optimized specifically for the bootstrap and is used in this work.

4.9 Application to Universality

In this section, we describe how we will use the numerical methods just reviewed in order to investigate the concept of universality.

Let us review our question. As mentioned in the introduction, in critical phenomena, members of a universality class generally have only three properties in common: the number of dimensions, the global symmetry group of the Hamiltonian, and the number of experimental "knobs" that need to be tuned in order to reach the critical point. The question is: why only three? Why is there not multiple universality classes with the same set of those three properties? This would be consistent with the renormalization group. Now, due to the severe consistency conditions imposed by the conformal bootstrap equations, a possible answer has emerged. The work of [150–153] suggests the answer is that there only exists a single CFT with any fixed set of those properties. Their evidence was in three dimensions. We give the analogous evidence in two dimensions for the case of the 2D Ising universality class.

We will formulate this question so that it can be investigated with the final numerical bootstrap algorithm presented in section 4.7. We want to show that the 2D Ising universality class is the only universality class that:

1. is in two dimensions

2. has a $\mathbb{Z}_2$ global symmetry

3. has exactly two relevant operators (one even and one odd under the $\mathbb{Z}_2$)

The relevant operators correspond to directions away from the fixed point's basin of at-

traction, which correspond to experimental knobs that need to be tuned. The two relevant operators in the Ising case correspond to the temperature and magnetic field in the magnetic transition or to the temperature and pressure in the liquid-vapor transition.

Denote the two relevant operators by σ and ϵ, where σ is $\mathbb{Z}_2$-odd and ϵ is $\mathbb{Z}_2$-even. The symmetry structure of the OPE is

$$\sigma \times \sigma \sim \mathbb{Z}_2\text{-even} \tag{4.68}$$

$$\epsilon \times \epsilon \sim \mathbb{Z}_2\text{-even} \tag{4.69}$$

$$\sigma \times \epsilon \sim \mathbb{Z}_2\text{-odd} \tag{4.70}$$

This allows us to make separate proposals about the spectrum of $\mathbb{Z}_2$-even and $\mathbb{Z}_2$-odd operators.

As in section 4.8, we will consider the combined set of 4-point functions, $\langle \sigma\sigma\sigma\sigma \rangle$, $\langle \epsilon\epsilon\epsilon\epsilon \rangle$, and $\langle \sigma\sigma\epsilon\epsilon \rangle$. Now, we need to propose a spectrum of operators that can appear in the above OPEs. The spectrum will be as follows:

$$l = 0,\ \mathbb{Z}_2\text{-odd:} \quad \Delta = \Delta_\sigma \text{ or } \Delta > 2$$

$$l = 0,\ \mathbb{Z}_2\text{-even:} \quad \Delta = \Delta_\epsilon \text{ or } \Delta > 2$$

$$l > 0 \quad \text{all operators consistent with unitarity bounds } (\Delta \geq l)$$

This means that the only relevant scalar operators we are allowing in the OPE are those with $\Delta = \Delta_\sigma$ and with $\Delta = \Delta_\epsilon$. All others must have have $\Delta > 2$, and therefore be irrelevant
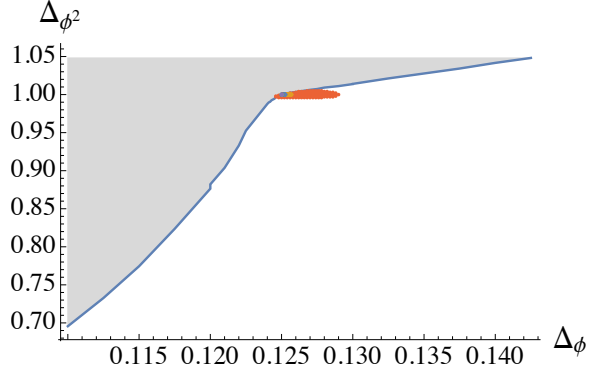
Figure 4.7: Multiple correlator results in 2D superimposed on the single correlator curve from figure 4.6. This time, everything *except* the red region is ruled out. The 2D Ising model has the exact values of $\Delta_\sigma = \frac{1}{8}$ and $\Delta_\epsilon = 1$. This figure has $\Delta_{\sigma'} = 4$ and $\Delta_{\epsilon'} = 3$. A zoomed-in view of the red region is in figure 4.8

.

since we are in two dimensions.

Having specified everything we need for the numerical bootstrap algorithm, all that remains now is to is pick numerical values of Δ_σ, Δ_ϵ and then search for a functional α. The ideal result would be that as we scan over Δ_σ and Δ_ϵ, we keep finding that the bootstrap equations cannot be satisfied (i.e. by finding the appropriate functional α) except for when $\Delta_\sigma = \frac{1}{8}$ and $\Delta_\epsilon = 1$, which are their values in the 2D Ising CFT. This would be very strong evidence that no other universality class exists with the stated properties (see the end of the following section for caveats).

4.10 Results

In this section, we present our numerical evidence that the CFT describing the 2D Ising universality class is the only $\mathbb{Z}_2$-symmetric CFT in two dimensions with exactly two relevant operators. The results in this section have not appeared in the literature previously.

Unfortunately, we were unable to attain the ideal numerical results mentioned at the

143

(a) Zoom in of red region in figure 4.7

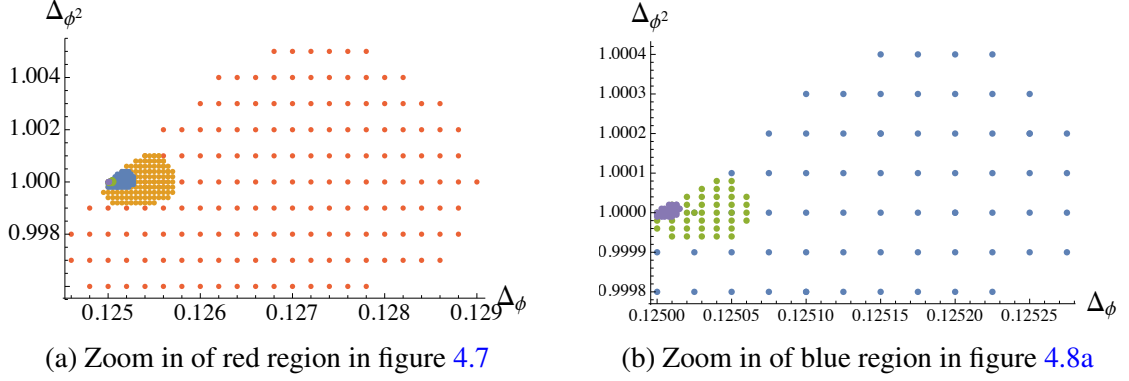(b) Zoom in of blue region in figure 4.8a

Figure 4.8: Zooming in on the red region of figure 4.7. The progressively smaller islands corresponds to increasing the number of derivatives Λ in the functional α defined in (4.60), where $\Lambda = 9, 11, 13, 15, 17$. The 2D Ising model has the exact values of $\Delta_\sigma = \frac{1}{8}$ and $\Delta_\epsilon = 1$.

end of last section. However, we did attain a similar but weaker result by making slightly stronger assumptions about the proposed spectrum. Specifically, we modified our proposed scalar spectrum to be

$$l = 0, \ \mathbb{Z}_2\text{-odd:} \quad \Delta = \Delta_\sigma \text{ or } \Delta \geq \Delta_{\sigma'}$$

$$l = 0, \ \mathbb{Z}_2\text{-even:} \quad \Delta = \Delta_\epsilon \text{ or } \Delta \geq \Delta_{\epsilon'}$$

where $\Delta_{\sigma'}, \Delta_{\epsilon'} \geq 2$. In other words, we assumed a larger gap to the irrelevant operators. Now, with $\Delta_{\sigma'} \gtrsim 3.3$ and $\Delta_{\epsilon'} \gtrsim 2.6$, we were indeed able to show that no CFT exists except for Δ_σ and Δ_ϵ very close to their Ising values. For $\Delta_{\sigma'} = 4$ and $\Delta_{\epsilon'} = 3$, the results are shown in figures 4.7 and 4.8. In figure 4.7, the results are superimposed on the single correlator bound that we found earlier in figure 4.6. Up to the sampling grid size, everything except the tiny region in red is ruled out. Figure 4.8 shows two progressively zoomed in versions of the same results. The increasingly smaller islands corresponds to increasing the number of derivatives Λ in the functional α defined in (4.60), where $\Lambda = 9, 11, 13, 15, 17$. It

appears that perhaps the island could shrink to zero size around the Ising values as $\Lambda \to \infty$.

To avoid confusion, let us be clear on what results are rigorous and what results have strong evidence, but were not rigorously established. First the rigorous part. We claim that the algorithm in section 4.7 rigorously rules out putative CFTs. Once a functional is found, it is merely a matter of numerical evaluation to show that the conformal bootstrap equation (4.42) cannot be satisfied. On the other hand, we then used this tool to provide evidence for a claim about universality. There are loopholes in this evidence. First, we sampled Δ_σ and Δ_ϵ on a grid surrounding their Ising values and checked one-by-one whether a functional exists or not. We did not check the continuously infinite number of values of Δ_σ and Δ_ϵ. Furthermore, there are infinitely many operators besides σ and ϵ. These are the irrelevant operators that have various subleading effects in critical phenomena such as finite-size corrections and corrections to scaling. Perhaps those could consistently differ between universality classes.[10] Finally, we were only focusing on universality classes that are described by unitary CFTs. Unitarity required the squared OPE coefficients to be positive, which was absolutely crucial to the whole numerical bootstrap program. It is currently completely unknown how to relax the constraint of unitarity.

In conclusion, in this chapter, we used the recently developed tools of the conformal bootstrap to provide strong evidence that the 2D Ising CFT is the unique unitary CFT in two dimensions with a $\mathbb{Z}_2$ symmetry and two relevant operators.

---

[10]However, there is also strong evidence that this is not the case [165–167].

Bibliography

[1] J. M. Maldacena. TASI 2003 lectures on AdS / CFT. `arXiv:hep-th/0309246 [hep-th]`.

[2] S. Weinberg, *The Quantum Theory of Fields: Volume 1, Foundations*. Cambridge University Press, 1995. `http://books.google.com/books?id=V7ggAwAAQBAJ`.

[3] S. Weinberg and E. Witten. Limits on massless particles. *Physics Letters B* **96** no. 1, (1980) 59 – 62. `http://www.sciencedirect.com/science/article/pii/0370269380902129`.

[4] J. M. Maldacena. The Large N limit of superconformal field theories and supergravity. *Adv.Theor.Math.Phys.* **2** (1998) 231–252, `arXiv:hep-th/9711200 [hep-th]`.

[5] S. Gubser, I. R. Klebanov, and A. M. Polyakov. Gauge theory correlators from noncritical string theory. *Phys.Lett.* **B428** (1998) 105–114, `arXiv:hep-th/9802109 [hep-th]`.

[6] E. Witten. Anti-de Sitter space and holography. *Adv.Theor.Math.Phys.* **2** (1998) 253–291, `arXiv:hep-th/9802150 [hep-th]`.

[7] A. Strominger and C. Vafa. Microscopic origin of the Bekenstein-Hawking entropy. *Phys.Lett.* **B379** (1996) 99–104, `arXiv:hep-th/9601029 [hep-th]`.

[8] S. W. Hawking. Breakdown of predictability in gravitational collapse. *Phys. Rev. D* **14** (Nov, 1976) 2460–2473. `http://link.aps.org/doi/10.1103/PhysRevD.14.2460`.

[9] A. Almheiri, D. Marolf, J. Polchinski, and J. Sully. Black Holes: Complementarity or Firewalls? *JHEP* **1302** (2013) 062, `arXiv:1207.3123 [hep-th]`.

[10] A. Almheiri, D. Marolf, J. Polchinski, D. Stanford, and J. Sully. An Apologia for Firewalls. `arXiv:1304.6483 [hep-th]`.

146

[11] D. Marolf and J. Polchinski. Gauge/Gravity Duality and the Black Hole Interior. *Phys.Rev.Lett.* **111** (2013) 171301, `arXiv:1307.4706 [hep-th]`.

[12] S. L. Braunstein, S. Pirandola, and K. Zyczkowski. Entangled black holes as ciphers of hidden information. *Physical Review Letters 110,* **101301** (2013) , `arXiv:0907.1190 [quant-ph]`.

[13] G. 't Hooft. Dimensional reduction in quantum gravity. `arXiv:gr-qc/9310026 [gr-qc]`.

[14] L. Susskind. The World as a hologram. *J.Math.Phys.* **36** (1995) 6377–6396, `arXiv:hep-th/9409089 [hep-th]`.

[15] L. Susskind, L. Thorlacius, and J. Uglum. The Stretched horizon and black hole complementarity. *Phys.Rev.* **D48** (1993) 3743–3761, `arXiv:hep-th/9306069 [hep-th]`.

[16] O. Aharony, S. S. Gubser, J. M. Maldacena, H. Ooguri, and Y. Oz. Large N field theories, string theory and gravity. *Phys.Rept.* **323** (2000) 183–386, `arXiv:hep-th/9905111 [hep-th]`.

[17] R. Sundrum. From Fixed Points to the Fifth Dimension. *Phys.Rev.* **D86** (2012) 085025, `arXiv:1106.4501 [hep-th]`.

[18] D. Bigatti and L. Susskind. TASI lectures on the holographic principle. `arXiv:hep-th/0002044 [hep-th]`.

[19] S. D. Mathur. The Information paradox: A Pedagogical introduction. *Class.Quant.Grav.* **26** (2009) 224001, `arXiv:0909.1038 [hep-th]`.

[20] M. Banados, C. Teitelboim, and J. Zanelli. The Black hole in three-dimensional space-time. *Phys.Rev.Lett.* **69** (1992) 1849–1851, `arXiv:hep-th/9204099 [hep-th]`.

[21] M. Banados, M. Henneaux, C. Teitelboim, and J. Zanelli. Geometry of the (2+1) black hole. *Phys.Rev.* **D48** (1993) 1506–1525, `arXiv:gr-qc/9302012 [gr-qc]`.

[22] S. Hawking and D. N. Page. Thermodynamics of Black Holes in anti-De Sitter Space. *Commun.Math.Phys.* **87** (1983) 577.

[23] J. M. Maldacena. Eternal black holes in anti-de Sitter. *JHEP* **0304** (2003) 021, `arXiv:hep-th/0106112 [hep-th]`.

[24] W. Israel. Thermo field dynamics of black holes. *Phys.Lett.* **A57** (1976) 107–110.

[25] G. T. Horowitz and D. Marolf. A New approach to string cosmology. *JHEP* **9807** (1998) 014, `arXiv:hep-th/9805207 [hep-th]`.

[26] V. Balasubramanian, P. Kraus, A. E. Lawrence, and S. P. Trivedi. Holographic probes of anti-de Sitter space-times. *Phys.Rev.* **D59** (1999) 104021, `arXiv:hep-th/9808017 [hep-th]`.

[27] P. C. Martin and J. S. Schwinger. Theory of many particle systems. 1. *Phys.Rev.* **115** (1959) 1342–1373.

[28] J. S. Schwinger. Brownian motion of a quantum oscillator. *J.Math.Phys.* **2** (1961) 407–432.

[29] K. T. Mahanthappa. Multiple production of photons in quantum electrodynamics. *Phys.Rev.* **126** (1962) 329–340.

[30] P. M. Bakshi and K. T. Mahanthappa. Expectation value formalism in quantum field theory. 1. *J.Math.Phys.* **4** (1963) 1–11.

[31] P. M. Bakshi and K. T. Mahanthappa. Expectation value formalism in quantum field theory. 2. *J.Math.Phys.* **4** (1963) 12–16.

[32] L. Keldysh. Diagram technique for nonequilibrium processes. *Zh.Eksp.Teor.Fiz.* **47** (1964) 1515–1527.

[33] Y. Takahasi and H. Umezawa. Thermo field dynamics. *Collect.Phenom.* **2** (1975) 55–80.

[34] J. Hartle and S. Hawking. Path Integral Derivation of Black Hole Radiance. *Phys.Rev.* **D13** (1976) 2188–2203.

[35] E. Witten. Quantum gravity in de Sitter space. `arXiv:hep-th/0106109 [hep-th]`.

[36] I. Ichinose and Y. Satoh. Entropies of scalar fields on three-dimensional black holes. *Nucl.Phys.* **B447** (1995) 340–372, `arXiv:hep-th/9412144 [hep-th]`.

[37] E. Keski-Vakkuri. Bulk and boundary dynamics in BTZ black holes. *Phys.Rev.* **D59** (1999) 104001, `arXiv:hep-th/9808037 [hep-th]`.

[38] J. M. Maldacena and A. Strominger. AdS(3) black holes and a stringy exclusion principle. *JHEP* **9812** (1998) 005, `arXiv:hep-th/9804085 [hep-th]`.

[39] M. Parikh and P. Samantray. Rindler-AdS/CFT. `arXiv:1211.7370 [hep-th]`.

[40] B. Czech, J. L. Karczmarek, F. Nogueira, and M. Van Raamsdonk. Rindler Quantum Gravity. *Class.Quant.Grav.* **29** (2012) 235025, `arXiv:1206.1323 [hep-th]`.

[41] S. Elitzur, A. Giveon, D. Kutasov, and E. Rabinovici. From big bang to big crunch and beyond. *JHEP* **0206** (2002) 017, `arXiv:hep-th/0204189 [hep-th]`.

[42] A. R. Steif. The Quantum stress tensor in the three-dimensional black hole. *Phys.Rev.* **D49** (1994) 585–589, `arXiv:gr-qc/9308032 [gr-qc]`.

[43] G. Lifschytz and M. Ortiz. Scalar field quantization on the (2+1)-dimensional black hole background. *Phys.Rev.* **D49** (1994) 1929–1943, `arXiv:gr-qc/9310008 [gr-qc]`.

[44] B. S. Kay, M. J. Radzikowski, and R. M. Wald. Quantum field theory on space-times with a compactly generated Cauchy horizon. *Commun.Math.Phys.* **183** (1997) 533–556, `arXiv:gr-qc/9603012 [gr-qc]`.

[45] M. Visser. The Quantum physics of chronology protection. `arXiv:gr-qc/0204022 [gr-qc]`.

[46] M. Berkooz and D. Reichmann. A Short Review of Time Dependent Solutions and Space-like Singularities in String Theory. *Nucl.Phys.Proc.Suppl.* **171** (2007) 69–87, `arXiv:0705.2146 [hep-th]`.

[47] J. McGreevy and E. Silverstein. The Tachyon at the end of the universe. *JHEP* **0508** (2005) 090, `arXiv:hep-th/0506130 [hep-th]`.

[48] A. de la Fuente and R. Sundrum. In preparation.

[49] P. Kraus, H. Ooguri, and S. Shenker. Inside the horizon with AdS / CFT. *Phys.Rev.* **D67** (2003) 124022, `arXiv:hep-th/0212277 [hep-th]`.

[50] J. S. Schwinger. Brownian motion of a quantum oscillator. *J.Math.Phys.* **2** (1961) 407–432.

[51] J. Schwinger. The special canonical group. *Proceedings of the National Academy of Sciences* **46** no. 10, (1960) 1401–1415. `http://www.pnas.org/content/46/10/1401.short`.

[52] S. Weinberg. Quantum contributions to cosmological correlations. *Phys.Rev.* **D72** (2005) 043514, `arXiv:hep-th/0506236 [hep-th]`.

[53] V. Balasubramanian and S. F. Ross. Holographic particle detection. *Phys.Rev.* **D61** (2000) 044007, `arXiv:hep-th/9906226 [hep-th]`.

[54] J. Louko, D. Marolf, and S. F. Ross. On geodesic propagators and black hole holography. *Phys.Rev.* **D62** (2000) 044041, `arXiv:hep-th/0002111 [hep-th]`.

[55] T. Hartman and J. Maldacena. Time Evolution of Entanglement Entropy from Black Hole Interiors. *JHEP* **1305** (2013) 014, `arXiv:1303.1080 [hep-th]`.

[56] L. Fidkowski, V. Hubeny, M. Kleban, and S. Shenker. The Black hole singularity in AdS / CFT. *JHEP* **0402** (2004) 014, `arXiv:hep-th/0306170 [hep-th]`.

[57] A. Hamilton, D. N. Kabat, G. Lifschytz, and D. A. Lowe. Local bulk operators in AdS/CFT: A Holographic description of the black hole interior. *Phys.Rev.* **D75** (2007) 106001, `arXiv:hep-th/0612053 [hep-th]`.

[58] I. Heemskerk, D. Marolf, J. Polchinski, and J. Sully. Bulk and Transhorizon Measurements in AdS/CFT. *JHEP* **1210** (2012) 165, arXiv:1201.3664 [hep-th].

[59] K. Papadodimas and S. Raju. An Infalling Observer in AdS/CFT. arXiv:1211.6767 [hep-th].

[60] S. Hemming, E. Keski-Vakkuri, and P. Kraus. Strings in the extended BTZ space-time. *JHEP* **0210** (2002) 006, arXiv:hep-th/0208003 [hep-th].

[61] J. Kaplan. Extracting data from behind horizons with the AdS / CFT correspondence. arXiv:hep-th/0402066 [hep-th].

[62] V. Balasubramanian and T. S. Levi. Beyond the veil: Inner horizon instability and holography. *Phys.Rev.* **D70** (2004) 106005, arXiv:hep-th/0405048 [hep-th].

[63] G. Festuccia and H. Liu. Excursions beyond the horizon: Black hole singularities in Yang-Mills theories. I. *JHEP* **0604** (2006) 044, arXiv:hep-th/0506202 [hep-th].

[64] E. J. Martinec and W. McElgin. Exciting AdS orbifolds. *JHEP* **0210** (2002) 050, arXiv:hep-th/0206175 [hep-th].

[65] F. Loran and M. Sheikh-Jabbari. O-BTZ: Orientifolded BTZ Black Hole. *Phys.Lett.* **B693** (2010) 184–187, arXiv:1003.4089 [hep-th].

[66] F. Loran and M. Sheikh-Jabbari. Orientifolded Locally AdS_3 Geometries. *Class.Quant.Grav.* **28** (2011) 025013, arXiv:1008.0462 [hep-th].

[67] S. Carlip. The (2+1)-Dimensional black hole. *Class.Quant.Grav.* **12** (1995) 2853–2880, arXiv:gr-qc/9506079 [gr-qc].

[68] U. H. Danielsson, E. Keski-Vakkuri, and M. Kruczenski. Vacua, propagators, and holographic probes in AdS / CFT. *JHEP* **9901** (1999) 002, arXiv:hep-th/9812007 [hep-th].

[69] C. W. Misner. The Flatter regions of Newman, Unti and Tamburino's generalized Schwarzschild space. *J.Math.Phys.* **4** (1963) 924–938.

[70] C. R. Cramer and B. S. Kay. The Thermal and two particle stress - energy must be ill defined on the 2-D Misner space chronology horizon. *Phys.Rev.* **D57** (1998) 1052–1056, arXiv:gr-qc/9708028 [gr-qc].

[71] J. Polchinski. String theory. Vol. 1: An introduction to the bosonic string.

[72] A. de la Fuente and R. Sundrum. In preparation.

[73] J. Bisognano and E. Wichmann. On the Duality Condition for a Hermitian Scalar Field. *J.Math.Phys.* **16** (1975) 985–1007.

[74] J. Bisognano and E. Wichmann. On the Duality Condition for Quantum Fields. *J.Math.Phys.* **17** (1976) 303–321.

[75] G. Sewell. Relativity of temperature and the Hawking effect. *Phys. Lett.* **79A** (1980) 23–24.

[76] G. L. Sewell. Quantum fields on manifolds: PCT and gravitationally induced thermal states. *Annals Phys.* **141** (1982) 201–224.

[77] W. G. Unruh and N. Weiss. Acceleration radiation in interacting field theories. *Phys.Rev.* **D29** (1984) 1656.

[78] T. Inami and H. Ooguri. One-Loop Effective Potential in Anti-de Sitter Space. *Prog.Theor.Phys.* **73** (1985) 1051.

[79] C. Burgess and C. Lutken. Propagators and effective potentials in anti-de Sitter space. *Phys.Lett.* **B153** (1985) 137.

[80] S. Aminneborg, I. Bengtsson, S. Holst, and P. Peldan. Making anti-de Sitter black holes. *Class.Quant.Grav.* **13** (1996) 2707–2714, `arXiv:gr-qc/9604005 [gr-qc]`.

[81] D. R. Brill, J. Louko, and P. Peldan. Thermodynamics of (3+1)-dimensional black holes with toroidal or higher genus horizons. *Phys.Rev.* **D56** (1997) 3600–3610, `arXiv:gr-qc/9705012 [gr-qc]`.

[82] S. Holst and P. Peldan. Black holes and causal structure in anti-de Sitter isometric space-times. *Class.Quant.Grav.* **14** (1997) 3433–3452, `arXiv:gr-qc/9705067 [gr-qc]`.

[83] D. Baumann. TASI Lectures on Inflation. `arXiv:0907.5424 [hep-th]`.

[84] **WMAP** Collaboration, G. Hinshaw *et al.* Nine-Year Wilkinson Microwave Anisotropy Probe (WMAP) Observations: Cosmological Parameter Results. *Astrophys.J.Suppl.* **208** (2013) 19, `arXiv:1212.5226 [astro-ph.CO]`.

[85] **Planck Collaboration** Collaboration, P. Ade *et al.* Planck 2013 results. XXII. Constraints on inflation. `arXiv:1303.5082 [astro-ph.CO]`.

[86] K. Freese, J. A. Frieman, and A. V. Olinto. Natural inflation with pseudo nambu-goldstone bosons. *Phys. Rev. Lett.* **65** (Dec, 1990) 3233–3236. `http://link.aps.org/doi/10.1103/PhysRevLett.65.3233`.

[87] S. Weinberg. The Cosmological Constant Problem. *Rev.Mod.Phys.* **61** (1989) 1–23.

[88] J. Polchinski, *String Theory: Volumes 1 and 2*. Cambridge University Press, 1998.

[89] **BICEP2 Collaboration** Collaboration, P. Ade *et al.* Detection of B-Mode Polarization at Degree Angular Scales by BICEP2. *Phys.Rev.Lett.* **112** (2014) 241101, `arXiv:1403.3985 [astro-ph.CO]`.

[90] R. Flauger, J. C. Hill, and D. N. Spergel. Toward an Understanding of Foreground Emission in the BICEP2 Region. *JCAP* **1408** (2014) 039, `arXiv:1405.7351 [astro-ph.CO]`.

[91] **Planck Collaboration** Collaboration, R. Adam *et al.* Planck intermediate results. XXX. The angular power spectrum of polarized dust emission at intermediate and high Galactic latitudes. `arXiv:1409.5738 [astro-ph.CO]`.

[92] E. Silverstein and A. Westphal. Monodromy in the CMB: Gravity Waves and String Inflation. *Phys.Rev.* **D78** (2008) 106003, `arXiv:0803.3085 [hep-th]`.

[93] L. McAllister, E. Silverstein, and A. Westphal. Gravity Waves and Linear Inflation from Axion Monodromy. *Phys.Rev.* **D82** (2010) 046003, `arXiv:0808.0706 [hep-th]`.

[94] R. Blumenhagen and E. Plauschinn. Towards Universal Axion Inflation and Reheating in String Theory. *Phys.Lett.* **B736** (2014) 482–487, `arXiv:1404.3542 [hep-th]`.

[95] T. W. Grimm. Axion Inflation in F-theory. *Phys.Lett.* **B739** (2014) 201–208, `arXiv:1404.4268 [hep-th]`.

[96] C. Long, L. McAllister, and P. McGuirk. Aligned Natural Inflation in String Theory. *Phys.Rev.* **D90** (2014) 023501, `arXiv:1404.7852 [hep-th]`.

[97] L. McAllister, E. Silverstein, A. Westphal, and T. Wrase. The Powers of Monodromy. `arXiv:1405.3652 [hep-th]`.

[98] X. Gao, T. Li, and P. Shukla. Combining Universal and Odd RR Axions for Aligned Natural Inflation. *JCAP* **1410** no. 10, (2014) 048, `arXiv:1406.0341 [hep-th]`.

[99] I. Ben-Dayan, F. G. Pedro, and A. Westphal. Towards Natural Inflation in String Theory. `arXiv:1407.2562 [hep-th]`.

[100] Z. Kenton and S. Thomas. D-brane Potentials in the Warped Resolved Conifold and Natural Inflation. `arXiv:1409.1221 [hep-th]`.

[101] N. Arkani-Hamed, H.-C. Cheng, P. Creminelli, and L. Randall. Extra natural inflation. *Phys.Rev.Lett.* **90** (2003) 221302, `arXiv:hep-th/0301218 [hep-th]`.

[102] S. Dimopoulos, S. Kachru, J. McGreevy, and J. G. Wacker. N-flation. *JCAP* **0808** (2008) 003, `arXiv:hep-th/0507205 [hep-th]`.

[103] N. Kaloper and L. Sorbo. A Natural Framework for Chaotic Inflation. *Phys.Rev.Lett.* **102** (2009) 121301, `arXiv:0811.1989 [hep-th]`.

[104] N. Kaloper, A. Lawrence, and L. Sorbo. An Ignoble Approach to Large Field Inflation. *JCAP* **1103** (2011) 023, `arXiv:1101.0026 [hep-th]`.

[105] S. Dubovsky, A. Lawrence, and M. M. Roberts. Axion monodromy in a model of holographic gluodynamics. *JHEP* **1202** (2012) 053, `arXiv:1105.3740 [hep-th]`.

[106] K. Harigaya, M. Ibe, K. Schmitz, and T. T. Yanagida. Chaotic Inflation with a Fractional Power-Law Potential in Strongly Coupled Gauge Theories. *Phys.Lett.* **B720** (2013) 125–129, `arXiv:1211.6241 [hep-ph]`.

[107] K. Harigaya and M. Ibe. Simple realization of inflaton potential on a Riemann surface. *Phys.Lett.* **B738** (2014) 301–304, `arXiv:1404.3511 [hep-ph]`.

[108] M. Dine, P. Draper, and A. Monteux. Monodromy Inflation in SUSY QCD. *JHEP* **1407** (2014) 146, `arXiv:1405.0068 [hep-th]`.

[109] K. Yonekura. Notes on natural inflation. *JCAP* **1410** no. 10, (2014) 054, `arXiv:1405.0734 [hep-th]`.

[110] I. P. Neupane. Natural Braneworld Inflation in Light of Recent Results from Planck and BICEP2. *Phys.Rev.* **D90** no. 12, (2014) 123502, `arXiv:1409.8647 [astro-ph.CO]`.

[111] N. Arkani-Hamed, L. Motl, A. Nicolis, and C. Vafa. The String landscape, black holes and gravity as the weakest force. *JHEP* **0706** (2007) 060, `arXiv:hep-th/0601001 [hep-th]`.

[112] A. de la Fuente, P. Saraswat, and R. Sundrum In preparation.

[113] R. Kallosh, A. D. Linde, D. A. Linde, and L. Susskind. Gravity and global symmetries. *Phys.Rev.* **D52** (1995) 912–935, `arXiv:hep-th/9502069 [hep-th]`.

[114] T. Banks and N. Seiberg. Symmetries and Strings in Field Theory and Gravity. *Phys.Rev.* **D83** (2011) 084019, `arXiv:1011.5120 [hep-th]`.

[115] Y. Hosotani. Dynamical Gauge Symmetry Breaking as the Casimir Effect. *Phys.Lett.* **B129** (1983) 193.

[116] B. Feng, M.-z. Li, R.-J. Zhang, and X.-m. Zhang. An inflation model with large variations in spectral index. *Phys.Rev.* **D68** (2003) 103511, `arXiv:astro-ph/0302479 [astro-ph]`.

[117] M. Li, W. Song, and T. Wang. Some low dimensional evidence for the weak gravity conjecture. *JHEP* **0603** (2006) 094, `arXiv:hep-th/0601137 [hep-th]`.

[118] M. Li, W. Song, Y. Song, and T. Wang. A Weak gravity conjecture for scalar field theories. *JHEP* **0705** (2007) 026, `arXiv:hep-th/0606011 [hep-th]`.

[119] T. Banks, M. Johnson, and A. Shomer. A Note on Gauge Theories Coupled to Gravity. *JHEP* **0609** (2006) 049, `arXiv:hep-th/0606277 [hep-th]`.

[120] Q.-G. Huang. Weak Gravity Conjecture with Large Extra Dimensions. *Phys.Lett.* **B658** (2008) 155–157, `arXiv:hep-th/0610106 [hep-th]`.

[121] Q.-G. Huang. Weak Gravity Conjecture for the Effective Field Theories with N Species. *Phys.Rev.* **D77** (2008) 105029, `arXiv:0712.2859 [hep-th]`.

[122] C. Cheung and G. N. Remmen. Naturalness and the Weak Gravity Conjecture. *Phys.Rev.Lett.* **113** (2014) 051601, `arXiv:1402.2287 [hep-ph]`.

[123] C. Cheung and G. N. Remmen. Infrared Consistency and the Weak Gravity Conjecture. *JHEP* **1412** (2014) 087, `arXiv:1407.7865 [hep-th]`.

[124] J. D. Bekenstein. Black holes and entropy. *Phys.Rev.* **D7** (1973) 2333–2346.

[125] L. Susskind. Some speculations about black hole entropy in string theory. `arXiv:hep-th/9309145 [hep-th]`.

[126] A. C. Wall. A proof of the generalized second law for rapidly changing fields and arbitrary horizon slices. *Phys.Rev.* **D85** no. 6, (2012) 104049, `arXiv:1105.3445 [gr-qc]`.

[127] A. W. Peet. The Bekenstein formula and string theory (N-brane theory). *Class.Quant.Grav.* **15** (1998) 3291–3338, `arXiv:hep-th/9712253 [hep-th]`.

[128] A. Sen. Microscopic and Macroscopic Entropy of Extremal Black Holes in String Theory. *Gen.Rel.Grav.* **46** (2014) 1711, `arXiv:1402.0109 [hep-th]`.

[129] T. Rudelius. On the Possibility of Large Axion Moduli Spaces. `arXiv:1409.5793 [hep-th]`.

[130] J. E. Kim, H. P. Nilles, and M. Peloso. Completing natural inflation. *JCAP* **0501** (2005) 005, `arXiv:hep-ph/0409138 [hep-ph]`.

[131] K. Choi, H. Kim, and S. Yun. Natural Inflation with Multiple Sub-Planckian Axions. *Phys.Rev.* **D90** (2014) 023545, `arXiv:1404.6209 [hep-th]`.

[132] S. H. H. Tye and S. S. C. Wong. Helical Inflation and Cosmic Strings. `arXiv:1404.6988 [astro-ph.CO]`.

[133] R. Kappl, S. Krippendorf, and H. P. Nilles. Aligned Natural Inflation: Monodromies of two Axions. `arXiv:1404.7127 [hep-th]`.

[134] I. Ben-Dayan, F. G. Pedro, and A. Westphal. Hierarchical Axion Inflation. `arXiv:1404.7773 [hep-th]`.

[135] Y. Bai and B. A. Stefanek. Natural Milli-Charged Inflation. `arXiv:1405.6720 [hep-ph]`.

[136] W. D. Goldberger and M. B. Wise. Modulus stabilization with bulk fields. *Phys.Rev.Lett.* **83** (1999) 4922–4925, `arXiv:hep-ph/9907447 [hep-ph]`.

[137] X. Wang, B. Feng, M. Li, X.-L. Chen, and X. Zhang. Natural inflation, Planck scale physics and oscillating primordial spectrum. *Int.J.Mod.Phys.* **D14** (2005) 1347, `arXiv:astro-ph/0209242 [astro-ph]`.

[138] C. Pahud, M. Kamionkowski, and A. R. Liddle. Oscillations in the inflaton potential? *Phys.Rev.* **D79** (2009) 083503, `arXiv:0807.0322 [astro-ph]`.

[139] R. Flauger, L. McAllister, E. Pajer, A. Westphal, and G. Xu. Oscillations in the CMB from Axion Monodromy Inflation. *JCAP* **1006** (2010) 009, `arXiv:0907.2916 [hep-th]`.

[140] T. Kobayashi and F. Takahashi. Running spectral index from inflation with modulations. *JCAP* **1** (Jan., 2011) 26, `arXiv:1011.3988 [astro-ph.CO]`.

[141] R. Easther and R. Flauger. Planck Constraints on Monodromy Inflation. *JCAP* **1402** (2014) 037, `arXiv:1308.3736 [astro-ph.CO]`.

[142] R. Flauger, L. McAllister, E. Silverstein, and A. Westphal. Drifting Oscillations in Axion Monodromy. `arXiv:1412.1814 [hep-th]`.

[143] T. Higaki and F. Takahashi. Natural and Multi-Natural Inflation in Axion Landscape. *JHEP* **1407** (2014) 074, `arXiv:1404.6923 [hep-th]`.

[144] J. E. Kim and G. Carosi. Axions and the Strong CP Problem. *Rev.Mod.Phys.* **82** (2010) 557–602, `arXiv:0807.3125 [hep-ph]`.

[145] K. G. Wilson. Renormalization group and critical phenomena. 1. Renormalization group and the Kadanoff scaling picture. *Phys. Rev.* **B4** (1971) 3174–3183.

[146] K. G. Wilson. Renormalization group and critical phenomena. 2. Phase space cell analysis of critical behavior. *Phys. Rev.* **B4** (1971) 3184–3205.

[147] K. G. Wilson and J. B. Kogut. The Renormalization group and the epsilon expansion. *Phys. Rept.* **12** (1974) 75–200.

[148] J. Cardy, *Scaling and Renormalization in Statistical Physics*. Cambridge Lecture Notes in Physics. Cambridge University Press, 1996. `https://books.google.com/books?id=Wt804S9FjyAC`.

[149] N. Goldenfeld, *Lectures on Phase Transitions and the Renormalization Group*. Frontiers in physics. Addison-Wesley, Advanced Book Program, 1992. `https://books.google.com/books?id=DdB1__nl7CYC`.

[150] F. Kos, D. Poland, and D. Simmons-Duffin. Bootstrapping Mixed Correlators in the 3D Ising Model. *JHEP* **11** (2014) 109, `arXiv:1406.4858 [hep-th]`.

[151] D. Simmons-Duffin. A Semidefinite Program Solver for the Conformal Bootstrap. *JHEP* **06** (2015) 174, `arXiv:1502.02033 [hep-th]`.

[152] F. Kos, D. Poland, D. Simmons-Duffin, and A. Vichi. Bootstrapping the O(N) Archipelago. *JHEP* **11** (2015) 106, `arXiv:1504.07997 [hep-th]`.

[153] F. Kos, D. Poland, D. Simmons-Duffin, and A. Vichi. Precision Islands in the Ising and $O(N)$ Models. `arXiv:1603.04436 [hep-th]`.

[154] D. Simmons-Duffin. TASI Lectures on the Conformal Bootstrap. `arXiv:1602.07982 [hep-th]`.

[155] S. Rychkov. EPFL Lectures on Conformal Field Theory in D>= 3 Dimensions. `arXiv:1601.05000 [hep-th]`.

[156] J. Polchinski. Scale and conformal invariance in quantum field theory. *Nuclear Physics B* **303** (June, 1988) 226–236.

[157] M. A. Luty, J. Polchinski, and R. Rattazzi. The *a*-theorem and the Asymptotics of 4D Quantum Field Theory. *JHEP* **01** (2013) 152, `arXiv:1204.5221 [hep-th]`.

[158] A. Dymarsky, Z. Komargodski, A. Schwimmer, and S. Theisen. On Scale and Conformal Invariance in Four Dimensions. *JHEP* **10** (2015) 171, `arXiv:1309.2921 [hep-th]`.

[159] A. Dymarsky, K. Farnsworth, Z. Komargodski, M. A. Luty, and V. Prilepina. Scale Invariance, Conformality, and Generalized Free Fields. *JHEP* **02** (2016) 099, `arXiv:1402.6322 [hep-th]`.

[160] D. Pappadopulo, S. Rychkov, J. Espin, and R. Rattazzi. OPE Convergence in Conformal Field Theory. *Phys. Rev.* **D86** (2012) 105043, `arXiv:1208.6449 [hep-th]`.

[161] H. Osborn. Conformal Blocks for Arbitrary Spins in Two Dimensions. *Phys. Lett.* **B718** (2012) 169–172, `arXiv:1205.1941 [hep-th]`.

[162] R. Rattazzi, V. S. Rychkov, E. Tonni, and A. Vichi. Bounding scalar operator dimensions in 4D CFT. *JHEP* **12** (2008) 031, `arXiv:0807.0004 [hep-th]`.

[163] M. A. Luty and T. Okui. Conformal technicolor. *JHEP* **09** (2006) 070, `arXiv:hep-ph/0409274 [hep-ph]`.

[164] D. Poland, D. Simmons-Duffin, and A. Vichi. Carving Out the Space of 4D CFTs. *JHEP* **05** (2012) 110, `arXiv:1109.5176 [hep-th]`.

[165] S. El-Showk and M. F. Paulos. Bootstrapping Conformal Field Theories with the Extremal Functional Method. *Phys. Rev. Lett.* **111** no. 24, (2013) 241601, `arXiv:1211.2810 [hep-th]`.

[166] S. El-Showk and M. F. Paulos. Extremal bootstrapping: go with the flow. `arXiv:1605.08087 [hep-th]`.

[167] S. El-Showk, M. F. Paulos, D. Poland, S. Rychkov, D. Simmons-Duffin, and A. Vichi. Solving the 3d Ising Model with the Conformal Bootstrap II. c-Minimization and Precise Critical Exponents. *J. Stat. Phys.* **157** (2014) 869, `arXiv:1403.4545 [hep-th]`.